

# Remote river rating in Zambia

A case study in the Luangwa river basin

a MSc study by Ivar Abas



# Remote river rating in Zambia

A case study in the Luangwa river basin

by

I. Abas

to obtain the degree of Master of Science  
at the Delft University of Technology,  
to be defended publicly on Friday December 21st, 2018.

Student number:	4102088
Project duration:	February 1st, 2018 – December 21st, 2018
Thesis committee:	Prof. dr. ir. H.H.G. Savenije, TU Delft
	Ir. W.M.J. Luxemburg, TU Delft
	Dr. ir. H. Winsemius, Deltares & TU Delft
	Prof. dr. ir. M. Kok, TU Delft
	Ir. A. Couasnon, VU Amsterdam

An electronic version of this thesis is available at <http://repository.tudelft.nl/>.



*"No man ever steps  
in the same river twice;  
for it's not the same river  
and he's not the same man."*

- HERACLITUS



# Acknowledgements

This thesis would not have been a success without the help and resources of the Water Resources Management Center of the University of Zambia, therefore I want to express my gratitude. In particular I want to thank Professor Imasiku Nyambe for helping me out with all kinds of issues during my stay in Zambia and for his enthusiasm throughout the project.

Besides the support of the University of Zambia I received a lot of help from the Zambian Water Resources Management Authority for which I express my deepest gratitude.

I want to thank my thesis committee for guiding me the way and for the endless patients and enthusiasm I encountered when I bothered them with questions. Thanks a lot for the inspiring sessions and the casual conversations after the colloquium drinks. A special thanks to Huub Savenije and Wim Luxemburg for accompanying me throughout my time at Delft University. From a small river called “de Kromme Rijn” in the Netherlands to the Pungue river in Mozambique and in the end all the way up to the Luangwa catchment in Zambia. Thanks a lot for the beautiful moments and the unforgettable experience and adventures.

Last but certainly not least I want to thank Henry Zimba and Hubert Samboko, my roommates and research buddies during my stay in Zambia. Henry I really enjoyed our soccer games at the campus and sincerely appreciated you showing me all of the beautiful things Zambia has to offer. Hubert thank you for your endless support during our long drives during fieldwork and the necessary distractions of the Zambian nightlife in the weekends. I hope to see you guys soon in the Netherlands and will do my best to repay the hospitality and kindness I have received during my unforgettable stay.

*I. Abas  
Delft, December 2018*



# Abstract

Direct measurement of river discharge is difficult, time consuming and costly. Therefore a rating curve is often used to estimate the river discharge. Limited measurements under extreme conditions result in extrapolation of the rating curve for high flow conditions. This induces uncertainties and errors in the stage-discharge relation. Recently there has been a gradual shift to more physically based rating curves, where the geometry of a river is included and no extrapolation is needed. This seems to be a promising shift to improve traditional river rating. However, the challenge now is to accurately determine the parameters bed roughness and hydraulic slope. The aim of this research is to develop and evaluate a method to better estimate the hydraulic parameters bed roughness and hydraulic slope. To do so a case study has been carried out in the Luangwa river catchment in Zambia.

The research methodology can be divided in six stages. The first stage consists of a literature review where the knowledge gap is identified and the research aim and supporting objectives are formulated. The second stage includes the data collection stage. Discharge, bathymetric and aerial data are collected for an upstream, middle and downstream location of the Luangwa river catchment. In the end, the downstream location of the Great East Road bridge is selected for further analysis and hydraulic modelling. The third stage is the data processing stage, where Unmanned Aerial Vehicle (UAV) data is transformed in a Digital Elevation Model (DEM) and the Acoustic Doppler Current Profiler (ADCP) measurements are processed. The fourth stage is the data analysis stage. In this stage the ADCP transects are investigated on their hydraulic behaviour and the vegetation and water parts are removed from the DEM. The fifth stage contains the hydraulic modelling stage. In this stage a 1D steady-state hydraulic model is build and calibrated on the conducted ADCP measurements. In this research the hydraulic model HEC-RAS is used. The final stage consists of comparing a more physically based rating curve from the hydraulic model with a traditional rating curve from the Zambian Water Resources Management Authority (WARMA).

This research presents different methods to estimate the hydraulic slope or under uniform flow conditions the bed slope. In the end the measurements of the global DEM and the Differential Global Positioning System (DGPS) measurements of the water surface level are used to obtain one value  $i_w = 4 \cdot 10^{-4}$  for the slope. This value is further on used in the steady-state hydraulic model.

The model output is evaluated by the Root Mean Squared Error (RMSE). The lowest value for the RMSE is obtained for a Manning's roughness coefficient of  $n = 0.040$ . According to literature this seems to be a reasonable value. A rating curve is composed by the HEC-RAS model and compared to the rating curve of WARMA. The more physically constructed rating curve, by the hydraulic model fits clearly in the 95% confidence interval of the WARMA rating curve. However, for high flows the rating curves diverge. The model sensitivity is evaluated by changing the Manning's roughness and changing the hydraulic slope. It becomes clear that it is important to estimate the bed roughness accurately. Finally some recommendations are made for a future survey and for future research.



# Contents

<b>List of Acronyms</b>	<b>ix</b>
<b>List of Figures</b>	<b>xi</b>
<b>List of Tables</b>	<b>xv</b>
<b>1 Introduction</b>	<b>1</b>
1.1 General introduction . . . . .	1
1.2 Problem statement . . . . .	2
1.3 Research aim and objectives . . . . .	2
1.4 Thesis layout . . . . .	4
<b>2 Theoretical background</b>	<b>5</b>
2.1 Traditional river rating . . . . .	5
2.1.1 Theory . . . . .	5
2.1.2 Limitations. . . . .	6
2.2 Physically based river rating . . . . .	6
2.3 Aerial photography and photogrammetry. . . . .	8
2.3.1 Photogrammetry. . . . .	8
2.3.2 Aerial photography . . . . .	9
2.4 Hydraulic modelling . . . . .	11
<b>3 Research area</b>	<b>13</b>
3.1 The Luangwa river catchment. . . . .	13
3.2 Site selection . . . . .	14
<b>4 Research equipment</b>	<b>17</b>
4.1 Unmanned Aerial Vehicle . . . . .	17
4.2 Ground Control Points . . . . .	18
4.3 Differential Global Positioning System . . . . .	18
4.4 Acoustic Doppler Current Profiler. . . . .	19
4.5 Garden hose with transparent tubes . . . . .	20
<b>5 Research methodology</b>	<b>21</b>
5.1 Simplification research methodology . . . . .	21
5.2 Data collection . . . . .	22
5.2.1 Wet river profile collection . . . . .	23
5.2.2 Dry river profile collection . . . . .	23
5.2.3 Estimation of the hydraulic slope . . . . .	24
5.3 Data processing. . . . .	26
5.3.1 Wet river profile . . . . .	26
5.3.2 Dry river profile . . . . .	27
5.4 Data analysis . . . . .	27
5.4.1 Wet river profile . . . . .	27
5.4.2 Dry river profile . . . . .	29
5.5 Hydraulic modelling . . . . .	29
5.5.1 General modelling approach. . . . .	29
5.5.2 Model calibration . . . . .	31
5.5.3 Model evaluation . . . . .	31
5.5.4 Parameter sensitivity. . . . .	32
5.6 Rating curve comparison . . . . .	32

<b>6</b>	<b>Results &amp; discussion</b>	<b>33</b>
6.1	Wet river profile . . . . .	33
6.2	Dry river profile . . . . .	36
6.3	Hydraulic slope estimation . . . . .	36
6.4	Hydraulic modelling . . . . .	38
6.5	Rating curve comparison . . . . .	39
<b>7</b>	<b>Conclusions &amp; recommendations</b>	<b>45</b>
7.1	Conclusions. . . . .	45
7.2	Recommendations . . . . .	46
7.2.1	Recommendations for a future survey . . . . .	46
7.2.2	Recommendations for future research . . . . .	46
	<b>Bibliography</b>	<b>47</b>
<b>A</b>	<b>Backwater derivation and calculation</b>	<b>51</b>
<b>B</b>	<b>Error estimation GCPs</b>	<b>55</b>
<b>C</b>	<b>Cross-sections analysis</b>	<b>57</b>
C.1	Bathymetry measurements . . . . .	58
C.1.1	Depth profiles . . . . .	58
C.2	Velocity profiles . . . . .	59
C.2.1	Downstream transect . . . . .	59
C.2.2	Middle transect . . . . .	59
C.2.3	Upstream transect . . . . .	60
C.2.4	Discharge summary tables. . . . .	61
C.3	Width versus depth . . . . .	62
C.4	Cross-sectional area versus depth. . . . .	62
C.5	Perimeter versus depth . . . . .	63
C.6	Hydraulic radius versus depth . . . . .	64
C.7	Conveyance versus depth . . . . .	64
C.8	Averaging depth profiles . . . . .	65
C.8.1	Downstream transect . . . . .	65
C.8.2	Middle transect . . . . .	66
C.8.3	Upstream transect . . . . .	66
<b>D</b>	<b>Additional graphs results</b>	<b>69</b>
D.1	Hydraulic slope estimation . . . . .	69
D.2	Model evaluation . . . . .	70
D.3	Rating curves . . . . .	71
<b>E</b>	<b>Manning values and calculations</b>	<b>79</b>

# List of Acronyms

<b>ADCP</b>	Acoustic Doppler Current Profiler
<b>ASTER</b>	Advanced Spaceborne Thermal Emission and Reflection Radiometer
<b>DEM</b>	Digital Elevation Model
<b>DGPS</b>	Differential Global Positioning System
<b>HEC-RAS</b>	Hydrologic Engineering Center River Analysis System
<b>HGL</b>	Hydraulic Grade Line
<b>GCPs</b>	Ground Control Points
<b>GDEM</b>	Global Digital Elevation Model
<b>GL</b>	Ground Level
<b>GSD</b>	Ground Sampling Distance
<b>RMSE</b>	Root Mean Squared Error
<b>UAV</b>	Unmanned Aerial Vehicle
<b>WARMA</b>	Water Resources Management Authority of Zambia



# List of Figures

1.1	Fictional rating curve, where extrapolation is applied for high flows. . . . .	2
1.2	Flowchart of steps needed to achieve research aim. . . . .	3
2.1	The principle of photogrammetry, a schematic representation including the required overlap (Government of Canada, 2016). . . . .	8
2.2	(a) Schematic definition of the Ground Sampling Distance. (b) Basic concepts of aerial photography (Government of Canada, 2016). . . . .	9
2.3	Longitudinal profile of a river reach, with variables of the energy equation. . . . .	11
3.1	Terrain analysis and watershed delineation of the Luangwa river basin. . . . .	13
3.2	Gauging stations WARMA and measurement locations: Mulopwe village, Mfuwe and Great East Road bridge. . . . .	14
3.3	Overview of different measurement sites: (a) Mulopwe village (b) Mfuwe (c) Great East Road bridge site 1 and (d) Great East Road bridge site 2. . . . .	15
3.4	The locations of respectively, the WARMA gauging station, the Great East Road bridge and the chosen measurement site for hydraulic modelling. . . . .	16
4.1	Examples of different pre-programmed flights in the applications: (a) Dronedeploy and (b) Litchi. . . . .	18
4.2	Ground Control Points at measurement locations: (a) the measurement location and (b) Mulopwe village. . . . .	18
4.3	Set-up of a Differential GPS with a base- and rover receiver and an external antenna. . . . .	19
4.4	ADCP measurements at (a) the measurement location and (b) Mfuwe. . . . .	20
4.5	(a) the wooden plank with transparent tubes and (b) the garden hose method being applied in the field. . . . .	20
5.1	A simplification of the six steps carried out in the research methodology. . . . .	21
5.2	The data collection categories; the wet river profile, the dry river profile and the hydraulic slope estimation. . . . .	22
5.3	The river profile divided into a wet and dry part, based on the ADCP measurement carried out on May 12, 2018. . . . .	22
5.4	Transects ADCP measurements for downstream location of the Great East Road bridge. . . . .	23
5.5	Slope determination area of interest, where GL = Ground level, HGL = Hydraulic Grade Line (Veldhuis, 2018). . . . .	25
5.6	A schematic sketch of the garden hose method. . . . .	25
5.7	DGPS measurements of the water surface level for a short and large distance. . . . .	26
5.8	An example of a processed ADCP measurement at the area of interest on May 12, 2018. . . . .	26
5.9	Processing procedure of aerial photographs in Agisoft PhotoScan. . . . .	27
5.10	Hydraulic parameters definition of a transect. . . . .	28
5.11	The DEM of the area of interest still containing vegetation and water. . . . .	29
5.12	The set-up of the geometry of the HEC-RAS model. . . . .	30
5.13	The requirements and outputs for a 1D steady-state HEC-RAS model. . . . .	31
6.1	Depth profiles for the downstream transect on the 12 <sup>th</sup> of May 2018. . . . .	33
6.2	Selection of depth profiles for the downstream transect on the 12 <sup>th</sup> of May 2018. . . . .	34
6.3	Conveyance versus modelled depth on the 12 <sup>th</sup> of May 2018. . . . .	35
6.4	Averaging the middle transect on the 12 <sup>th</sup> of May 2018. . . . .	35
6.5	(a) DEM without water or vegetation and (b) orthophoto of the area of interest. . . . .	36
6.6	Bed slope estimation from the ASTER GDEM data (Broekema, 2018). . . . .	36
6.7	DGPS measurements of the water surface elevation over a large distance. . . . .	37

6.8	The RMSE for varying Manning's coefficients, both measurement days combined. . . . .	38
6.9	The discharge stage measurements of WARMA. . . . .	39
6.10	Determination of stage-discharge relationship WARMA measurements. . . . .	40
6.11	The simulated stage discharge values for the HEC-RAS model. . . . .	40
6.12	Determination of stage-discharge relationship HEC-RAS model. . . . .	41
6.13	Comparison of rating curve WARMA with the HEC-RAS rating curve. . . . .	42
6.14	Rating curve sensitivity for changes in Manning's coefficient and constant hydraulic slope. . . . .	42
6.15	Rating curve sensitivity for changes in hydraulic slope and constant bed roughness. . . . .	43
6.16	Rating curve sensitivity for changes in hydraulic slope with new optimum bed roughness values. . . . .	43
6.17	Rating curve comparison with error bounds and the sensitivity of a change in bed roughness. . . . .	44
B.1	GCP locations and error estimates. X (Easting) and Y (Northing) errors are represented by ellipse shape. Z (altitude) error is represented by ellipse color. . . . .	55
C.1	Transects ADCP measurements for downstream location of the Great East Road bridge. . . . .	57
C.2	Depth profiles for the downstream transect on the 27 <sup>th</sup> of April 2018. . . . .	58
C.3	Depth profiles for the downstream transect on the 12 <sup>th</sup> of May 2018. . . . .	58
C.4	Selection of depth profiles for the downstream transect on the 12 <sup>th</sup> of May 2018. . . . .	58
C.5	Velocity profiles for the downstream transect on the 27 <sup>th</sup> of April 2018. . . . .	59
C.6	Velocity profiles for the downstream transect on the 12 <sup>th</sup> of May 2018. . . . .	59
C.7	Velocity profiles for the middle transect on the 27 <sup>th</sup> of April 2018. . . . .	59
C.8	Velocity profiles for the middle transect on the 12 <sup>th</sup> of May 2018. . . . .	60
C.9	Velocity profiles for the upstream transect on the 27 <sup>th</sup> of April 2018. . . . .	60
C.10	Velocity profiles for the upstream transect on the 12 <sup>th</sup> of May 2018. . . . .	60
C.11	Top width versus modelled depth on the 27 <sup>th</sup> of April 2018. . . . .	62
C.12	Top width versus modelled depth on the 12 <sup>th</sup> of May 2018. . . . .	62
C.13	Cross-sectional area versus modelled depth on the 27 <sup>th</sup> of April 2018. . . . .	62
C.14	Cross-sectional area versus modelled depth on the 12 <sup>th</sup> of May 2018. . . . .	63
C.15	Perimeter versus modelled depth on the 27 <sup>th</sup> of April 2018. . . . .	63
C.16	Perimeter versus modelled depth on the 12 <sup>th</sup> of May 2018. . . . .	63
C.17	Hydraulic radius versus modelled depth on the 27 <sup>th</sup> of April 2018. . . . .	64
C.18	Hydraulic radius versus modelled depth on the 12 <sup>th</sup> of May 2018. . . . .	64
C.19	Conveyance versus modelled depth on the 27 <sup>th</sup> of April 2018. . . . .	64
C.20	Conveyance versus modelled depth on the 12 <sup>th</sup> of May 2018. . . . .	65
C.21	Averaging the downstream transect on the 27 <sup>th</sup> of April 2018. . . . .	65
C.22	Averaging the downstream transect on the 12 <sup>th</sup> of May 2018. . . . .	65
C.23	Averaging the middle transect on the 27 <sup>th</sup> of April 2018. . . . .	66
C.24	Averaging the middle transect on the 12 <sup>th</sup> of May 2018. . . . .	66
C.25	Averaging the upstream transect on the 27 <sup>th</sup> of April 2018. . . . .	66
C.26	Averaging the downstream transect on the 12 <sup>th</sup> of May 2018. . . . .	67
D.1	Hydraulic slope estimation from the ASTER GDEM data (Broekema, 2018). . . . .	69
D.2	(a) DEM in python with water surface and (b) DEM of only the floodplain, where the slope is estimated (Broekema, 2018). . . . .	69
D.3	DGPS measurements of the water surface elevation over a large distance. . . . .	70
D.4	DGPS measurements of the water surface over a short distance. . . . .	70
D.5	The RMSE for varying Manning's coefficients for both measurement days. . . . .	70
D.6	The RMSE for varying Manning's coefficients on April 27, 2018. . . . .	71
D.7	The RMSE for varying Manning's coefficients on May 12, 2018. . . . .	71
D.8	The discharge stage measurements of WARMA. . . . .	72
D.9	Determination of stage-discharge relationship WARMA measurements. . . . .	72
D.10	The discharge stage measurements and corresponding rating curve of WARMA. . . . .	72
D.11	The simulated stage discharge values for the HEC-RAS model, where $i_w=4e-4$ and $n=0.040$ . . . . .	73
D.12	Determination of stage-discharge relationship HEC-RAS model, where $i_w=4e-4$ and $n=0.040$ . . . . .	73
D.13	Comparison of rating curve WARMA with the HEC-RAS rating curve. . . . .	73
D.14	Determination of stage-discharge relationship HEC-RAS model, where $i_w=4e-4$ and $n=0.032$ . . . . .	74
D.15	Determination of stage-discharge relationship HEC-RAS model, where $i_w=4e-4$ and $n=0.048$ . . . . .	74

---

D.16 Rating curve sensitivity for changes in Manning's coefficient and constant hydraulic slope. . . . .	74
D.17 Determination of stage-discharge relationship HEC-RAS model, where $i_w=2e-4$ and $n=0.040$ . . . . .	75
D.18 Determination of stage-discharge relationship HEC-RAS model, where $i_w=8e-4$ and $n=0.040$ . . . . .	75
D.19 Rating curve sensitivity for changes in hydraulic slope and constant bed roughness. . . . .	75
D.20 Determination of stage-discharge relationship HEC-RAS model, where $i_w=2e-4$ for $n=0.028$ . . . . .	76
D.21 Determination of stage-discharge relationship HEC-RAS model, where $i_w=8e-4$ $n=0.058$ . . . . .	76
D.22 Rating curve sensitivity for changes in hydraulic slope with new optimum bed roughness values. . . . .	76
D.23 Determination of the 95% confidence interval of the WARMA rating curve. . . . .	77
D.24 Rating curve comparison with error bounds of the 95% confidence interval and WARMA measurements. . . . .	77
D.25 Rating curve comparison with error bounds and the sensitivity of a change in bed roughness. . . . .	77
E.1 Manning's roughness values for main channel and flood plain (Chow, 1959). . . . .	79



# List of Tables

4.1	Specifications of the DJI Phantom 4 aircraft and camera. . . . .	17
6.1	The different hydraulic slope estimations. . . . .	37
6.2	The rating curve coefficients for the WARMA stage-discharge relation. . . . .	39
6.3	The rating curve coefficients for the HEC-RAS stage-discharge relation. . . . .	41
A.1	Variables for both backwater estimations. . . . .	53
A.2	Variables for the first order approximation. . . . .	53
A.3	Variables for the empirical fit to Bresse. . . . .	53
B.1	GCP errors for X, Y and Z. . . . .	56
C.1	Discharge summary table of the ADCP measurements on the 27 <sup>th</sup> of April 2018. . . . .	61
C.2	Discharge summary table of the ADCP measurements on the 12 <sup>th</sup> of May 2018. . . . .	61
E.1	Parameter values for plain Manning calculation. . . . .	80



# Introduction

## 1.1 General introduction

Many watersheds in the world are ungauged or poorly-gauged, which results in a lack of concurrent datasets and limited hydrological data (Pan and Nichols, 2013; Sivapalan et al., 2003). River discharge, the volumetric rate of water flow passing a cross section of a river, is an essential hydrological parameter for rainfall-runoff modelling, hydropower generation, flood prediction and many other hydrological applications (Pan et al., 2016; Petersen-Øverleir, 2005).

Directly measuring river discharge is often difficult, costly and time consuming. Rivers can be very dynamic and cross-sections change over time. Moreover, river channels can be irregular resulting in variable flow velocities or non-uniform flow. To measure the river discharge a transverse cross-section is often divided into sub-sections, where a number of flow velocities at different flow depths are determined. From those measurements a mean flow velocity is calculated per sub-section. The river discharge is obtained by taking the sum of all mean flow velocities multiplied by a sub-section's area. This method is known as the velocity-area method (Herschy, 2009; Mosley and McKerchar, 1992).

A more recent technique to measure the discharge is the Acoustic Doppler Current Profiler (ADCP) method, which is in principle based on the velocity-area method. The ADCP method uses a boat to traverse a cross-section and collects measurements of velocity and river depth. The water velocity is measured by using the Doppler principle and assigned to a given depth cell in the water column. The Doppler principle is based on the reflection of sound waves by a moving particle, which results in a frequency change of the sound waves detected by multiple beams underneath the ADCP. The beams located under a different angle can transmit and receive the sound signals. From this, a three-dimensional water velocity is obtained. The area is measured by tracking the river bed and the position of the boat (Gordon, 1989; Herschy, 2009). A disadvantage of the ADCP method are the costs for purchasing an ADCP, the prices start around 25,000 USD (Olivier Hoes, personal communication, December 10, 2018)

To save time, labour and costs the river discharge is commonly estimated by a rating curve, relating water level to river discharge. A rating curve is constructed by fitting a curve through a number of measurements of water level and discharge. The river discharge is then determined by using the rating curve relation to transform water level measurements into discharge values.

Figure 1.1 shows a conceptual rating curve and the problem of extrapolation, which is applied for extreme flow conditions. Normally there are limited or no measurements under extreme conditions, due to flooding. This can result in inaccessibility of the area of interest or damaged equipment making it impossible to carry out measurements. Extrapolation is applied for extreme flow conditions, which can induce errors and uncertainties in the stage-discharge relationship.

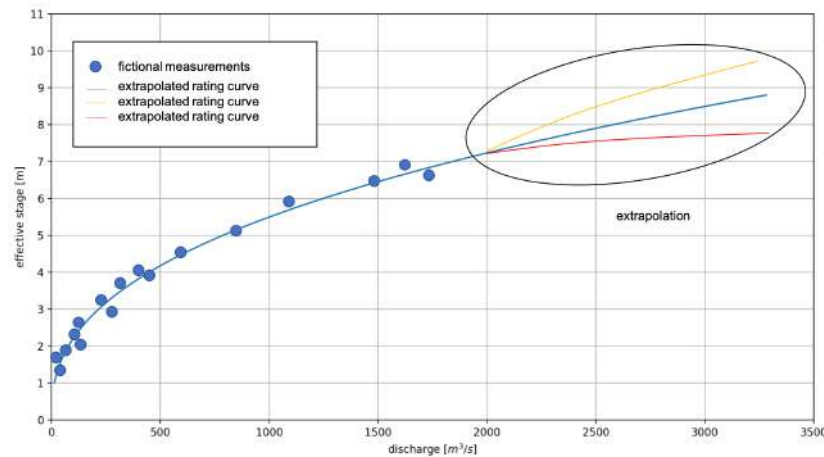


Figure 1.1 Fictional rating curve, where extrapolation is applied for high flows.

The last couple of decades there has been a tremendous development of remote sensing and other space- or airborne data sources, which have led to a shift from a data-poor to a data-rich environment (Bates, 2012; Yan et al., 2015). Scientist around the world have focussed on how to integrate those observations in hydrological or hydraulic modelling (Hrachowitz et al., 2013; Sivapalan et al., 2003; Yan et al., 2015). In general there is a gradual shift to more physically based models to evaluate the potential of different sources of remote sensing data, especially in the field of flood inundation modelling (Bates, 2012). There is even literature that shows methods to indirectly estimate the river discharge by using satellite images or remotely sensed cross-sectional inundation areas in combination with information about the river bathymetry (Gleason and Smith, 2014; Pan et al., 2016).

This research aims to improve the estimation of the hydraulic parameters bed roughness and hydraulic slope, and to develop a method for the construction of a more physically based rating curve. The rating curve is constructed by using a hydraulic model of a river reach, which contains geometric information of the river profile. The under water river profile is measured by using an ADCP and the remaining dry floodplains are mapped with an Unmanned Aerial Vehicle (UAV).

## 1.2 Problem statement

Direct measurement of river discharge is difficult, time consuming and costly. That is why many watersheds around the world are ungauged or poorly-gauged. In gauged areas where observations of water level and river discharge are available, a rating curve is often used to estimate the river discharge. Traditionally this rating curve is constructed using a power-law function and conventional regression, which can lead to inaccurate flow regimes in situations where the flow is unsteady and e.g. hysteresis occurs (Parodi and Ferraris, 2004; Petersen-Øverleir, 2006). Furthermore there are limited or no measurements under extreme conditions. In practice extrapolation is used to estimate the extremes, which induce uncertainties and errors in the constructed rating curve. Recently there has been a gradual shift to more physically based river rating, where the geometry of a river is included in the power-law expression (Strijker, 2017; Veldhuis, 2018). This seems to be a promising method to improve traditional river rating, but there is need for verification. Currently the biggest challenge in more physically based river rating lies in accurately estimating the hydraulic parameters bed roughness and hydraulic slope. In order to improve this method it is important to get more insight in accurately determine those parameters and be able to construct a more physically based rating curve.

## 1.3 Research aim and objectives

Almost all hydraulic and hydrological models use discharge data as input or output parameter. Rating curves are a tool to transfer measured water levels to discharges. Uncertainties and errors in rating curves lead to biased models. Rating curves therefore should contain more physically based parameters rather than primarily being based on curve fitting and extrapolation, as is the case for traditional river rating.

Furthermore to be able to improve a more physically based rating curve it is important to accurately estimate the parameters bed roughness and hydraulic slope. This research has therefore the following aim:

***Develop and evaluate a method to improve remote river rating by better estimating the hydraulic parameters bed roughness and hydraulic slope by combining innovations in the field of hydraulic modelling with UAV photogrammetry.***

In order to achieve the above mentioned research aim, the following research questions are formulated:

1. How can the hydraulic slope accurately be estimated?
2. How can a hydraulic model of a river reach be used to better estimate the bed roughness?
3. Can a hydraulic model be used to construct a more physically based rating curve, and how can it be compared to traditional river rating in terms of accuracy?

To answer the formulated research questions, the following research work plan is developed.

- Collect discharge, bathymetric and aerial data in the Luangwa river basin at a location upstream, in the middle and downstream of the river catchment.
- Find a way to combine geometrical information of the river profile from under- and above the water surface.
- Identify the possibility of excluding extrapolation in traditional rating curves by incorporating the geometric profile of a river reach.
- Construct a more physically based rating curve at one of the measured locations.
- Compare the constructed physically based rating curve with a traditional rating curve at one of the measured locations.
- Develop a 1D steady-state hydraulic model of a river reach at one of the measured locations.
- Based on the proceedings of the above objectives, identify the challenges and limitations on estimating the bed roughness and hydraulic slope by using a 1D steady-state hydraulic model in combination with a highly accurate DEM of the area of interest.

Figure 1.2 shows the steps of this study, which need to be taken in order to achieve the research goal and answer the formulated research questions.

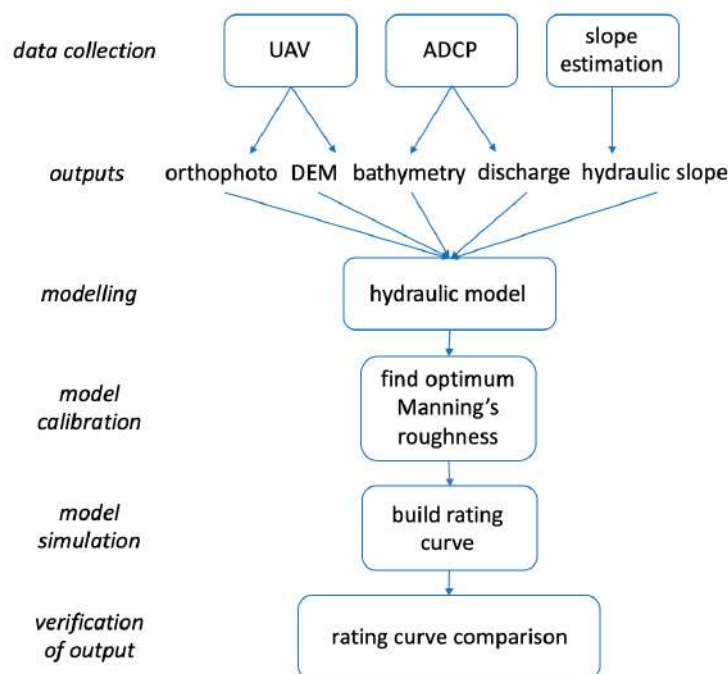


Figure 1.2 Flowchart of steps needed to achieve research aim.

## 1.4 Thesis layout

This master thesis is organised in seven chapters. The initial chapter provides a general introduction and outlines the importance of a more physically based river rating approach.

Chapter 2: *Theoretical background* provides a detailed description of the difference between traditional and more physically based river rating. Furthermore the concept of photogrammetry is explained. The chapter is concluded by additional information of the hydraulic model used in this research and the underlying equations.

Chapter 3: *Research area* describes the Luangwa catchment and the site selection procedure. An overview is given of the different measurement locations. One measurement site is in the end selected for building the hydraulic model. This site is used to compare a more physically based rating curve, produced by the hydraulic model with a traditional rating curve developed by the Zambian Water Resources Management Authority (WARMA).

Chapter 4: *Research equipment* provides a detailed description of the equipment used in this research.

Chapter 5: *Research methodology* describes the different stages of the used research methodology. The stages are step by step explained in detail.

Chapter 6: *Results & discussion* presents and discusses the results of this research. Such as the discharge and bathymetry measurements, terrain analysis, hydraulic slope estimation, finding optimum Manning's roughness and rating curve computation and comparison.

Chapter 7: *Conclusions & recommendations* lists the conclusions and recommendation for future work.

# 2

## Theoretical background

This chapter contains the theoretical background of this research. First of all the theory of traditional river rating will be explained and its limitations. Secondly a more physically based approach will be presented. Moreover, the theory of photogrammetry will be explained. Finally the chapter will be concluded by information about the hydraulic model used in this research and the underlying principles of the model will be explained.

### 2.1 Traditional river rating

#### 2.1.1 Theory

Traditional river rating is based on the stage-discharge relation. The stage-discharge relation expresses the relationship between the water level (also referred to as stage) and the river discharge. In order to obtain a continuous record of discharge data, the river stage is recorded and the discharge is computed from the stage-discharge relationship (Herschy, 2009; Luxemburg and Coenders, 2015). The most applied function to approximate the rating curve is the power-law function (Bjerklie et al., 2005; Leon et al., 2006; Petersen-Øverleir, 2005; Rantz, 1982). The power law function is given below:

$$Q = a(h - h_0)^b \quad (2.1)$$

where  $Q$  is the discharge [ $\text{m}^3/\text{s}$ ],  $h$  is the water stage [m],  $h_0$  represents the water level at zero flow [m] and  $a$  [ $\text{m}^{2-b}/\text{s}$ ] and  $b$  [-] are coefficients, which are determined through curve fitting.

To be able to establish a reliable and stable stage-discharge relationship, river properties need to be taken into account. Discharge measurements are carried out over a range of stages in order to come up with a reliable curve. The lower and medium stages are normally not too difficult to measure, because the area is still accessible and the river is not at its widest. The challenges are with the higher stages, where measurements are sometimes not possible due to flooding of the area or damaged equipment. Extrapolation is applied for higher stages, which can induce errors and uncertainties in the rating curve (Petersen-Øverleir, 2014).

If the river channel is stable over time, which means it does not shift course, relatively a few measurements are needed although in practice very few rivers have completely stable characteristics. The calibration procedure cannot be carried out once and for all, but needs to be repeated frequently in order to keep the stage-discharge relation reliable. In particular, surveys are required after floods, when the cross-sectional area or even the river course might have been changed.

To define the stage-discharge relation in sand bed rivers, several discharge measurements a month may be required because of the random shifts of a rivers geometry. A suitable location would be a stable site e.g. a rock bottom. A stable site where the stage-discharge relation does not change over time is called a permanent control. When a section does change over time it is referred to as a shifting control (DHV Consultants BV and Delft Hydraulics, 1999; Herschy, 2009; Luxemburg and Coenders, 2015).

Furthermore it is important that a stage-discharge relationship is as unique as possible. Therefore the selected site should not be under influence of any backwater effects. Ideally, a straight river section is selected

where the streamlines are parallel and the flow is relatively uniform. As a rule of thumb the river section is approximately straight a 100 m upstream and downstream from the gauging station (Luxemburg and Coenders, 2015; Rantz, 1982).

### 2.1.2 Limitations

The main shortcoming of the traditional method is that the rating curve is not physically based, but depends only on mathematical parameters. In other words it is based on curve fitting, which includes uncertainties and errors in the inter- and extrapolation and the form of the rating curve (Petersen-øverleir, 2014; Strijker, 2017). In general, sufficient measurements during low or moderate flows are available, but little during peak flow conditions. In practice extrapolation is required to cover the full range of flows, which can induce uncertainties and errors in the stage-discharge relation (DHV Consultants BV and Delft Hydraulics, 1999; Herschy, 2009; Strijker, 2017).

Strijker (2017) showed that the exponent  $b$  in equation 2.1 has a minor influence on the rating curve for regular flow conditions, while under high flow conditions it can have a significant influence. Limited observations in the extrapolation zone can result in an unreliable rating curve, this is an important limitation of traditional river rating. The coefficient  $a$  in the power law function includes the physical parameters bed roughness and hydraulic slope and is in practice normally used as a calibration parameter (DHV Consultants BV and Delft Hydraulics, 1999; Strijker, 2017; Veldhuis, 2018).

Another limitation of the traditional method is that the stage-discharge relation has a limited validity in time. Therefore the rating curve needs calibration as frequently as required by the rate of change in the stage-discharge relation (Luxemburg and Coenders, 2015). Factors that can change the relationship between water stage and discharge are (Herschy, 2009; Rantz, 1982):

- Degradation or aggradation of the river bed.
- Cross-sectional changes caused by growth and decay of aquatic weeds.
- Cross-sectional and river course changes after floods.
- Over-bank flow or spilling and ponding in areas adjoining the stream channel.

The rate of change in the stage-discharge relation strongly depends on the dynamic character of the river and the river morphology. Sand-bed rivers for example require more frequent calibration.

## 2.2 Physically based river rating

More physically based river rating is based on capturing the river geometry in the power-law expression. The flow in a river is a function of the river geometry, the river slope and the bed roughness. The most commonly used equations are the Chézy and the Manning(-Strickler) formulas. They are based on steady and uniform flow, also referred to as normal flow (Chow, 1959). The equations are derived from the 1D Saint Venant or shallow water equations, under the assumption that the resistance force balances the downstream component of the gravitational force (Ankum, 2002; Battjes and Labeur, 2014). The shallow water equations can be divided in the continuity equation and the momentum equation. The continuity equation, without lateral inflow can be described by the following equation:

$$\underbrace{\frac{\partial A}{\partial t}}_{\text{storage}} + \underbrace{\frac{\partial Q}{\partial x}}_{\text{net mass transport}} = 0 \quad \text{continuity equation} \quad (2.2)$$

$$\underbrace{\frac{\partial Q}{\partial t}}_{\text{local inertia}} + \underbrace{\frac{\partial}{\partial x} \left( \frac{Q^2}{A} \right)}_{\text{advective inertia}} + \underbrace{gA \frac{\partial h}{\partial x}}_{\text{gravity forcing}} + \underbrace{c_f \frac{Q^2}{Ad}}_{\text{resistance}} = 0 \quad \text{momentum equation} \quad (2.3)$$

If steady flow is considered, the  $\partial/\partial t$  term in the momentum equation drops. For small Froude numbers ( $Fr \ll 1$ ), which is the case for subcritical flow, the advective inertia can be neglected as well, which leads to a reduced momentum equation where the resistance force balances the gravitational force:

$$gA \frac{\partial h}{\partial x} = -c_f \frac{Q^2}{Ad} \quad (2.4)$$

When assuming a rectangular channel where  $A = Bd$  and the width  $B$  is constant the equation can be further reduced. Fill in the piezometric head  $h = z_b + d$  and  $Q = uA$  and the equation reduces to the following form:

$$gd\left(\frac{\partial d}{\partial x} + \frac{\partial z_b}{\partial x}\right) = -c_f u^2 \quad (2.5)$$

If the flow is uniform, which means that the flow is spatially constant the water depth does not change in longitudinal direction. This drops the  $\partial d/\partial x$  term in the reduced momentum equation. Fill in the bed slope  $i_b = \partial z_b/\partial x$  and the dimensionless friction coefficient  $c_f = g/C^2$  and after rearranging some terms the Chézy equation is obtained:

$$u = C\sqrt{di_b} \quad \text{or} \quad Q = AC\sqrt{di_b} \quad (2.6)$$

The Manning's formula can be obtained from the Chézy equation by filling in  $C = R^{(1/6)}/n$  and  $R \approx d$ , which is valid for rectangular channels where the width is much larger than the depth. Under uniform flow conditions  $i_b = i_w$ , which results in the following expression:

$$u = \frac{R^{1/6}}{n} \sqrt{Ri_w} \quad \text{or} \quad Q = n^{-1} \sqrt{i_w} AR^{2/3} \quad (2.7)$$

where  $Q$  is the discharge [ $\text{m}^3/\text{s}$ ],  $n$  is the Manning roughness coefficient [ $\text{s}/\text{m}^{1/3}$ ],  $i_w$  is the hydraulic slope or friction slope [ $\text{m}/\text{m}$ ],  $A$  is the cross-sectional area [ $\text{m}^2$ ] and  $R$  is the hydraulic radius [ $\text{m}$ ], which is the ratio of the cross-sectional area to its wetted perimeter. The hydraulic radius is a function of the water level  $h$  and is expressed by the following equation (Chow, 1959):

$$R = \frac{A}{P} = f(h) \quad (2.8)$$

where  $P$  is the wetted perimeter [ $\text{m}$ ].

The main difference between Chézy and Manning is the presents of the water depth in Chézy's roughness coefficient, while the Manning's roughness value is independent of the water depth (Manning, 1891). In this research the Manning equation is used, while this is also used by the hydraulic model. Furthermore the Manning's equation is simple and many years of experience have shown that it produces reliable results, under the assumption of steady and uniform flow (Hersch, 2009).

The Manning's equation can be rewritten in the same form as the power-law function:

$$Q = \underbrace{n^{-1} \sqrt{i}}_{a_1} \underbrace{AR^{2/3}}_{\underbrace{a_2(h-h_0)^b}_C} \quad (2.9)$$

where the first part  $a_1$  includes the bed roughness and the hydraulic slope, and the second part  $C$  represents the geometry of a river also referred to as the conveyance.

The conveyance term  $C$  [ $\text{m}^{8/3}$ ] in this research is defined as  $a_2(h-h_0)^b$ , and should not be mistaken with the also commonly used conveyance term  $n^{-1}AR^{2/3}$  that includes the bed roughness, for example used in the hydraulic model HEC-RAS (Brunner, 2016a) or lecture notes of the course river engineering at TU Delft (Vriend et al., 2011). The conveyance of the river  $C$  can completely be described by the geometry of a river section. The geometry of a river can be measured in the field. This can be done by aerial photography for the floodplains and by means of an ADCP for the part of the river under water. In this research both techniques are used, more information about this will follow in chapter research methodology.

Due to the fact that the conveyance part of the Manning's equation can be measured in the field, the only coefficient, which needs to be determined is  $a_1$ . As mentioned before coefficient  $a_1$  consists of the physical parameters bed roughness and hydraulic slope. Especially the bed roughness is considered to be difficult to determine and one could take a different roughness value for the main channel than e.g. the floodplain. However, Chow (1959) showed that a uniform Manning's coefficient can be used for the combined river profile of

main channel and floodplain due to parameter compensation. Floodplains normally contain more vegetation and usually therefore have a higher roughness value than the main channel, but this can be compensated by the decrease in roughness caused by a higher water level. The most common methods to determine the bed roughness are: selecting  $n$  from a table with qualitative descriptions of the channel characteristics, selecting it from photographs, which have typical roughness values, or estimate it by means of empirical relations, where the roughness is linked to the hydraulic variables (Chow, 1959; Wu and Wang, 1999). In practice however, the bed roughness is often used as a calibration parameter.

## 2.3 Aerial photography and photogrammetry

### 2.3.1 Photogrammetry

(Stereo-) photogrammetry is the science of making measurements from photographs (Walford, 2017). This research makes use of aerial photography, where air photos are taken from an Unmanned Aerial Vehicle (UAV) using a highly-accurate camera. Overlapping photographs are used to identify common points on each image (Government of Canada, 2016; Pix4D, 2018c). A line of sight can be constructed, from the camera location to the point of interest. It is the intersection of those lines that determine the three dimensional location ( $x, y, z$ ) of a particular point (Balogh and Kiss, 2014; Corrigan, 2017). This technique is called "structure from motion" and is used to create a 3D surface model and a highly-accurate digital elevation model (DEM). The DEM will be used to map the height differences of the floodplains of a river section. Figure 2.1 shows the principle of photogrammetry and a range of the required front- and side overlap.

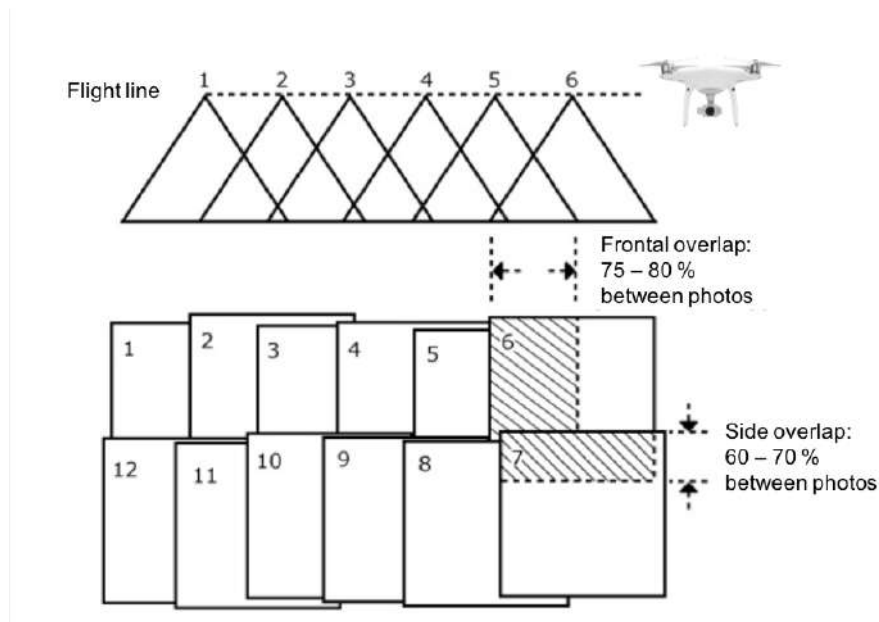


Figure 2.1 The principle of photogrammetry, a schematic representation including the required overlap (Government of Canada, 2016).

### 2.3.2 Aerial photography

The accuracy of aerial photography is largely dependent on the quality of the images captured. In order to collect a high quality image dataset the following factors need to be taken into account:

1. Weather conditions
2. Area size
3. Flight speed
4. Flight altitude
5. Maximum flight time
6. Ground Sampling Distance
7. Camera settings

First of all it is important to check the weather conditions when going into the field. The DJI Phantom 4 is not waterproof and can therefore only be used under dry weather conditions (DJI, 2017). Even if the drone would have been waterproof the rain will reduce the quality of the captured images. Therefore aerial photography needs to be taken in good weather with good light and visibility. Overcast conditions with high clouds are ideal for flying, while too much sunlight can cause over-exposure or unwanted shadows (Bridle, 2007).

The following characteristics mainly determine the quality of the image dataset: visible detail of the image, amount of incoming light and the overlap of images. Dependent on the application it is important to capture as much detail in one picture as possible. The Ground Sampling Distance (GSD) expresses the distance between two consecutive pixel centres measured on the ground (DroneDeploy, 2017a; Pix4D, 2018a). The bigger the value of the GSD, the lower the spatial resolution of the image and the less visible details are captured. Figure 2.2 (a) shows a schematic representation of the GSD.

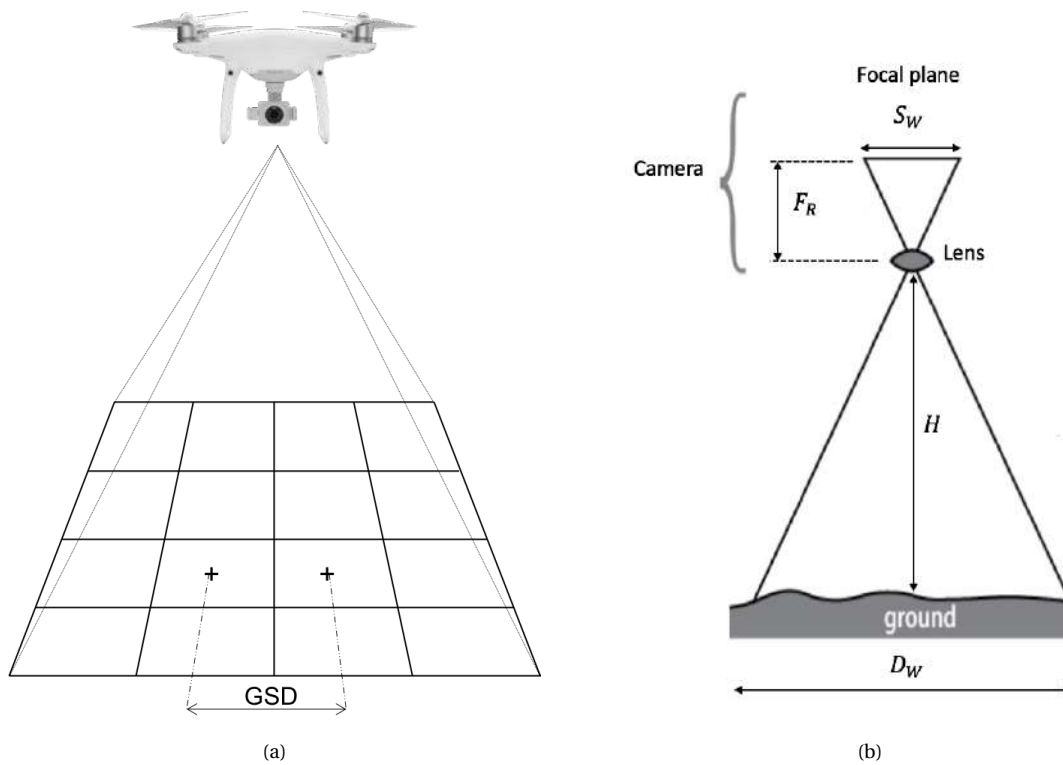


Figure 2.2 (a) Schematic definition of the Ground Sampling Distance. (b) Basic concepts of aerial photography (Government of Canada, 2016).

The GSD distance can be calculated by the following formula (Pix4D, 2018d)

$$GSD = \frac{S_w \cdot H \cdot 100}{F_r \cdot I_{mW}} \quad (2.10)$$

where  $S_w$  is the sensor width of the camera [mm],  $H$  is the flight altitude [m],  $F_r$  is the focal length of the camera [mm] and  $I_{mW}$  is the image width [pixels].

Figure 2.2 (b) shows some basic principles of aerial photography (Government of Canada, 2016). The distances  $D_W$  and  $D_H$  can be calculated by the following expressions (Pix4D, 2018d)

$$D_W = \frac{GSD \cdot I_{mW}}{100} \quad D_H = \frac{GSD \cdot I_{mH}}{100} \quad (2.11)$$

where  $D_W$  is the width of a single image footprint on the ground [m],  $D_H$  is the height of a single image footprint on the ground [m] and  $I_{mH}$  is the image height [pixels].

The blurriness of a picture depends on the Ground Sampling Distance (GSD) with respect to the flight speed. The flight speed is determined by the maximum flight time, the required GSD and the size of the research area. With a higher flight speed it is possible to map a larger area, however if the flight speed is too high the GSD can become very large, which results in a blurry image dataset. It therefore depends on the application which GSD is acceptable.

The size of the area of interest determines which flight altitude is reasonable. If the flight altitude is chosen the GSD for a flight can be calculated, while the GSD is determined by the flight altitude and the camera specifications (Pix4D, 2018b). Once the GSD is known the flight speed can be chosen based on the maximum flight time of the UAV battery, the required GSD and the size of the research area.

The amount of incoming light is also an important parameter for aerial photography. Lighting can be influenced by the shutter speed, ISO and aperture. The shutter speed is the speed at which the camera shutter opens and closes. A lower shutter speed results in a brighter image. ISO is in very basic terms a camera setting which can darken or brighten an image. The higher the ISO number the brighter the image. ISO is a good tool to help capture images in dark environments. However, raising your ISO has consequences. A photo taken at a too high ISO will show a lot of noise. Brightening a photo is therefore always a trade-off (Mansurov, 2018b). Aperture is an important variable in photography because it affects many different variables of an image. It can add dimension to images by blurring the background and can alter the exposure to light making the images brighter or darker. Aperture is a hole within in the lens of your camera, through which light can travel into the body of the camera. Aperture is basically the iris of the camera and can be shrunk or enlarged, allowing respectively less or more light to reach the camera body (Mansurov, 2018a).

Finally in aerial photography it is important to have front- and side overlap between images, as explained in subsection 2.3.1 (Government of Canada, 2016; Pix4D, 2018c). The overlap is needed for the post-processing software so it can reconstruct a 3D surface model or/and a Digital Elevation Model (DEM).

## 2.4 Hydraulic modelling

This research uses the hydraulic modelling software HEC-RAS for steady flow analysis. The HEC-RAS model was developed by the Hydrologic Engineering Center of the US Army Corps of Engineers. The model is widely applied and used for steady flow simulation, unsteady flow simulation, sediment transport computations and water quality analysis. In this research only one-dimensional steady flow is simulated (Brunner, 2016b).

In the steady state flow analysis the HEC-RAS model solves the energy equation for open channel flow (Brunner, 2016a), which is a simplification of the Bernoulli equation. The Bernoulli equation takes the elevation head, pressure head and velocity head into account. However, for open channels it is assumed that changes in the atmospheric pressure are negligible, which reduces the Bernoulli equation to the following form:

$$H = z_b + d + \frac{u^2}{2g} \quad (2.12)$$

where  $H$  is the energy head [m],  $z_b$  is the bottom elevation [m],  $d$  is the water depth [m] and  $u^2/2g$  is the velocity head [m].

HEC-RAS solves the energy equation. It calculates water surface profiles from one cross-section to another by means of an iterative procedure called the standard step method (Henderson, 1966). The energy equation can be expressed as follows:

$$z_{b1} + d_1 + \frac{a_1 u_1^2}{2g} + H_e = z_{b2} + d_2 + \frac{a_2 u_2^2}{2g} \quad (2.13)$$

where  $z_{b1}$  and  $z_{b2}$  are the main channel elevations [m],  $d_1$  and  $d_2$  are the water depths in [m],  $u_1$  and  $u_2$  are the averaged cross-sectional velocities [m/s],  $a_1$  and  $a_2$  are the velocity weighting coefficients of the sections one and two,  $g$  is the gravitational acceleration [m/s<sup>2</sup>] and  $H_e$  is the energy head loss from cross-section one to cross-section two [m].

Figure 2.3 shows the longitudinal profile of a river reach and the terms of the energy equation. Also the bed slope  $i_b$  [m/m] and the energy slope  $i_w$  [m/m] are indicated. Finally the piezometric head or stage  $h$  [m] is given, which is a measurement of a water pressure above a geodetic datum.

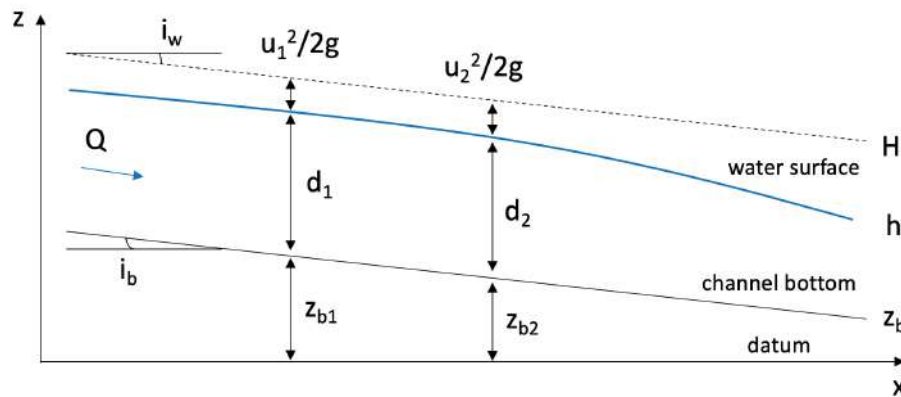


Figure 2.3 Longitudinal profile of a river reach, with variables of the energy equation.

The energy head loss between cross-sections consists of friction losses, and contraction or expansion losses and is given by the following expression (Brunner, 2016b).

$$H_e = L \bar{i}_w + C_{loss} \left| \frac{a_2 u_2^2}{2g} - \frac{a_1 u_1^2}{2g} \right| \quad (2.14)$$

where  $L$  [m] is the discharge weighted reach length,  $i_w$  is the friction slope [m/m] and  $C_{loss}$  [-] is the expansion or contraction loss coefficient.

The discharge weighted reach length can be calculated by (Brunner, 2016b):

$$L = \frac{L_{lob}\bar{Q}_{lob} + L_{ch}\bar{Q}_{ch} + L_{rob}\bar{Q}_{rob}}{\bar{Q}_{lob} + \bar{Q}_{ch} + \bar{Q}_{rob}} \quad (2.15)$$

where  $L_{lob}$ ,  $L_{ch}$ ,  $L_{rob}$  [m] are the cross-section reach lengths for flow in respectively, the left overbank, main channel and right overbank.  $\bar{Q}_{lob}$ ,  $\bar{Q}_{ch}$ ,  $\bar{Q}_{rob}$  [m<sup>3</sup>/s] are the average flows between the sections for the left overbank, main channel and right overbank.

The standard step method numerically solves the backwater equation through an iterative procedure (Chow, 1959). The backwater equation is given by the following expression:

$$\frac{dd}{dx} = \frac{i_b - i_w}{1 - Fr^2} \quad (2.16)$$

The derivation of the backwater equation from the momentum balance and from the energy equation is provided in appendix A. The computation procedure of the standard step method consists of the following steps (Brunner, 2016b):

1. A water surface level is assumed at the upstream cross-section, in case of subcritical flow conditions.
2. Per section (left overbank, main channel and right overbank) the conveyance and roughness values are determined, based on the assumed water surface elevation.
3. Then the friction slope  $i_w$  is calculated and equation 2.14 is solved.
4. Once this is done the energy equation 2.13 can be solved for the new water surface level.
5. Compare the calculated value of the water surface level with the assumed level in step 1; repeat the steps until the values agree to the user-defined tolerance e.g. 0.003 m.

# 3

## Research area

### 3.1 The Luangwa river catchment

The Luangwa river originates in the Mafinga Hills in the North-Eastern part of Zambia close to the border with Tanzania and Malawi. The river has a length of approximately 850 km and flows in South-Western direction. The river drains into the Zambezi river, shaping a broad valley along its course. The naturally created river valley is known for its abundant wildlife and relatively unaltered surroundings (WARMA, 2016).

The Luangwa river can be considered as one of the biggest tributaries of the Zambezi river. The catchment area is approximately 160,000 km<sup>2</sup> and is the third largest basin in Zambia (The World Bank, 2010). Figure 3.1 shows a terrain analysis and the stream and tributaries of the Luangwa river.

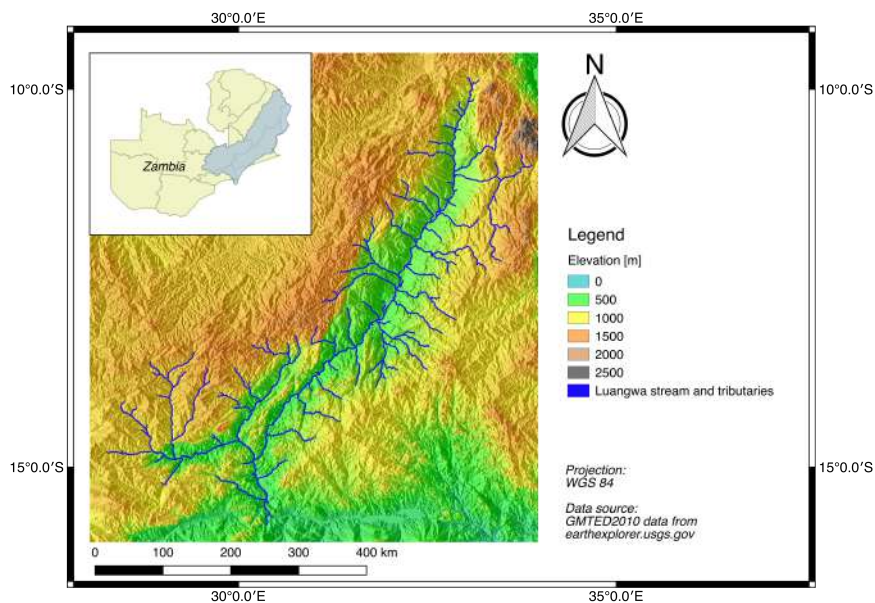


Figure 3.1 Terrain analysis and watershed delineation of the Luangwa river basin.

During the rainy season (December to March) the Luangwa generally floods whereas in the dry season the water level can considerably drop. The mean annual precipitation in the Luangwa basin is 1,021 mm resulting in a mean annual discharge of 518 m<sup>3</sup>/s (The World Bank, 2010).

### 3.2 Site selection

This research is focused on the Luangwa catchment. To get insight in the river basin it is divided into three different parts, respectively an upper, middle and downstream part. To select appropriate measurement locations the following selection criteria are considered:

- The measurement site needs to be accessible.
- The location has a large (dry) floodplain/sand plateau.
- The location should not be influenced by backwater effects.
- The river section is preferably straight.
- There should be a gauging station close-by.

First of all the river section of interest should be accessible, while a boat is needed for discharge measurements and a lot of equipment is used for other data collection. Secondly, a large sand plateau is preferred. This makes it possible to map the height differences by using Ground Control Points (GCPs) in combination with aerial photography.

Furthermore the measurement site should not be too close to a bridge or confluence or any other downstream activity which can cause backwater effects. Backwater effects influence the relationship between water level and discharge and therefore need to be avoided (DHV Consultants BV and Delft Hydraulics, 1999; Mueller et al., 2013). This should be taken into account, while selecting a suitable location.

Another criteria to be considered is the straightness of the river section. It is preferred to carry out discharge measurements in a straight river section, where streamlines are parallel to each other and the flow is relatively uniform. River bends are therefore not a suitable location because of spiral flow, eddies and excessive turbulence (Mueller et al., 2013; Rantz, 1982).

Finally, to be able to compare a constructed physics based rating curve with a traditional rating curve a gauging station should be close-by where historical data is available. Moreover the measurement site should be close to the gauging station to avoid tributary inflow and storage effects under conditions of rapidly changing stage (Rantz, 1982).

Taking into account the above mentioned selection criteria the following measurement locations are selected: Mulopwe village (upstream), Mfuwe (middle) and Great East Road bridge (downstream). Figure 3.2 shows the gauging station network of the Zambian Water Resources Management Authority (WARMA) and the selected gauging stations for this research. WARMA is responsible for preserving and protecting Zambia's ground and surface water resources and regulate the abstraction, allocation, use, development and management of water resources in a sustainable manner.

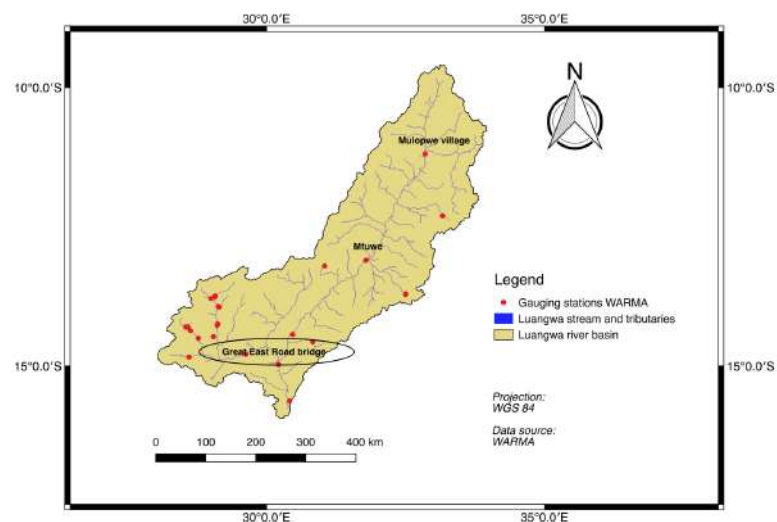


Figure 3.2 Gauging stations WARMA and measurement locations: Mulopwe village, Mfuwe and Great East Road bridge.

Mulopwe village is located approximately 80 km from the river source and lies in the upper part of the Luangwa catchment. It is extremely remote and difficult to reach. The river at this site is much smaller in terms of width and discharge, compared to the more downstream measurement locations. The gauging station was located a couple of hundred meters from the measurement site and the measurement site was only reachable by boat. Figure 3.3 shows an overview of the different measurement locations.



Figure 3.3 Overview of different measurement sites: (a) Mulopwe village (b) Mfuwe (c) Great East Road bridge site 1 and (d) Great East Road bridge site 2.

The measurement site in the middle of the Luangwa river basin is called Mfuwe. The river at this point forms a naturally barrier of one of the finest national parks of Africa, respectively South Luangwa National Park. The river is home to large populations of crocodiles and hippos, which makes it challenging for water management research. A couple of hundred meters downstream of the entrance of the South Luangwa National Park was a large (dry) floodplain, which was perfect for this research.

The downstream measurement sites are located near the Great East Road bridge. Site 1 is located downstream of the bridge and site 2 upstream of the bridge. Measurement site 1 is located a couple of hundred meters downstream of the bridge. This site has a large (dry) floodplain on the right riverbank and is relatively straight over a length of approximately 300 m. Measurement site 2 is located on the opposite side of the river then the gauging station of WARMA and therefore is a good location to compare differences. However, site 2 is relatively close to the bridge, which can have some negative influences on the rating curve due to backwater effects.

In the end only the downstream measurement location of the Great East Road bridge is selected for further analysis and area of interest for building a hydraulic model. This location is chosen because there are no structures, abstractions or confluences nearby, which can cause backwater effects. Furthermore the location is only a couple of kilometres from the gauging station of WARMA, which has the largest available discharge dataset. Also during fieldwork ADCP measurements are carried out at two different dates, which is an advantage for calibration of the hydraulic model. Because of the above mentioned reasons this location is the most suitable location for building a hydraulic model and in the end rating curve comparison. Figure 3.4 shows the chosen modelling location in more detail.



Figure 3.4 The locations of respectively, the WARMA gauging station, the Great East Road bridge and the chosen measurement site for hydraulic modelling.

If from this point onwards in the report is referred to the area of interest or measurement site the location, which is shown in figure 3.4 is considered.

# 4

## Research equipment

### 4.1 Unmanned Aerial Vehicle

For this study a DJI Phantom 4 aircraft has been used. The DJI Phantom 4 is the fourth generation of DJI's consumer aircraft's, insuring that DJI continues to be one of the leading manufacturers of aerial drones. The Phantom 4 is a small quadcopter that measures about 0.60 m from wing-to-wing and has a built-in camera in combination with a gimbal to maximize camera stability (Drone World, 2018). The gimbal is a stabilizing element, which makes sure that the camera even under extreme wind conditions can capture clear and stable images. Table 4.1 shows some specifications of the aircraft and the camera (DJI, 2017; 2018).

Table 4.1 Specifications of the DJI Phantom 4 aircraft and camera.

<b>Specifications DJI phantom 4</b>	
<b>aircraft</b>	
weight (including battery and propellers)	1380 g
maximum speed	20 m/s
range	± 5 km
battery type	LiPo 4S 5350 mAh
battery voltage	15.2
<b>camera</b>	
effective pixels	12.4 M
focal length	3.61 mm
sensor size	6.17x4.55 mm
image size (pixels)	4000x3000

The Phantom 4 can be controlled by several mobile applications in combination with the remote controller of DJI. There are applications, which are able to pre-program e.g. a flight path, aircraft speed, camera tilt, required overlap and other functions. For this study the following applications have been used: Dronedeploy, Pix4Dcapture and Litchi. Every application has his on advantage, that is why it is depended on local conditions which application was used. Figure 4.1 presents examples of way-point missions in Dronedeploy and Litchi.



Figure 4.1 Examples of different pre-programmed flights in the applications: (a) Dronedeploy and (b) Litchi.

## 4.2 Ground Control Points

Ground Control Points (GCPs) are characteristic points on the ground with known coordinates (DroneDeploy, 2017b; 2018; Pix4D, 2018e). Their coordinates have been measured by surveying equipment e.g. a differential GPS. The GCPs used in this research are squared and have the dimensions 0.40x0.40 m. The markers are made out of plastic and have a black and white checker pattern. The material is ideal for outdoor conditions, while it is water resistant and easy to clean.



Figure 4.2 Ground Control Points at measurement locations: (a) the measurement location and (b) Mulopwe village.

## 4.3 Differential Global Positioning System

The Global Positioning System (GPS), is one of the most successful satellite systems to date. GPS works with an one way radio ranging system, which provides information about real-time position and a very accurate time reference. The information provided about Positioning, Navigation and Timing (PNT) is useful for multiple commercial purposes, the army and civil society in general. The concept of GPS positioning is based on lateration. This means that the GPS receiver can compute its position, by measuring its distance to a number of GPS satellites, and using the known positions of those satellites to calculate its position. In order to estimate the three positional coordinates and the time offset of the receiver at least 4 satellites need to be tracked. The quality of the GPS position is largely dependent on the number of available satellites and their orientation with respect to the receiver. A good position accuracy can be received when enough satellites are tracked on all sides of the receiver. The accuracy of standalone positioning lies in the order of magnitude 5-15 meters, under reasonable satellite visibility (Bakker, 2017).

Differential GPS (DGPS) is a technique to improve the GPS Standard Positioning Service accuracy. Instead of using one receiver DGPS combines data from a roving receiver with data from a (reference) base station. The position of the rover is computed relative with respect to the base station (Trimble Navigation Limited, 2013). Several errors, such as the atmospheric errors are almost identical for both receivers, in close proximity to each other. In relative positioning those errors cancel out, which significantly improves the accuracy (Bakker, 2017). This research uses Real Time Kinematic (RTK) positioning, where data processing already occurs in the field as data is logged, providing immediate centimetre level accuracy (Trimble Navigation Limited, 2003; Wanninger, 2008). A RTK survey requires a GPS receiver as base station and at least one GPS receiver as a rover, both receivers have to (Trimble Navigation Limited, 2003):

- Observe and track carrier phase measurements. A carrier phase observable provides the exact number of wavelengths from the antenna phase center to the satellite.
- Log data at common times and epochs, where epochs is a continuous time system for all satellites.
- Track at least four common satellites in space at each location.
- Observe during good PDOP, which is a measure for the geometrical balance of satellites above the measuring position.

A good RTK survey requires the following (Trimble Navigation Limited, 2003):

- Initializing prior to data collection.
- Maintaining the lock to satellites while moving with the rover.
- Maintaining the lock to base station radio signal while moving with the rover.

RTK is ideal for collecting GPS measurements for the GCPs, while it is a fast and very accurate (centimetre accuracy) method. Figure 4.3 shows the set-up of the Differential GPS with a base and rover receiver. The base is connected to an external antenna, for improved tracking and communication.



Figure 4.3 Set-up of a Differential GPS with a base- and rover receiver and an external antenna.

## 4.4 Acoustic Doppler Current Profiler

An Acoustic Doppler Current Profiler (ADCP) has been used to map the bathymetry and estimate the discharge of the Luangwa river. As mentioned in the introduction an ADCP makes use of the Doppler principle where the sound wave reflections of a moving particle are detected by a frequency change of the sound. From this frequency change a three-dimensional water velocity is obtained, integrated over the transverse cross-section this gives the river discharge. According to the manufacturer the accuracy of the water velocity profiling is in order of magnitude mm/s, but this is obtained during ideal test conditions (Teledyne Marine, 2014). However in practice it is likely that the accuracy is lower.

For this study a Teledyne RiverRay ADCP of the Water Resources Management Centre of the University of Zambia (UNZA) has been used. The fieldwork has been conducted in the months April, May and the beginning of June 2018. In the first months a motorised boat of the Water Resources Management Authority (WARMA) has been used to survey the river with the ADCP. At the end of the fieldwork the water level unfortunately dropped so drastically that it was too low to use the motorised boat. With help of a local fisherman and its hand-crafted canoe it was possible to get some ADCP measurements. Figure 4.4 shows an example of an ADCP measurement with a motorised boat and one with a hand-crafted canoe.



(a)



(b)

Figure 4.4 ADCP measurements at (a) the measurement location and (b) Mfuwe.

#### 4.5 Garden hose with transparent tubes

The garden hose method for estimating the hydraulic slope uses a garden hose with transparent tubes. One transparent tube is connected to the garden hose and the other one is hanging loose. Both tubes are nailed to a wooden plank, whereas on top a small levelling instrument is connected. Figure 4.5 shows an impression of the garden hose with the transparent tubes being used in the field. The garden hose method will be explained in more detail in chapter research methodology subsection 5.2.3.



(a)



(b)

Figure 4.5 (a) the wooden plank with transparent tubes and (b) the garden hose method being applied in the field.

# 5

## Research methodology

This chapter discusses the research methodology. First the methodology is simplified in a flow chart and the different steps are explained. The sections explain the different steps of the research methodology in more detail.

### 5.1 Simplification research methodology

This research can be simplified in six different steps. Figure 5.1 presents a flow chart containing these steps. The first step is the literature review, where the knowledge gap is identified and the research aim and questions are formulated. The second step contains the data collection phase. In this step fieldwork is conducted and data is collected. First of all discharge measurements and bathymetry measurements are carried out by using an ADCP. Secondly the river profile above the water surface is mapped, by taking aerial photographs with an UAV. Finally the hydraulic slope data is collected by making use of different collection methods.

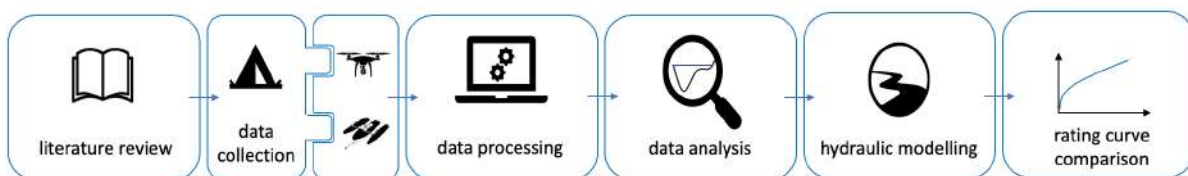


Figure 5.1 A simplification of the six steps carried out in the research methodology.

The third step of the research methodology is the data processing stage. In this step the discharge and bathymetry measurements are processed by the ADCP software called WinRiver II and replotted in Python. The aerial photographs of the UAV are processed with photogrammetry software. In this research the software programs Agisoft PhotoScan and Pix4D Mapper are compared. The fourth stage is the data analysis step where the outputs, the ADCP transects and the DEM are analysed. The fifth step includes the modelling stage of the area of interest, where the hydraulic model is build with the modelling tool HEC-RAS. The river geometry, under- and above the water surface are included in the model. The model is calibrated on the carried out discharge and stage measurements and an optimum value for the Manning's roughness  $n$  is found. With this information a rating curve is constructed, which will be compared in the sixth and final step of the research methodology. In this step a traditional rating curve, the rating curve of WARMA is compared with a more physically based rating curve from the hydraulic model.

## 5.2 Data collection

The data collection can be divided into three categories; the wet river profile, the dry river profile and the data collection for estimating the hydraulic slope. The measurements can be carried out in random order. Figure 5.2 shows the different categories of the data collection stage. The categories are explained in more detail in the following subsections.



Figure 5.2 The data collection categories; the wet river profile, the dry river profile and the hydraulic slope estimation.

One of the data collection activities contains the ADCP measurements, where the river discharge and bathymetry (wet river profile) are measured. Figure 5.3 shows the definition of the river profile what is considered to be wet and dry. Basically the wet river profile is considered the area, which is measured by the ADCP and everything above the water surface is called the dry river profile.

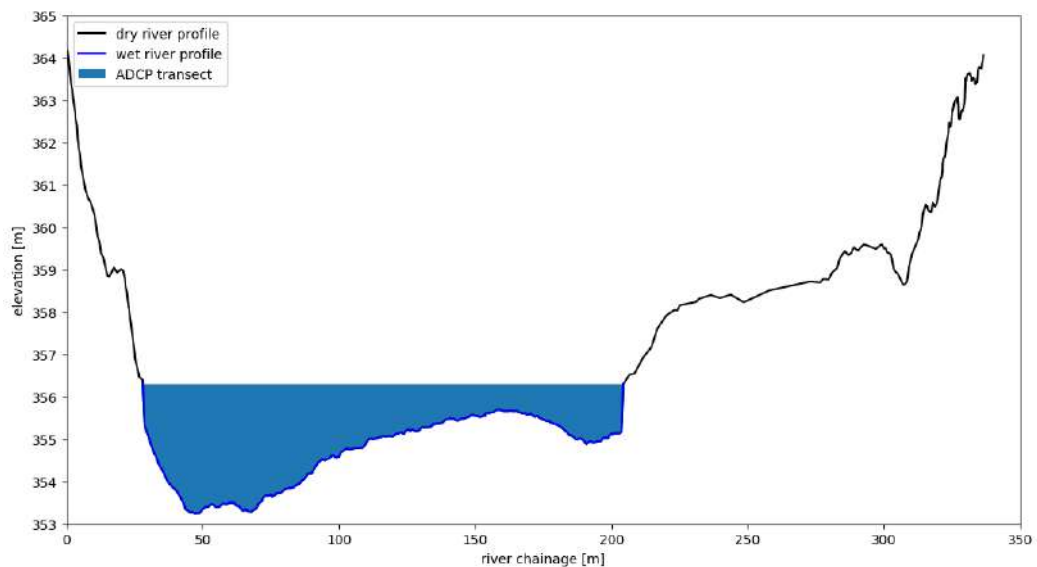


Figure 5.3 The river profile divided into a wet and dry part, based on the ADCP measurement carried out on May 12, 2018.

The dry river profile is collected by making use of an UAV equipped with a highly accurate camera. The UAV is used to capture aerial photographs in order to map the height differences of the dry floodplain. Finally data is collected to estimate the hydraulic slope, the different methods used are explained in more detail in subsection 5.2.3.

### 5.2.1 Wet river profile collection

This research is, in the end concentrated on one measurement location, the downstream location of the Great East Road bridge, as explained in chapter research area, see figure 3.4 for the location. At this location two discharge and bathymetry measurement campaigns are carried out. Respectively on the 27<sup>th</sup> of April and the 12<sup>th</sup> of May 2018. Chosen is for three transects, an upstream, a middle and a downstream transect. Every transect is measured four times.

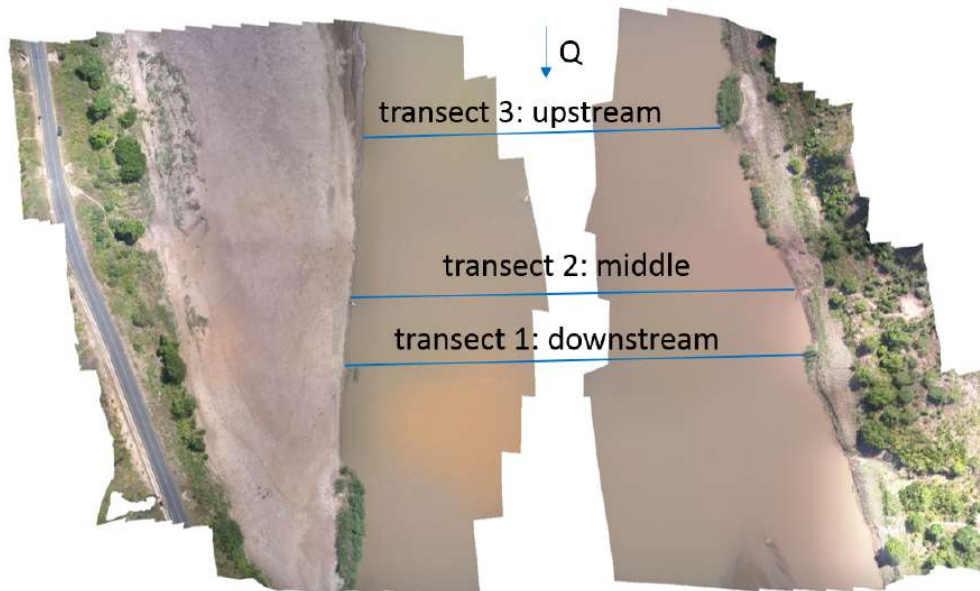


Figure 5.4 Transects ADCP measurements for downstream location of the Great East Road bridge.

### 5.2.2 Dry river profile collection

The dry river profile collection can be divided into two parts. The positioning of the GCPs and the collection of aerial photographs.

#### Positioning of Ground Control Points

The first part includes the surveying of the GCPs. In order to produce a georeferenced orthophoto and to obtain a DEM with centimetre accuracy level, GCPs are needed. These are control points within an image where the positions are known. GCPs have three main functions:

- Photographs can be georeferenced
- Improves the accuracy of the DEM
- Makes error estimation possible

The GCPs can be surveyed making it possible to reconstruct a scene in the "real world" by assigning the right orientation and world coordinates. They also improve the accuracy of output such as a DEM, by refining parameters and optimisation of variables. The final function of GCPs is that it allows the photogrammetry software to estimate errors between the taken photographs and the GCPs coordinates.

It is recommended to use between the 10-15 GCPs evenly distributed within the area of interest (Agisoft LLC, 2017; 2018). Make sure the GCPs cover the natural variation in elevation. Greater accuracy can be achieved by using more GCPs, however this is a trade off. Surveying the GCPs with a DGPS takes time and one could argue which accuracy is needed. In this research an accuracy level of centimetres is more than sufficient, while the measurements are combined with ADCP measurements, which are also in order of magnitude centimetre accuracy (Olivier Hoes, personal communication, December 12, 2018).

### Collection of aerial photographs

An UAV is used to collect aerial photographs. The accuracy of the photographs are largely dependent on the quality of the images captured. Therefore the factors described in chapter: Theoretical background subsection 2.3.2 needs to be taken into account. Furthermore a side- and front overlap needs to be determined and a flight plan can be pre-programmed using one of the available UAV applications. In this research Litchi, DroneDeploy and Pix4D are compared.

### 5.2.3 Estimation of the hydraulic slope

For estimation of the hydraulic slope data collection is needed. In case of uniform flow the bed slope equals the hydraulic slope (Henderson, 1966). The hydraulic slope and, under uniform flow conditions, the bed slope can be estimated by the following methods:

- Global DEM
- Local DEM (averaging dry river profile)
- Local DEM (conveyance method)
- The garden hose method
- DGPS measurements of water surface (short distance)
- DGPS measurements of water surface (large distance)

First of all the hydraulic slope can be calculated by using a global DEM of the area of interest. In this research the Advanced Spaceborne Thermal Emission and Reflection Radiometer (ASTER) Global Digital Elevation Model (GDEM) is used. ASTER GDEM data can be downloaded for free from the USGS Earth explorer website and has a spatial resolution of 30x30 m. The satellite data is loaded into QGIS and a polyline is drawn following the centreline of the river. This can be achieved by using a Google Earth plugin in QGIS. The polyline is drawn in such a way that the line covers roughly 10 kilometres upstream and 10 kilometres downstream of the area of interest, see also (Broekema, 2018; Veldhuis, 2018). The slope can be found by linear regression.

Secondly the hydraulic slope might be estimated by making use of the local DEM and focus on the elevation data of the dry river profile (Broekema, 2018). An important assumption in this method is that is assumed that the slope of the floodplain is equal to the slope of the river channel, which can only be assumed under the following conditions:

- The flow is uniform
- The characteristic length scale of the bed form should be much smaller than the river reach length (in longitudinal direction), which is investigated. This can be expressed as follows (Broekema, 2018)

$$\frac{\text{river reach length [m]}}{\text{characteristic bed form length [m]}} > 30 \quad (5.1)$$

It basically means that the river reach length needs to be long enough so that the characteristic bed form length is abundantly present to be averaged out.

- The DEM of the river reach should be long enough (order of magnitudes of kilometres in longitudinal direction), to avoid local effects of sedimentation.

To be able to determine the slope, the distance in longitudinal direction and elevation data are needed. Normally this is done for dry rivers (Veldhuis, 2018), but Broekema (2018) showed this for only the dry river profile, while there was still a considerable part of the river profile which was under water. The elevation data are averaged per column in transverse direction, to average out local effects, and are then plotted against the longitudinal distance. Linear regression is applied to the average floodplain column data and a slope is determined. More detailed information concerning this method can be found in the bachelor thesis of (Broekema, 2018).

The third method also uses the local DEM, but now makes use of the conveyance in longitudinal direction (Veldhuis, 2018). The method uses the relation between the conveyance and the effective stage. If the water surface slope would be equal to the bed slope, the conveyance  $C$  will remain constant in longitudinal direction, under the assumption that  $Q$ ,  $n$  and  $i$  are constant. Figure 5.5 shows this principle. If the water surface slope in downstream direction would be zero,  $C$  would increase in downstream direction as the water depth  $d$  would increase. Note that in this case uniform flow would not be valid any more.

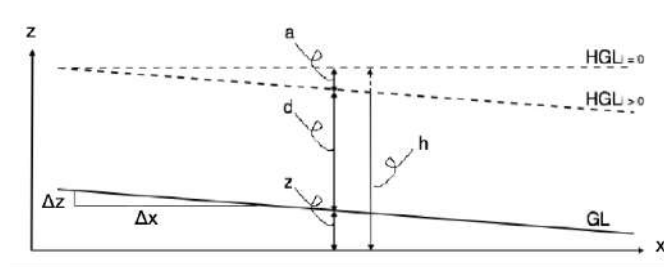


Figure 5.5 Slope determination area of interest, where GL = Ground level, HGL = Hydraulic Grade Line (Veldhuis, 2018).

To be able to determine the slope the variation of the conveyance is calculated in downstream direction. Instead of assuming a constant value for the water level (water surface slope of zero) a slope is enforced on the water surface. By iteration a slope can be found that results in a constant  $C$  over  $x$ , such that  $\Delta C/\Delta x = 0$ . More detailed information on the conveyance method can be found in the master thesis of (Veldhuis, 2018).

The fourth method is a practical method and good for insight, but not very accurate. This method uses a garden hose with a length of 20m and two transparent tubes see 4.5. One end is put under water at the upstream end and at the downstream end two transparent tubes are attached. Under uniform flow conditions, when the hydraulic slope equals the bed slope, the slope can be estimated by dividing the difference in bed elevation by the length of the garden hose. This is allowed while under uniform flow conditions the depth and velocity head in longitudinal direction are constant (Broekema, 2018; Vriend et al., 2011). Figure 5.6 shows the principle of the garden hose method.

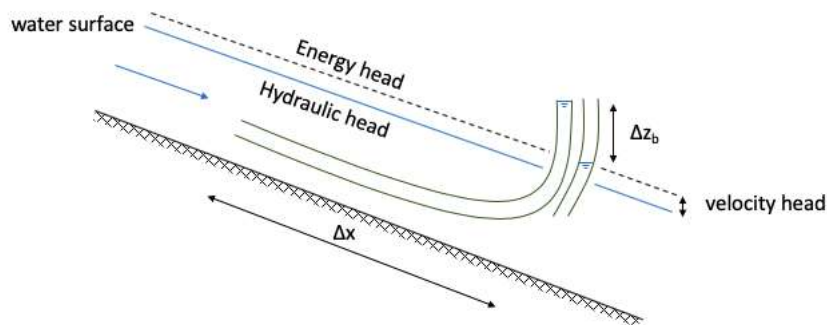


Figure 5.6 A schematic sketch of the garden hose method.

The difference in bed elevation corresponds in this situation with the water level difference in the transparent tubes. This difference is measured with a ruler. The biggest drawback of this method is that sometimes air bubbles make it difficult to measure the difference in the transparent tubes and that it is important to make sure the end of the garden hose is perpendicular to the flow to exclude the velocity head (order of magnitude 0.02m, when a velocity of 0.2 m/s is assumed). In practice this is difficult, which makes this method good for insight but not very accurate.

The final two methods for slope estimation uses a DGPS to measure the water surface elevation at two or more points along the river. One method uses a large distance between points and the other one short distances. Figure 5.7 shows where the DGPS measurements are taken.



Figure 5.7 DGPS measurements of the water surface level for a short and large distance.

The large distance DGPS measurements are preferred while the hydraulic slope is expected to be small, and on short distances can conflict with the measurement accuracy of the DGPS, which is in centimetre accuracy level. The centreline of the river is followed, in case of the large distance DGPS measurements to determine the longitudinal distance between DGPS measurements and the hydraulic slope is then calculated by dividing the difference in water surface elevation by the longitudinal distance of the river centreline. In case of the shoreline (short distance) measurements the difference in water surface elevation is divided by the longitudinal distance of the land-water boundary between the points.

## 5.3 Data processing

### 5.3.1 Wet river profile

For this research a Teledyne RiverRay ADCP is used to carry out discharge and bathymetry measurements. The data is processed by the Teledyne software called Winriver II. The data is exported and replotted in Python. Figure 5.8 shows an example of such a replotted profile.

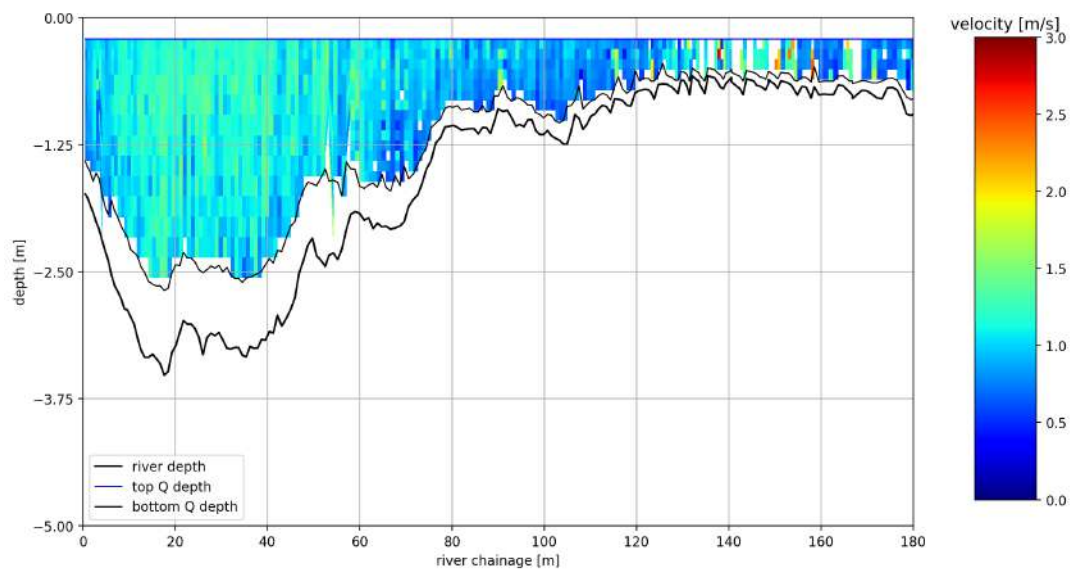


Figure 5.8 An example of a processed ADCP measurement at the area of interest on May 12, 2018.

### 5.3.2 Dry river profile

The dry river profile is surveyed by an UAV and the aerial photographs are processed by photogrammetry software. In the end only the Litchi flights are used in this research, while this flight contained raw images and the total Root Mean Squared Error (RMSE) of the GCPs where the smallest, see appendix B for the error estimations of the GCPs. In this research Pix4D Mapper and Agisoft Photoscan are used to come up with a DEM of the dry river profile. After comparison of both software's it is decided to only use Agisoft PhotoScan. This is because filtering out vegetation is easier and Agisoft can also process raw images, whereas in Pix4D this option is not available.

Generally the processing procedure of Agisoft PhotoScan includes four stages (Agisoft LLC, 2018). Figure 5.9 shows a schematic of these stages. The first stage is the the camera alignment stage. In this stage common points on photographs are identified and matched. This method is known as "structure from motion". Moreover, the camera positions of each picture are defined and the camera calibration parameters are refined. As a result of the first stage the sparse point cloud and a set of calibration parameters are formed.

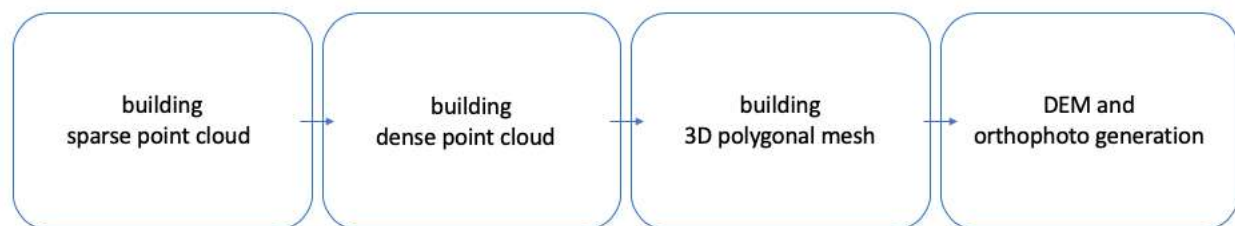


Figure 5.9 Processing procedure of aerial photographs in Agisoft PhotoScan.

The second stage is the generation of the dense point cloud. The dense point cloud is build by PhotoScan based on the estimated camera positions and the photographs themselves. There are several processing algorithms available in PhotoScan but in general these algorithms search systematically to identify best matches between pictures. This results in significantly more 3D points then for the sparse point cloud. The dense point cloud can be edited prior to export or proceeding to the next stage. The cloud is edited in case of an area with a lot of vegetation, where the vegetation can significantly influence the outcome of the DEM.

The third stage is building the 3D polygonal mesh. PhotoScan reconstructs a mesh representing an object surface, based on the dense point cloud. It may be necessary to edit the mesh. Correction tools are available in PhotoScan such as: decimating the mesh, removal of detached components, closing holes, smoothing and other tools. In this research decimation of the mesh and closing holes is used.

The fourth stage is the DEM and orthophoto generation stage. The Inverse Distance Weighting interpolation method is used to fill the gaps in the dense point cloud. The DEM can now be generated. The size can be set manually, where in this research is chosen to set the raster to a resolution of 10x10 cm. This with respect to the computational time and the wanted accuracy. Besides the DEM also the orthophoto can be generated.

## 5.4 Data analysis

### 5.4.1 Wet river profile

As explained in subsection 5.3.1 the ADCP measurements are processed by the WinRiver II software package. After processing the results are replotted and analysed in Python. This is done, while Python offers more flexibility for data analysis and manipulation. The purpose of the analysis of the ADCP measurements is to investigate the hydraulic behaviour of the different transects and to find out if they behave similar. If that is the case the position of where the transects are measured is of minor importance and it can be assumed that the transects taken on the 27<sup>th</sup> of April and 12<sup>th</sup> of May 2018 are more or less on the same positions. Furthermore if different transects behave hydraulically the same, it would not matter that much if rating curves are compared of exactly the same position. This is promising for this research, while the more physically based rating curve is constructed a couple of kilometres from the gauging station of WARMA.

First of all the bathymetry measurements are analysed. The depth profiles of a transect are plotted against the river chainage. A visual inspection is carried out to identify the outliers. To see if these outliers can be discarded the hydraulic behaviour of the transects is researched. In order to see the hydraulic behaviour of a transect an artificial range of water levels  $h$  is build. The range of  $h$  is from the minimum channel elevation up to the maximum water level measured in one transect. The following hydraulic parameters are plotted against this  $h$ : top width, cross-sectional area, perimeter, hydraulic radius and the conveyance.

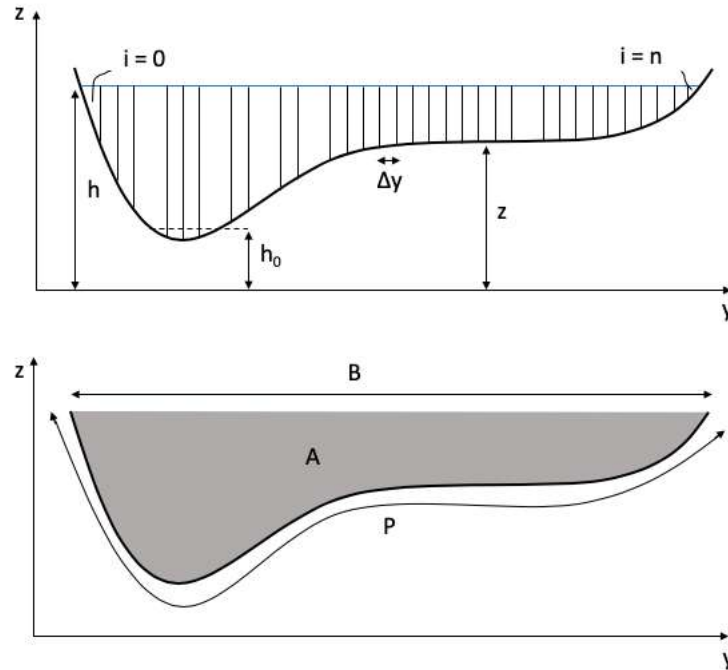


Figure 5.10 Hydraulic parameters definition of a transect.

$$A = \sum_{i=0}^n \frac{(h - z_i) + (h - z_{i+1})}{2} \Delta y \quad (5.2)$$

$$B = \sum_{i=0}^n \Delta y_i \quad (5.3)$$

$$P = \sum_{i=0}^n \sqrt{((h - z_i) - (h - z_{i+1}))^2 + \Delta y^2} \quad (5.4)$$

$$R = \frac{A}{P} \quad (5.5)$$

$$C = AR^{2/3} \quad (5.6)$$

Figure 5.10 shows how the hydraulic parameters are defined. Furthermore the mathematical definitions of the considered hydraulic parameters are given.  $h_0$  stands for the stage of zero flow. In this research it is assumed that  $h_0 = 0$ , while this is the case for the closest gauging station and the river cross-section at the gauging station and the area of interest show a similar shape.

### 5.4.2 Dry river profile

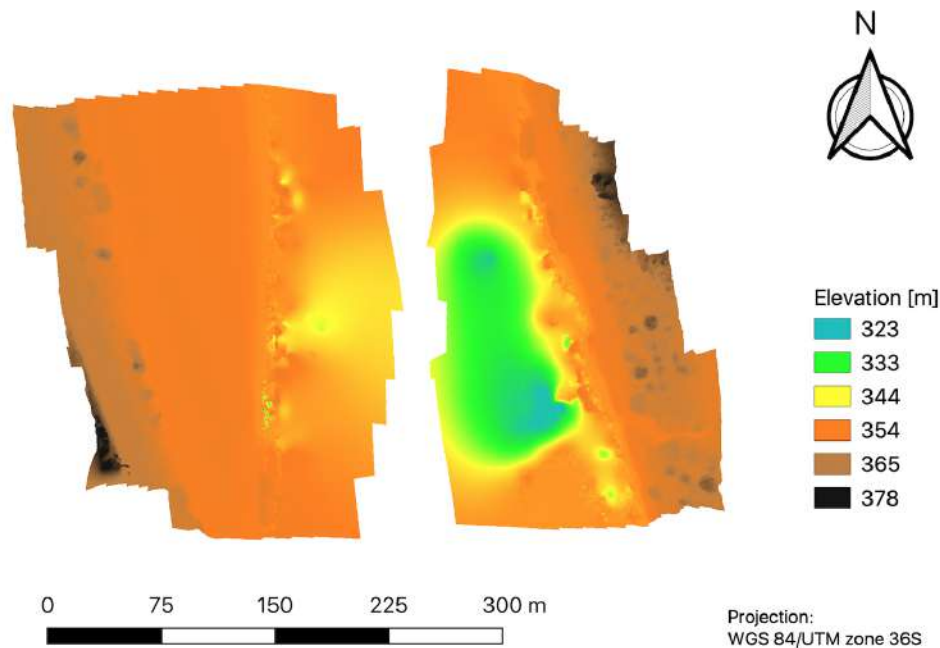


Figure 5.11 The DEM of the area of interest still containing vegetation and water.

## 5.5 Hydraulic modelling

### 5.5.1 General modelling approach

To construct a more physically based rating curve and to find an optimum value for the Manning's roughness  $n$  a hydraulic model, called HEC-RAS is used. The wet- and dry river profile measurements are combined into three cross-sections at the area of interest. Figure 5.12 shows the geometry of the model set-up.

The ADCP measurements are used to construct the under water profile and the DEM is used to construct the profile above the water surface, as is shown in figure 5.3. When setting up a hydraulic model it is important that the area of interest is out of the influence zone of any backwater effects, caused by disturbances downstream. Therefore backwater calculations are carried out, which can be found in appendix A. Appendix A derives the backwater equation from the 1D shallow water equations (Vriend et al., 2011). After the derivation the backwater lengths are calculated. The largest backwater length, approximately 11km is used in order to make sure the area of interest is not influenced by backwater effects. The downstream cross-section in figure 5.12 is copied and placed 11km downstream of the river model, under the assumption of a hydraulic slope.

A common method to obtain more cross-sections in HEC-RAS is to apply interpolation between the cross-sections. Interpolation is applied between the upstream and the middle, and the middle and the downstream cross-section. Cross-sections are generated every meter to smoothen the river's geometry.

In this study a 1D steady-state model is used, for rating curve comparison. Chosen is for steady-state because (Brunner, 2016c):

- The river system is not tidally influenced.
- There are no big tributaries, resulting in a minimised lateral inflow.
- No dynamic events such as a dambreak or floods are considered.

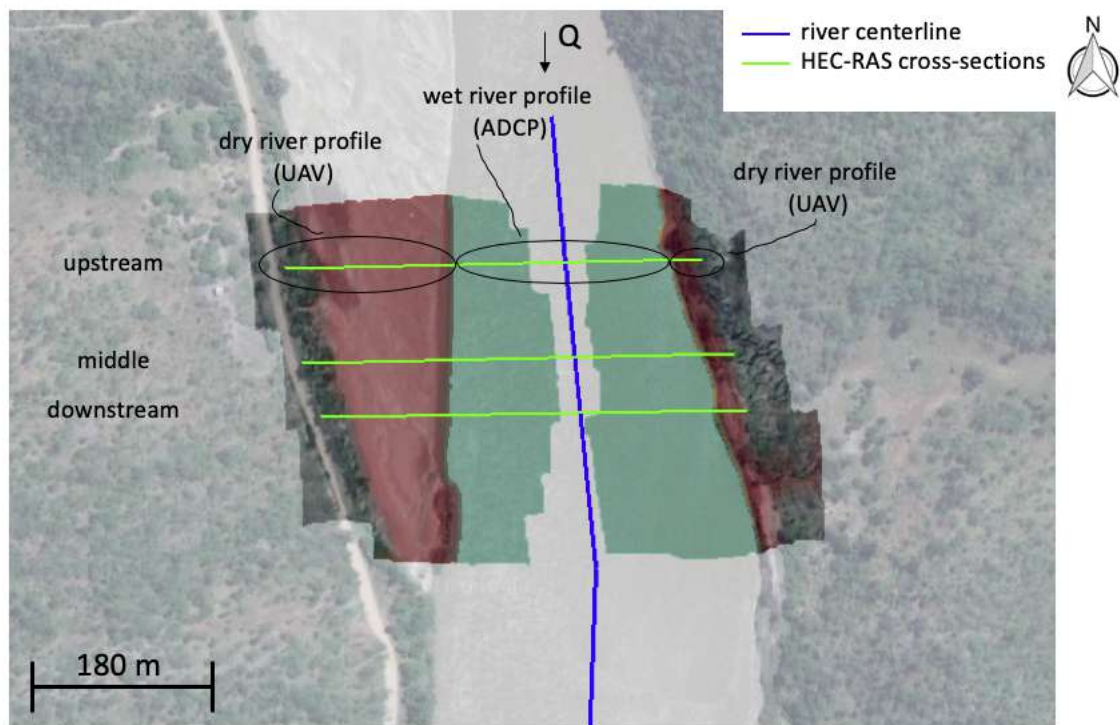


Figure 5.12 The set-up of the geometry of the HEC-RAS model.

Chosen is for 1D instead of 2D mainly for practical reasons. For example it is easier to construct the model geometry in HEC-RAS, because one could manually combine the wet- and the dry river profile in the geometric data editor. In 2D a mesh needs to be created of a merged HEC-RAS terrain, which would include the dry and wet profile measurements. However, the model did not merge the two terrains properly. If one would have measured in the dry season, perhaps the river would have been dry. In that case only UAV measurements would have been needed and the entire river geometry would be included in one terrain model. No merging is needed and it would have been easier to model in 2D.

Another option to model a 2D flow area in HEC-RAS is using a 1D model and connect it with a 2D flow area. Basically the 2D flow area is then connected as a lateral structure (Brunner, 2016b;c). However, this works under the assumption that the 2D flow area is lower than the edge between 1D/2D. In this case the floodplain has a lateral slope towards the river, which would not apply for the calculations in HEC-RAS.

For rating curve comparison a 2D model or a 1D model combined with a 2D flow area would be interesting, especially for intermediate discharges. In this case the floodplain starts to participate and while the area of interest is quiet flat a lot of energy will be dissipated. In theory therefore a rating curve build by a 1D model could be different, for the intermediate stage, than a 1D/2D or a 2D modelled rating curve.

In this research only a 1D steady-state HEC-RAS model is used for estimating an optimum bed roughness and in the end rating curve construction. Figure 5.13 shows the requirements and outputs for a 1D steady-state HEC-RAS model.

Besides geometric information the HEC-RAS model also needs steady flow data for carrying out a steady flow simulation. Part of this steady flow data is defining the boundary conditions, for upstream and downstream of the river model. In case of subcritical flow water level information needs to be provided at the downstream boundary and discharge information at the upstream boundary (Vriend et al., 2011). The normal depth assumption is used to calculate the water level at the downstream boundary and the measured discharges on respectively the 27<sup>th</sup> of April and 12<sup>th</sup> of May 2018 for the upstream boundary. Furthermore a uniform Manning's roughness is assumed for all cross-sections and the model is simulated for varying Manning's values.

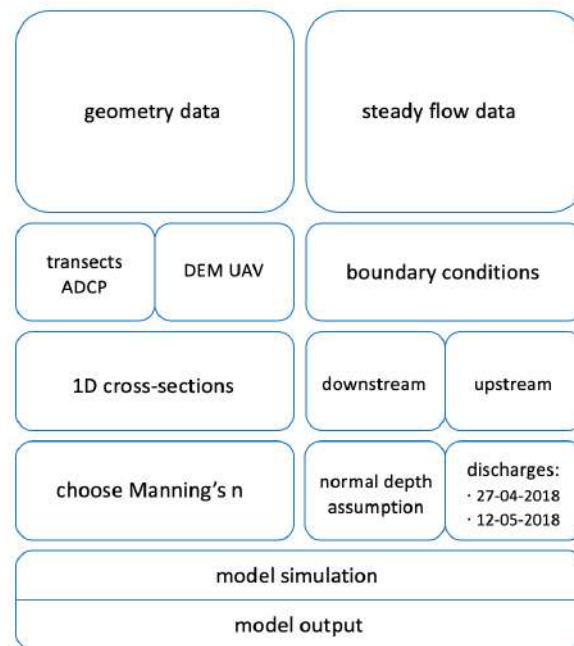


Figure 5.13 The requirements and outputs for a 1D steady-state HEC-RAS model.

### 5.5.2 Model calibration

In order to use model outputs for research purposes the model needs to be scientifically sound and robust. Model calibration can be defined as the process of estimating model parameters by comparing model simulation results with observed data under the same assumed conditions (Moriassi et al., 2007). The steady-state HEC-RAS model is calibrated by an iterative process of finding an optimal Manning's roughness coefficient  $n$  for the modelled river reach by comparing the simulated water surface elevations with the observed data. In other words the purpose is to find the Manning's value, which leads to the best performance of the model evaluation parameter, which is described in the following subsection. Bed roughness is highly variable as it depends on various factors such as channel alignment, bed material, nature of sediments, surface roughness and obstructions in the river channel. Chow (1959) showed that Manning's coefficient  $n$  can vary for the main channel and its floodplains, see appendix E for different Manning's roughness values. It is possible in HEC-RAS to choose a different  $n$  for the main channel than for the floodplains. However, in this research it is decided to use one Manning's coefficient, while the floodplains are not covered by more vegetation than the river channel. Therefore it is assumed that the roughness values of floodplain and main channel are more or less the same. The Luangwa river is a sand-bed river, with some weeds and stones. Based on the table presented by (Chow, 1959) in the appendix E, a range for  $n$  is chosen from 0.025 - 0.060. This range will be used to find an optimum roughness value and with this value a rating curve will be constructed.

### 5.5.3 Model evaluation

To get insight in the performance of the HEC-RAS model in terms of accuracy the Root Mean Squared Error (RMSE) is used as model evaluation criterion. The RMSE is a widely used measure of the differences between the observed values and predicted values by a model. The differences are also referred to as prediction errors. The RMSE represents the quadratic mean of the errors into one single measure and is therefore a measure for the model accuracy. The RMSE value is always positive and the lower the better the model performance (Lamichhane and Sharma, 2018; Moriassi et al., 2007). The RMSE can be expressed as follows:

$$RMSE = \sqrt{\sum_{i=1}^n (Y_i^{obs} - Y_i^{sim})^2} \quad (5.7)$$

#### **5.5.4 Parameter sensitivity**

Uncertainty of a parameter can influence the outcome of the model (Lamichhane and Sharma, 2018). Therefore the model sensitivity is investigated by changing the Manning's roughness  $n$ . Based on the table of (Chow, 1959) it is decided to change the Manning's optimum value with 20%, to see the impact on the constructed rating curve. Furthermore the sensitivity of the hydraulic slope is investigated. It would be convenient to also change this parameter by 20% and compare the different rating curves. However, the hydraulic slope can vary a lot locally therefore it is decided to change this with a factor two. This is arbitrary of course, but local measurements of the hydraulic slope show that, the slope can vary a lot locally. See for further explanation section 6.3 in the results and discussion chapter.

#### **5.6 Rating curve comparison**

The final step of the research methodology is the rating curve comparison step. In this step the more physically based rating curve produced by the hydraulic model will be compared with a traditional rating curve constructed by WARMA. The 95% confidence interval of the WARMA rating curve will be used to generally judge the accuracy of the more physically constructed rating curve.

# 6

## Results & discussion

This chapter presents the findings of this research. It focuses on rating curve comparison at the area of interest. To be able to construct a more physically based rating curve first the results of the analysis of the wet- and dry river profile is presented. Secondly the hydraulic slope is estimated by several methods, and an average value for the hydraulic slope is obtained. Furthermore the results of the steady-state HEC-RAS model will be presented and discussed and a comparison will be made between the constructed physically based rating curve and the traditional rating curve of the Zambian Water Resources Management Authority (WARMA). It is recommended to read this chapter with the appendices C and D, because a lot of additional information is given in the appendices.

### 6.1 Wet river profile

The ADCP measurements on the 12<sup>th</sup> of May 2018 are used to build up the hydraulic model in HEC-RAS, while on this day also UAV measurements were available, which made it possible to build up the river's geometry. As explained in chapter: research methodology three transects are measured across the area of interest, an upstream, middle and downstream transect. Each transect is measured four times. First of all the transect measurements are visually inspected. Figure 6.1 shows the depth profiles of all the transects.

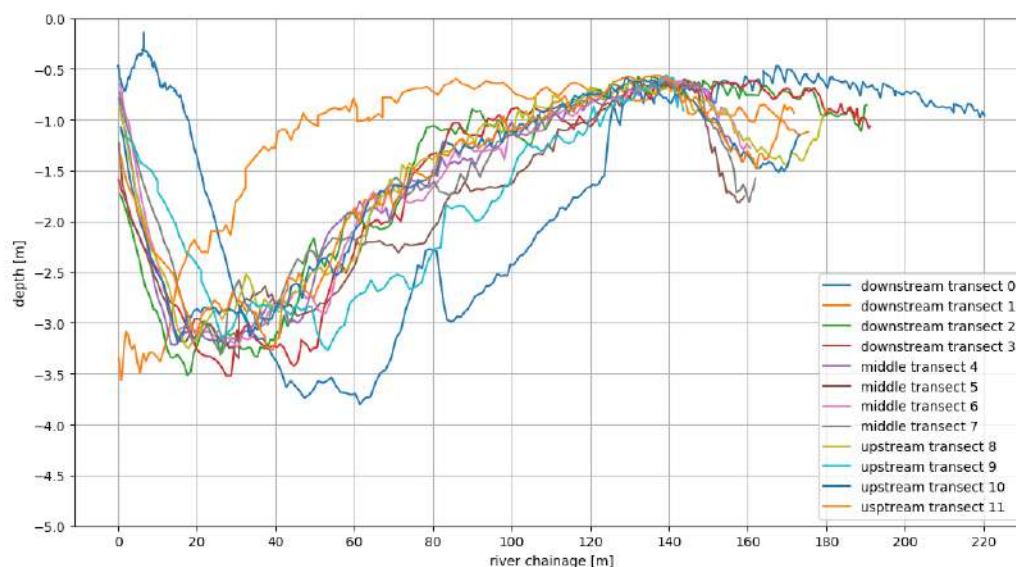


Figure 6.1 Depth profiles for the downstream transect on the 12<sup>th</sup> of May 2018.

It can be seen from figure 6.1 that there are transect measurements, which show a different shape and length for the same transect. It is likely that this is caused by an incorrect ADCP measurement. A correct ADCP measurement is carried out in a straight line from one river bank to the other. In practice this is almost impossible to achieve, because of the wide river channel and the strong river flow, especially in the middle of a transect. Therefore it is easy to have a slightly different transect route, which can cause a different depth profile and length. After discarding the extreme outliers the profile plot shows a more similar shape, see figure 6.2.

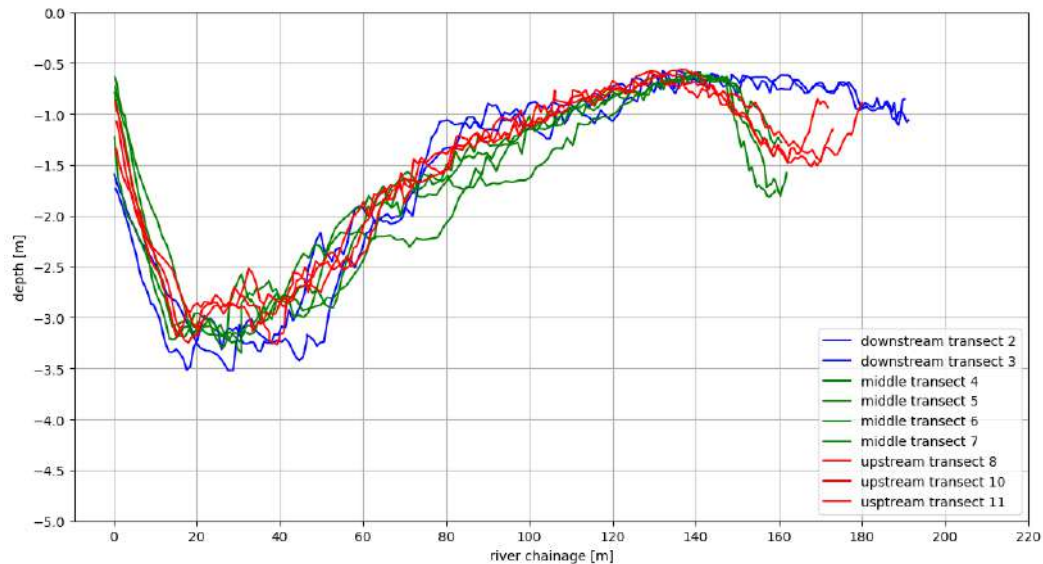


Figure 6.2 Selection of depth profiles for the downstream transect on the 12<sup>th</sup> of May 2018.

Figure 6.2 shows two different types of transects. The middle and the upstream transect show a shallow part with a small secondary channel, whereas the downstream transect has no secondary channel. This arises the question if the transects behave hydraulically the same.

To see if the transects behave hydraulically the same an artificial depth is created ranging from the minimum channel elevation up to the measured water level on the 12<sup>th</sup> of May 2018. This artificial depth is plotted against hydraulic parameters such as: top width, cross-sectional area, perimeter, hydraulic radius and conveyance. Figure 6.3 shows the conveyance, which include the cross-sectional area and the hydraulic radius. Appendix C provides a more detailed analysis including figures of the other hydraulic parameters.

Hydraulically the transects seem to behave similar, although around 140-150m the downstream transect shows a more constant conveyance. This is caused by a reduced hydraulic radius. In case of the downstream transect, there is no secondary channel but a large shallow area. In this area the perimeter is relatively large compared to the cross-sectional area, which leads to a reduced hydraulic radius and a more constant conveyance.

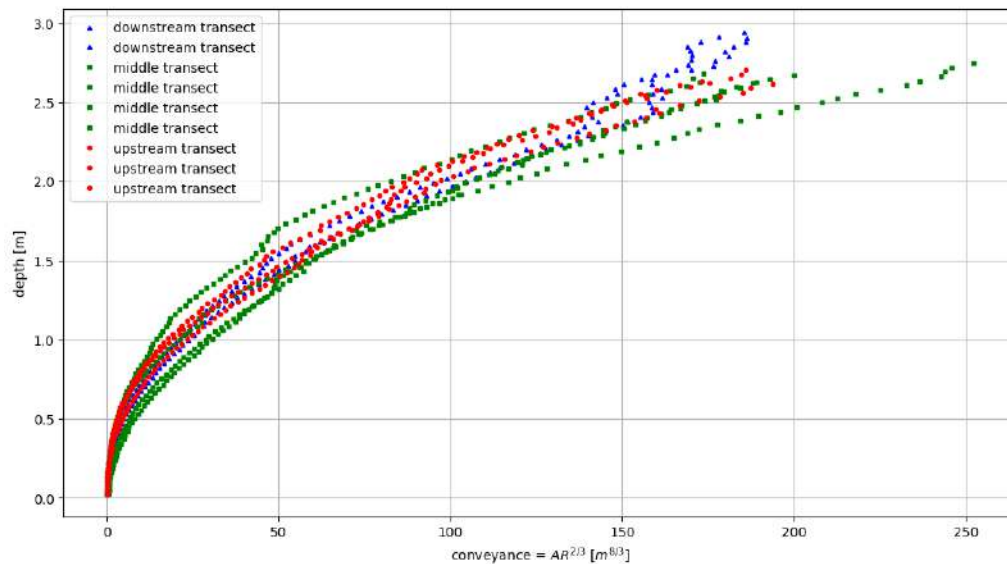


Figure 6.3 Conveyance versus modelled depth on the 12<sup>th</sup> of May 2018.

As mentioned before the transects are needed for building the hydraulic model in HEC-RAS. Therefore an average of the transect measurements needs to be calculated. Figure 6.4 shows how this is done for the middle transect. The other transects are plotted in appendix C.

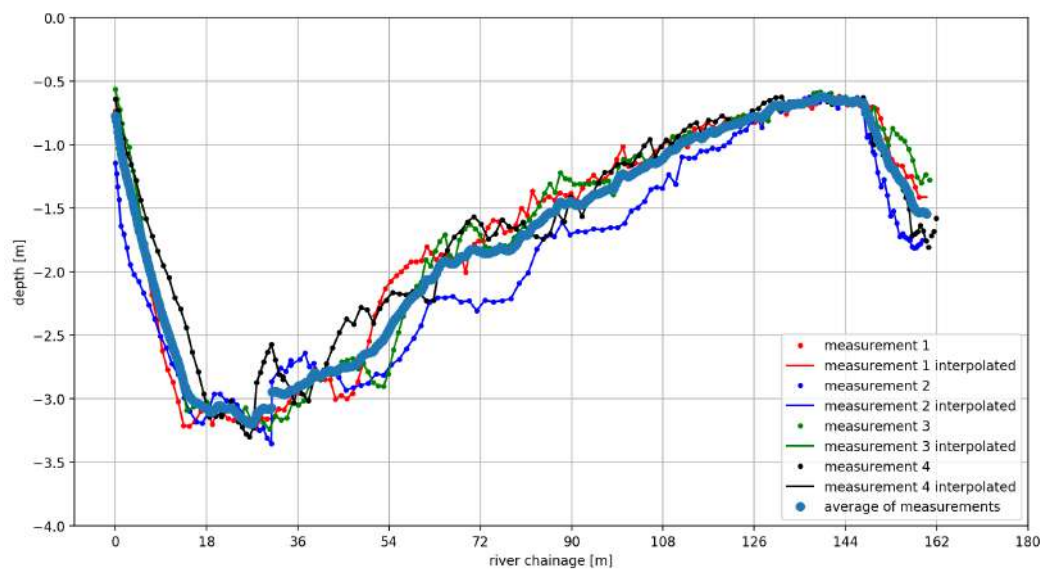


Figure 6.4 Averaging the middle transect on the 12<sup>th</sup> of May 2018.

Because of different lengths first the measurements are approximated by interpolation. After that an average is calculated. The averaged measurements for upstream, middle and downstream transects are combined with UAV measurements, as can be seen from figure 5.12 in the research methodology chapter.

## 6.2 Dry river profile

As described in the research methodology the water surface needs to be excluded from the DEM. The water is flowing and reflects light, which result in unreliable and incorrect elevation data. Furthermore vegetation also influences a DEM. To filter out the vegetation a tool in Agisoft Photoscan is used, called Classify Ground Points (Agisoft LLC, 2018). Figure 6.5 shows the edited DEM and the orthophoto of the measurement site.

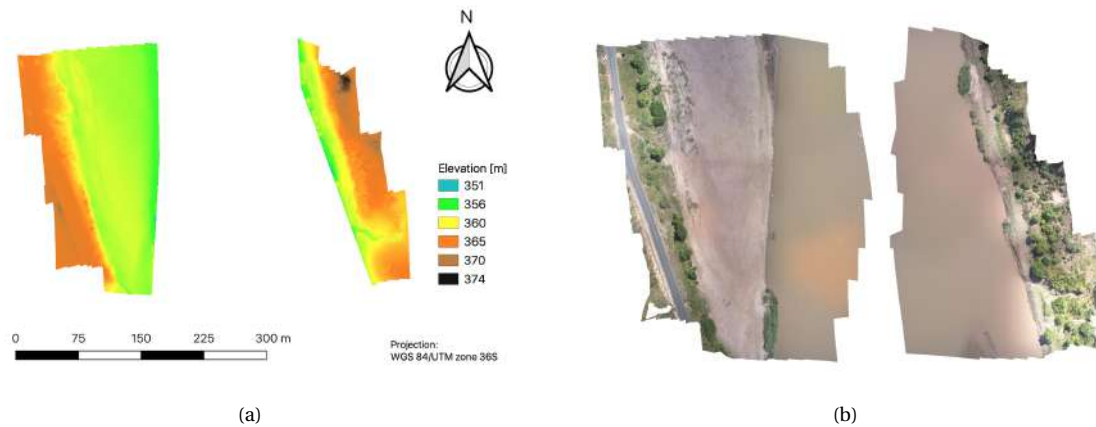


Figure 6.5 (a) DEM without water or vegetation and (b) orthophoto of the area of interest.

## 6.3 Hydraulic slope estimation

The bed slope and under uniform flow conditions the hydraulic slope can be estimated by a global DEM, local DEM, the garden hose method or DGPS measurements over a short or large distance. Figure 6.6 shows the estimation of the bed slope from ASTER GDEM data. An upstream starting point is chosen from where elevations are collected in downstream flow direction. In total a stretch of 25 km is sampled. Linear regression is applied to estimate the bed slope. For further explanation this research refers to (Broekema, 2018).

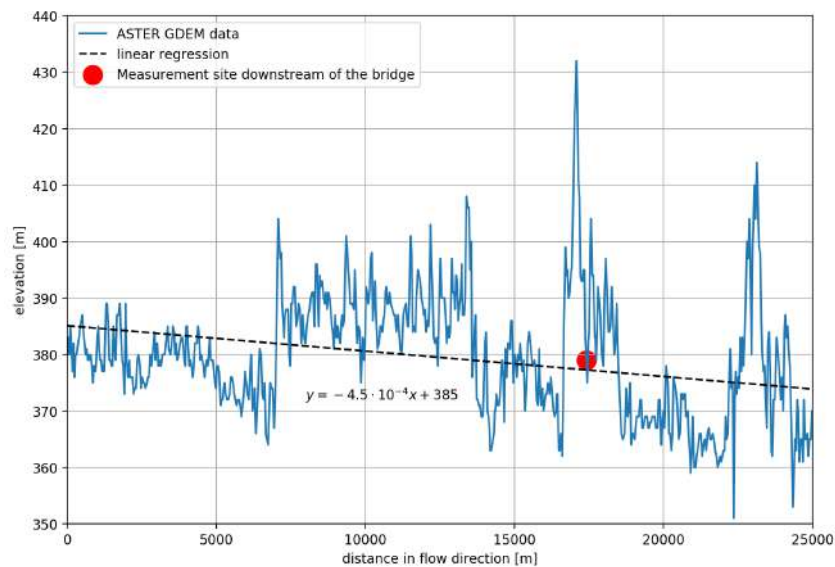


Figure 6.6 Bed slope estimation from the ASTER GDEM data (Broekema, 2018).

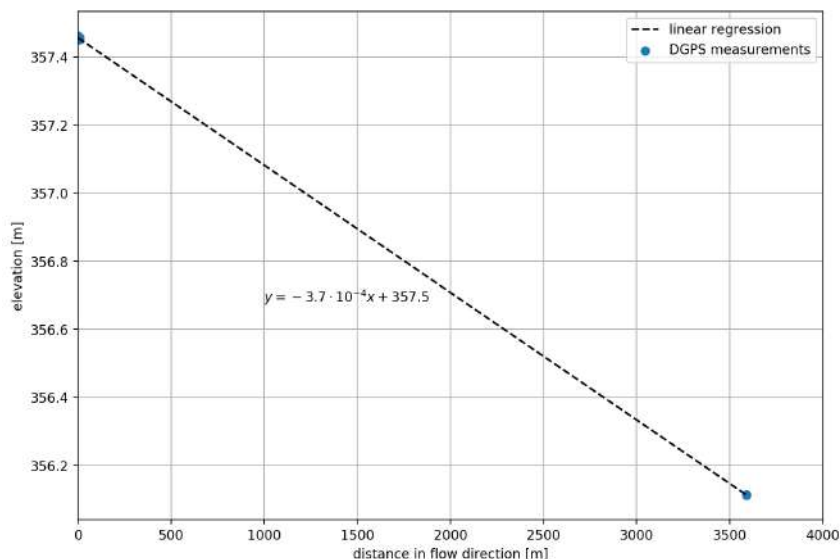


Figure 6.7 DGPS measurements of the water surface elevation over a large distance.

Table 6.1 The different hydraulic slope estimations.

Method	Estimated hydraulic slope [m/m]
global DEM	$-4.5 \cdot 10^{-4}$
local DEM (averaging floodplain)	+
local DEM (conveyance method)	+
garden hose method	$-7.5 \cdot 10^{-4}$
DGPS measurements large distance	$-3.7 \cdot 10^{-4}$
DGPS measurements short distance	$-2.2 \cdot 10^{-4}$

The slope estimations by the different methods are summarised in table 6.1. The table shows a positive slope for the methods using the local DEM. Broekema (2018) showed that it is likely this is caused by the short longitudinal length of the DEM. It is advised to fly a longer longitudinal stretch, order of magnitude a couple of kilometres, to make sure local sedimentation effects are averaged out.

The other estimates of the slope are within in the same order of magnitude. However the most reliable measurements are the estimated slopes from the DGPS measurements over a large distance. The DGPS is the most accurate instrument, while it measures up to centimetre accuracy level. However, the short distance measurements are tricky, while the slope is small and one could be conflicting with the instrument accuracy level. This is probably the reason while the DGPS measurement over a short distance gives a value of a different order of magnitude. Another reason might be that the hydraulic slope can vary a lot locally. This is why further on in the sensitivity analysis is chosen to vary the hydraulic slope a lot. A plot of the DGPS measurements over a short distance can be found in D.4 in appendix additional graphs results.

As explained in subsection 5.2.3 of the research methodology the garden hose method is a good method for insight, but in practice it is difficult to obtain accurate results. Table 6.1 shows a larger value for the slope measured by the garden hose method, compared to the other estimates. This can be caused by the inclusion of the velocity head at the upstream end of the garden hose, it is likely the garden hose end was in this case not perpendicular to the flow.

The global DEM contains a lot of outliers, but over a large distance gives a reasonable result, because these outliers are averaged out. In the end the slope obtained from the global DEM is averaged with the slope of the DGPS over a large distance, while these values are close to one and other and the both give a reasonable result. If the DGPS measurements over large distance and the global DEM value are averaged a hydraulic slope of  $i_w = -4.1 \cdot 10^{-4}$  is obtained. For simplicity a hydraulic slope of  $i_w = -4 \cdot 10^{-4}$  is used in the hydraulic model of HEC-RAS.

## 6.4 Hydraulic modelling

The observed water surface elevations at the three measured transects on both measurement days are compared with the simulated water surface elevations for various Manning's values. To evaluate the model performance in terms of model accuracy the statistical parameter RMSE is calculated. Figure 6.8 shows the model evaluation criteria for varying Manning's roughness values.

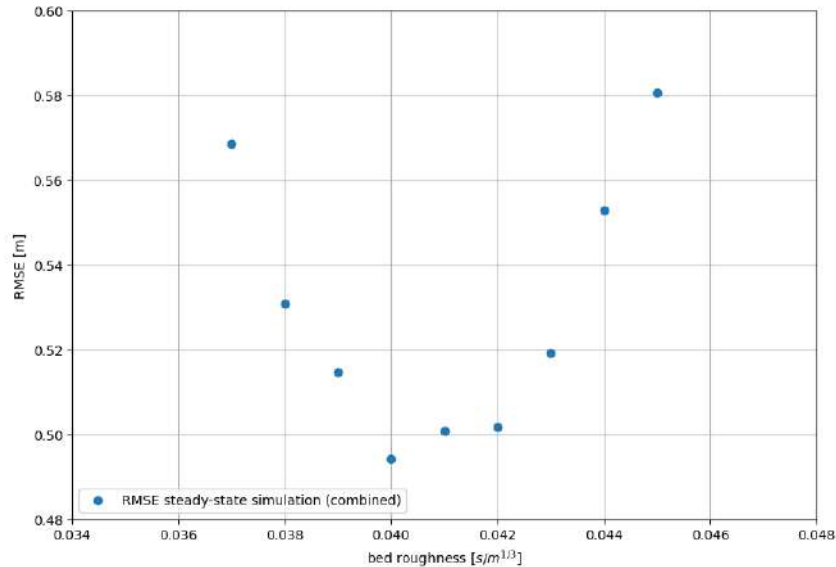


Figure 6.8 The RMSE for varying Manning's coefficients, both measurement days combined.

From figure 6.8 can be concluded that a Manning's coefficient of  $n = 0.040$  gives the best performance for the model evaluation parameter, if one would take both measurement days into account. This value is used to build up a rating curve in HEC-RAS One could also choose to optimise per measurement day. For April 27, 2018 a Manning's roughness value of  $n = 0.044$  would than be the optimum and for May 12, 2018 this would be  $n = 0.034$ . The graphs of the RMSE per measurement day can be found in figure D.7 and figure D.6 in the appendix additional graphs results. In this case a higher discharge gives a higher roughness value. It would be interesting to do some additional research on this however due to constraints in time this is chosen to be listed as a recommendation for future research.

To see how these roughness values obtained from the hydraulic model relate to plain Manning, some hand-calculations are carried out. For simplicity a rectangular channel is assumed where  $R \approx d$ . The values used for this calculation can be found in appendix E in table E.1. The calculations result in a Manning's value of  $n_1 = 0.050$  on April 27, 2018 and a value of  $n_2 = 0.048$  on May 12, 2018. Still a higher roughness value is observed for a higher discharge, but the differences between the roughness values are significantly smaller in the hand-calculations than for the roughness values from the hydraulic model.

## 6.5 Rating curve comparison

The gauging station of WARMA is approximately 4 kilometres from the measurement site, see figure 3.4 in chapter research area. A dataset of discharge and stage measurements, taken by WARMA between 1948 and 2002, is used to construct a rating curve. Figure 6.9 shows the discharge and stage measurements.

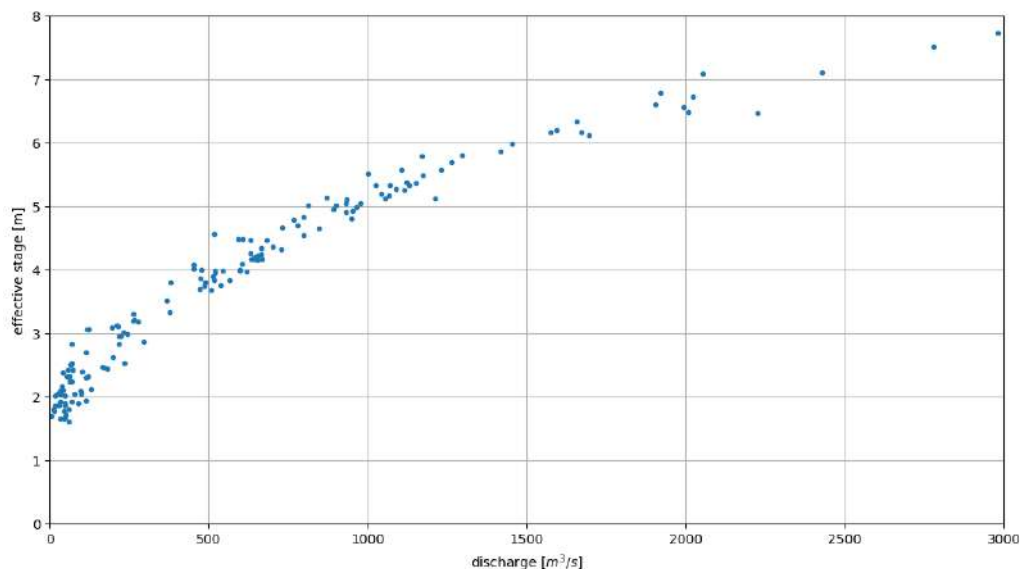


Figure 6.9 The discharge stage measurements of WARMA.

Figure 6.9 shows a dense concentration of measurements for low discharges and minor measurements for high flows. It is more difficult to take measurements during high flow conditions, areas can be flooded or equipment can be damaged. One could also argue up to which point it is save to take discharge measurements. Despite these challenges the rating curve includes some high flow measurements, which make the rating curve more reliable. The stage-discharge relation can be expressed in the following form:

$$Q = a(h - h_0)^b \quad (6.1)$$

where  $h_0$  is the stage for zero flow. The stage of zero flow can be estimated by plotting  $\log(h)$  versus  $\log(Q)$  and apply linear regression over only the low stages. Manually adjust the  $h_0$  value until the highest  $R^2$  is reached. In this case that is reached for  $h_0 = 0$ .

Figure 6.10 shows the  $\log(h)$  versus  $\log(Q)$ . In this case the stage-discharge relation becomes:

$$\log(Q) = \log(a) + b \log(h - h_0) \quad (6.2)$$

Linear regression is applied to determine the coefficients  $a$  en  $b$  for the stage-discharge relation of WARMA. Table 6.2 presents the values of the rating coefficients.

Table 6.2 The rating curve coefficients for the WARMA stage-discharge relation.

Coefficients	Values
$\log(a)$	0.78
$a$	6.05
$b$	3.13

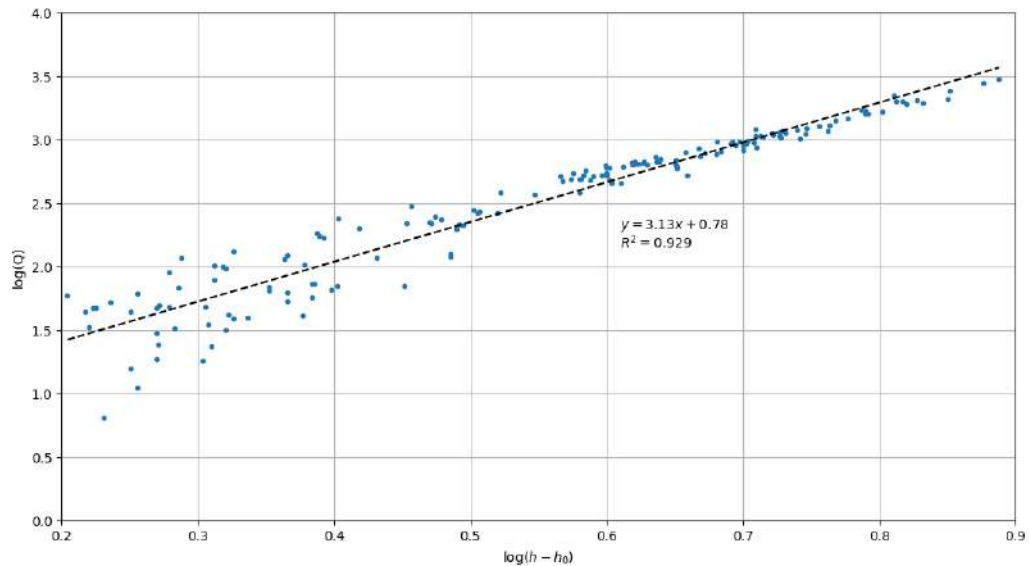


Figure 6.10 Determination of stage-discharge relationship WARMA measurements.

Figure 6.11 shows the simulated stage discharge relation for the steady-state HEC-RAS model. To be able to construct a rating curve in HEC-RAS, theoretical steady-state discharges are assumed. The discharges range from 100 - 5000  $m^3/s$  and are divided in steps of 100  $m^3/s$ . The maximum channel depths are calculated for the range of discharges for the most upstream transect, while this is as close as possible to the gauging station of WARMA. The maximum channel depth is used, because it is assumed that  $h_0 = 0$ . Based on this assumption the river stage  $h$  is equal to the maximum channel depth.

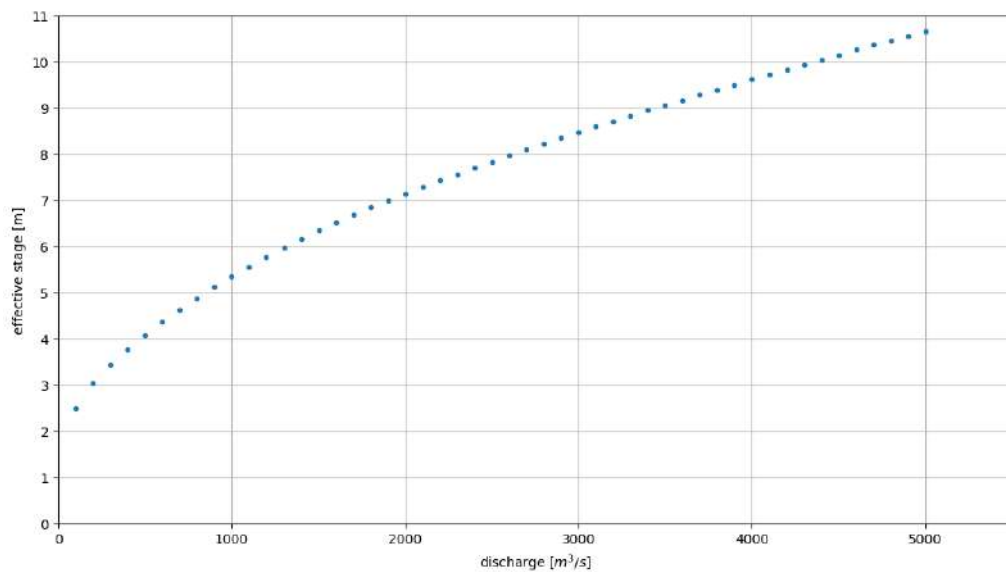


Figure 6.11 The simulated stage discharge values for the HEC-RAS model.

To determine the corresponding rating curve coefficients,  $\log(Q)$  is plotted versus  $\log(h)$ . Figure 6.12 shows the  $\log(Q)$  versus  $\log(h)$  graph. From linear regression the coefficients can be determined. Table 6.3 shows the values of the rating curve coefficients belonging to the simulated stage-discharge relation.

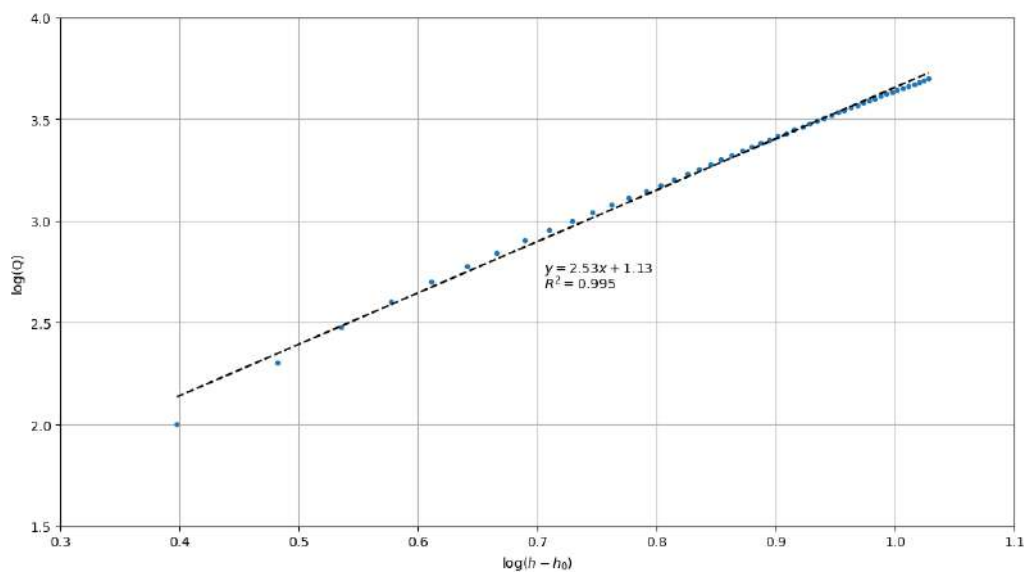


Figure 6.12 Determination of stage-discharge relationship HEC-RAS model.

Table 6.3 The rating curve coefficients for the HEC-RAS stage-discharge relation.

Coefficients	Values
$\log(a)$	1.13
$a$	13.54
$b$	2.52

The rating curve produced by HEC-RAS includes the wet- an dry river profile and therefore is much more physically based than the rating curve of WARMA. Figure 6.13 shows both rating curves in one graph. Besides the two rating curves also the stage and discharge measurements are visualised as well as the 95% confidence interval of the WARMA rating curve. The 95% confidence interval is obtained after a logarithmic transformation. This is done because the measurements of WARMA are not normally distributed. After the logarithmic transformation linear regression is applied and an upper and lower limit is determined by adding and subtracting two times the standard deviation (Dekking et al., 2005), see figure D.23 in appendix D.

Both rating curves are extremely close to each other up to a discharge of roughly  $500 \text{ m}^3/\text{s}$ . From that point onward the rating curves diverge, but the constructed more physically rating curve still remains within the 95% confidence interval of WARMA.

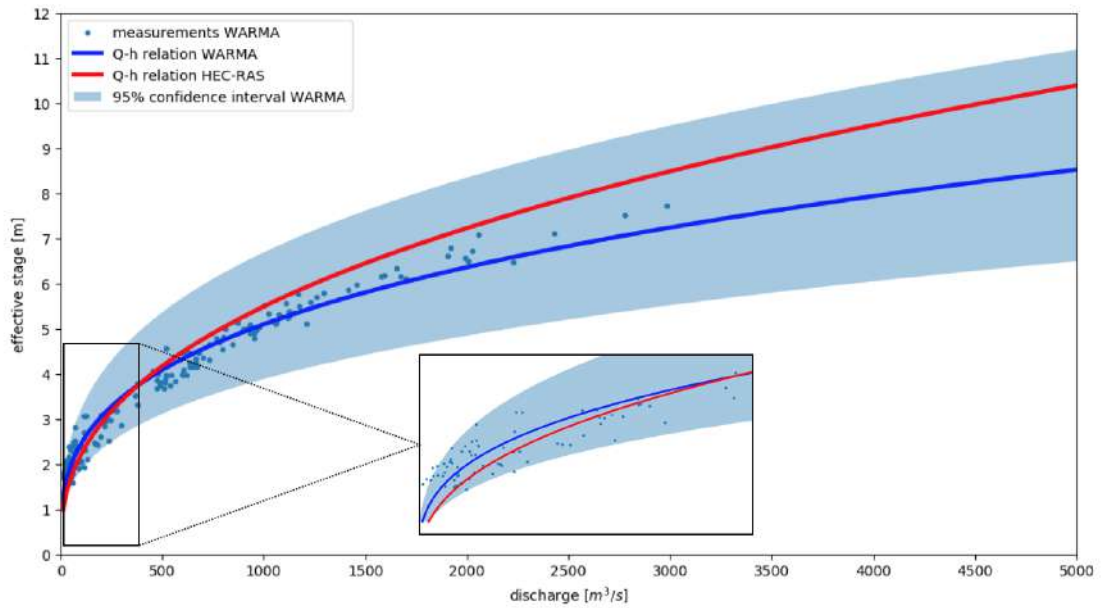


Figure 6.13 Comparison of rating curve WARMA with the HEC-RAS rating curve.

As mentioned in the research methodology it is important to know how sensitive the model output is for uncertainty in input parameters. In this case there are two main parameters that can influence the constructed rating curve, namely the hydraulic slope and the Manning's roughness coefficient. To see how uncertainty of those parameters can influence the outcome of the model 20% is added or subtracted from the Manning's coefficient and the hydraulic slope is adjusted with a factor two, while the slope can vary a lot locally. Figure 6.14 shows the sensitivity for  $n$ , and figure 6.15 shows the model sensitivity for the hydraulic slope  $i_w$ , when  $n$  is kept constant.

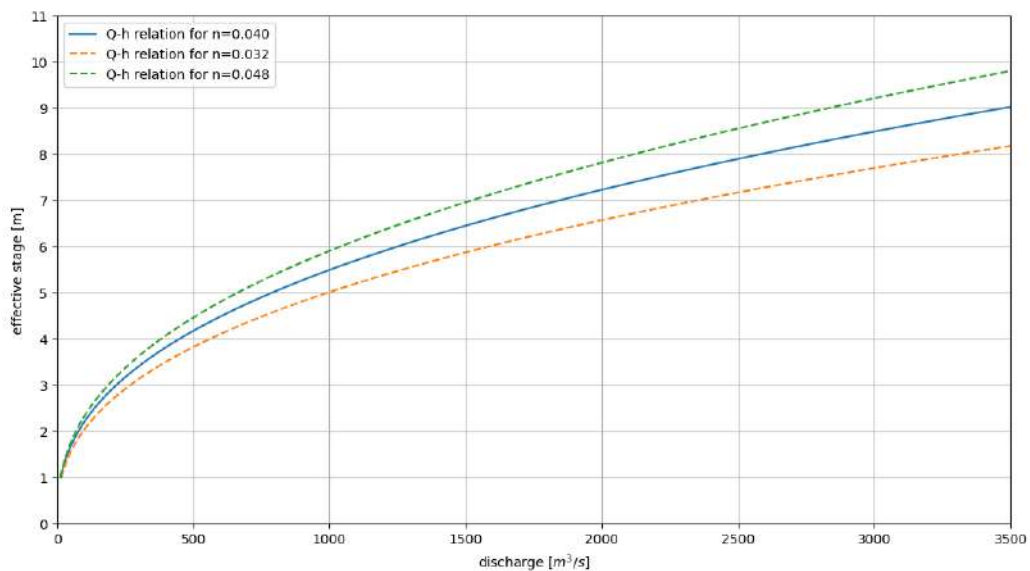


Figure 6.14 Rating curve sensitivity for changes in Manning's coefficient and constant hydraulic slope.

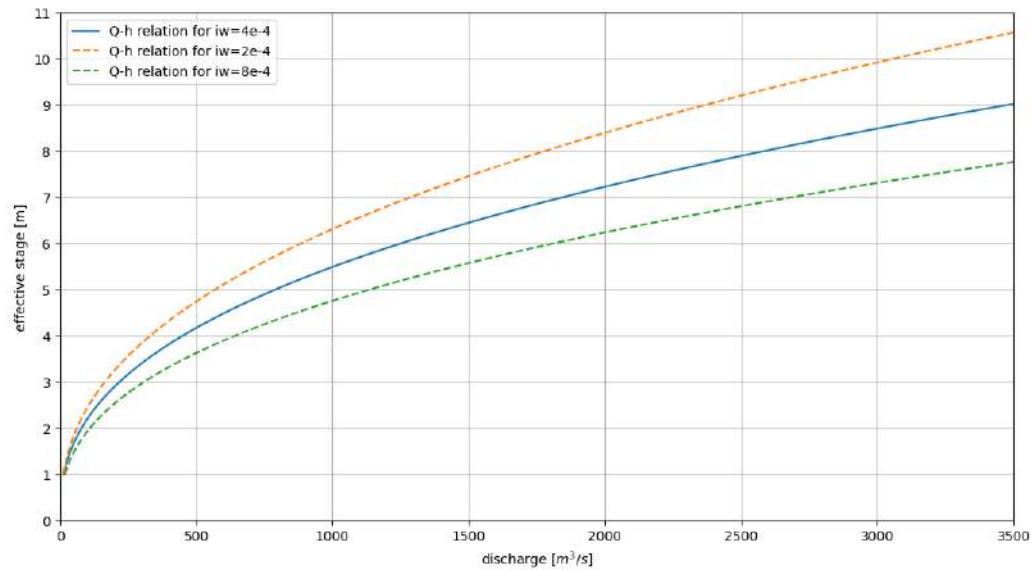


Figure 6.15 Rating curve sensitivity for changes in hydraulic slope and constant bed roughness.

However, the hydraulic slope and the bed roughness are related. Therefore if one would change the hydraulic slope a different optimal value for  $n$  will be found. Figure 6.16 shows this principle. It can be seen that a different hydraulic slope leads to a different optimum  $n$ , which almost lead to the original rating curve constructed in HEC-RAS with an  $i_w = 4e-4$  and a value  $n = 0.040$ .

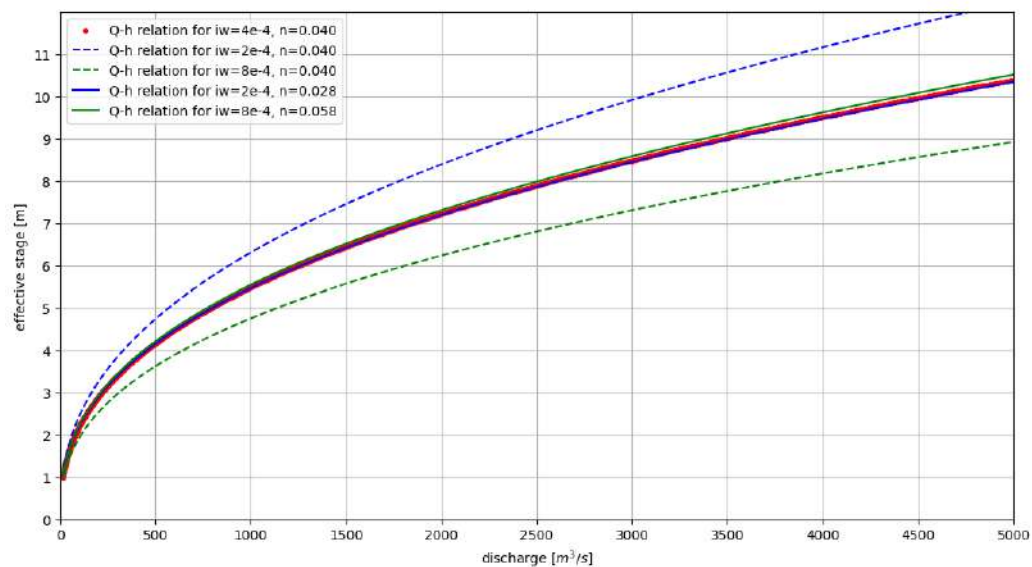


Figure 6.16 Rating curve sensitivity for changes in hydraulic slope with new optimum bed roughness values.

Now that is clear that a change in hydraulic slope leads to a different  $n$ , which in the end does not change the rating curve much it is important to see if a change in bed roughness still stays within the 95% confidence interval. In order to see this 6.13 and 6.14 are combined into figure 6.17.

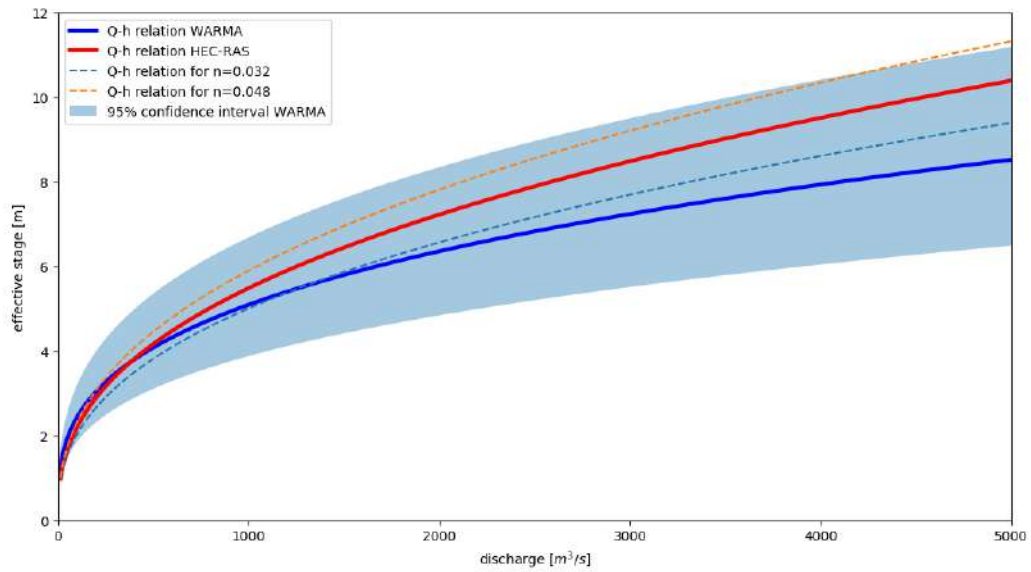


Figure 6.17 Rating curve comparison with error bounds and the sensitivity of a change in bed roughness.

From figure 6.17 it becomes clear that it is very important to accurately estimate the bed roughness, because it can significantly change the model output. However, even with an uncertainty in the bed roughness most of the rating curves would stay within the 95% confidence interval of the WARMA rating curve.



## Conclusions & recommendations

This chapter lists the main conclusions and recommendations. First the conclusions will be discussed and the research aim and objectives will be addressed. Finally the recommendations will be presented.

### 7.1 Conclusions

Discharge, bathymetric and aerial data are collected between April and June 2018 at several measurement locations in the Luangwa river catchment. Four sites are selected based on the formulated selection criteria; an upstream, middle and two downstream locations. In the end the downstream measurement location of the Great East Road bridge is selected for further analysis and hydraulic modelling. This location is chosen because there are no structures, abstractions or confluences nearby, which can cause backwater effects. Furthermore the location is only a couple of kilometres from the gauging station of WARMA, which has the largest available discharge dataset. Therefore this location is the most suitable location for rating curve comparison. Although the locations are a few kilometres apart it is assumed that the cross-sections behave hydraulically the same and therefore a rating curve comparison is possible.

The data analysis of the ADCP measurements on April 27 and May 12, 2018 provide insight in the hydraulic behaviour of the transects at the area of interest. It can be concluded that, after removing the incorrect ADCP measurements, the transects behave the same for several hydraulic parameters. The conveyance for transects without a secondary channel can become constant in shallow areas, while the hydraulic radius decreases in those areas. Despite this phenomena the hydraulic parameters show similar hydraulic behaviour. Interpolation seems to be a good method to average the transect measurements. The three averaged transects for the area of interest are further on used to build up the geometry of the hydraulic model.

The DEM which is generated by the photogrammetry software needs additional processing. The elevation values of the water surface are not reliable, while the water is flowing and light is reflected. Therefore the water surface needs to be cut out. This can be done in the software package QGIS. Furthermore vegetation leads to "noise" in the generated DEM. To be able to include the geometry of the river in a proper way, this vegetation needs to be filtered out. Agisoft PhotoScan offers a filtering tool to filter out vegetation, the obtained DEM after filtering seems good enough for building the geometry of the dry river profile in the hydraulic model.

The hydraulic slope, or under uniform flow conditions the bed slope can be estimated by the following methods: global DEM, local DEM, garden hose and DGPS measurements of the water surface. From the results of the different estimations it can be concluded that using a local DEM of approximately a longitudinal stretch of 300m gives the worst results. The garden hose method seems a good method for insight, but in practice it is difficult to obtain accurate results. This is caused by practical reasons such as the end of the garden hose not being perpendicular to the stream, which can result in an additional velocity head term at the upstream end or air bubbles along the hose. The slope estimation by the global DEM and in particular the estimation of the water surface elevation by the DPGS measurements over longer distances are promising. The values are close to each other and therefore they are averaged. A hydraulic slope of  $i_w = 4 \cdot 10^{-4}$  is assumed. This value is used in the hydraulic model to level out the different cross-sections.

In HEC-RAS the geospatial data of the wet- and dry river profile is combined into three cross-sections. To obtain more cross-sections interpolation is applied between these cross-sections. To make sure the area of interest is out of the influence zone of backwater effects, caused by disturbances downstream, the downstream cross-section is copied and placed 11km downstream. Besides geometrical information, steady flow data and boundary conditions need to be specified in order to run a 1D steady-state model. The observed water surface levels are compared with the simulated water surface levels, for various Manning's values. The model accuracy is evaluated by taking the RMSE. The lowest RMSE for both measurement days is obtained for a bed roughness of  $n = 0.040$ .

With an optimum value for the Manning's roughness a rating curve is constructed. The rating curve is compared with the rating curve of WARMA and clearly fits into the 95% confidence interval of the WARMA rating curve. By using a hydraulic model, which contains the entire river geometry one can get rid of extrapolation, which is an advantage compared to traditional river rating. The sensitivity of the hydraulic model is evaluated by changing the bed roughness and changing the hydraulic slope. It becomes clear that it is important to estimate the roughness accurately, while this can significantly change the model output.

## 7.2 Recommendations

### 7.2.1 Recommendations for a future survey

1. Find a measurement location where a gauging station is present and a complete discharge dataset is available. The measurement location should provide enough space for carrying out the UAV and ADCP measurements. The rating comparison is then easier, while both methods are carried out at the same location.
2. Make sure the ADCP transects measured on different dates are at the same position. A change in the river bed will also be captured and the hydraulic behaviour can be well studied.
3. It would be easier to map the river geometry in the dry season, when the Luangwa river is almost run dry. The whole area can be covered by the UAV and no additional ADCP measurements are needed. Some ADCP measurements are required for calibration, but one could do that for example at the beginning of the wet season, where there is water present in the river, but no bank full discharge is reached. The discharge measurements also become more accurate in that case.
4. To be able to make a decent estimate for the bed slope, and under uniform flow conditions the hydraulic slope, from a local DEM a longitudinal stretch of at least a kilometre needs to be measured by the UAV. The dry season would be ideal for estimating the bed slope, while the amount of water is at its minimum.

### 7.2.2 Recommendations for future research

1. The relationship between discharge and bed roughness is shortly addressed in this research. In other words what happens with the Manning's roughness value for an increase in discharge. It is interesting to do some further research on this.
2. Only a 1D steady-state model is used in this research, which is an obvious limitation. It is interesting to construct a rating curve from a 2D model or a 1D/2D model and especially focus on the differences in the rating curve for intermediate stages. It is likely that in these situations local accelerations can play a more dominant role, which can lead to a different form of the rating curve.
3. It is interesting to compare a HEC-RAS model with another hydraulic model. In theory one should get the same or a similar result, but this is not considered in this research.
4. This research can be a step forward to in the end estimate the discharge indirectly from space. This research uses a discharge-stage relationship, but with the same equipment used one could also make a discharge-chainage relationship. In that case the river chainage can be estimated from satellites and a river discharge can be estimated. This is recommended as a topic for future research.

# Bibliography

- Agisoft LLC (2017). Tutorial (Beginner level): Orthomosaic and DEM Generation with Agisoft PhotoScan Pro 1.2 (without Ground Control Points). Technical report. DOI 10.1006/mpev.1996.0003.
- Agisoft LLC (2018). Agisoft Photoscan User Manual - Version 1.4. Technical report.
- Ankum, P. (2002). *Design of Open-Channels and Hydraulic Structures*. Lecture notes, Delft University of Technology.
- Bakker, d. P. (2017). GPS Positioning Surveying and Mapping. Reader, Delft University of Technology.
- Balogh, A. and Kiss, K. (2014). Photogrammetric processing of aerial photographs acquired by UAVs. *Hungarian Archaeology*, (40):1–8.
- Bates, P. (2012). Integrating remote sensing data with flood inundation models: How far have we got? *Hydrological Processes*, 26(16):2515–2521. DOI 10.1002/hyp.9374.
- Battjes, J. and Labeur, R. (2014). *Open Channel Flow*. Lecture notes, Delft University of Technology.
- Bjerklie, D., Moller, D., Smith, L., and Dingman, S. (2005). Estimating discharge in rivers using remotely sensed hydraulic information. *Journal of Hydrology*, 309(1-4):191–209.
- Bridle, R. (2007). Timing and Weather. Retrieved from [http://www.findaerialphotography.com/timing\\_weather.php](http://www.findaerialphotography.com/timing_weather.php). Accessed on: August 30, 2018.
- Broekema, K. (2018). *Drone gebaseerde hoogte modellering voor rivier hellingen*. Bachelor thesis.
- Brunner, G. (2016a). HEC-RAS River Analysis System - Hydraulic Reference Manual, Version 5.0. Technical report, US Army Corps of Engineers. ISBN CPD-68.
- Brunner, G. (2016b). HEC-RAS River Analysis System - User's Manual, Version 5.0. Technical Report February, US Army Corps of Engineers. ISBN 6092583828.
- Brunner, G. (2016c). HEC-RAS River Analysis System - User's Manual 2D, Version 5.0. Technical Report November, US Army Corps of Engineers. ISBN CPD-68.
- Chow, V. (1959). *Open-channel hydraulics*. McGraw-Hill Book Company, New York. ISBN 0070107769.
- Corrigan, F. (2017). Introduction To UAV Photogrammetry And Lidar Mapping Basics. Retrieved from <https://www.dronezon.com/learn-about-drones-quadcopters/introduction-to-uav-photogrammetry-and-lidar-mapping-basics/>. Accessed on: August 30, 2018.
- Dekking, F., Kraaikamp, C., Lopuhaä, H., and Meester, L. (2005). *A Modern Introduction to Probability and Statistics*. Springer-Verlag, Delft. ISBN 1852338962.
- DHV Consultants BV and Delft Hydraulics (1999). How to establish stage discharge rating curve. Technical report.
- DJI (2017). Phantom 4 User Manual. Technical report.
- DJI (2018). Phantom 4 Specs. Retrieved from <https://www.dji.com/phantom-4/info>. Accessed on: August 30, 2018.
- Drone World (2018). About DJI Phantom 4 - General Info. Retrieved from <https://www.drone-world.com/about-dji-phantom-4-general-information>. Accessed on: August 30, 2018.

- DroneDeploy (2017a). Accuracy in Drone Mapping: What You Need to Know. Retrieved from <https://blog.dronedeploy.com/accuracy-in-drone-mapping-what-you-need-to-know-10322d8512bb>. Accessed on: August 30, 2018.
- DroneDeploy (2017b). What Are Ground Control Points (GCPs) and How Do I Use Them? Retrieved from <https://blog.dronedeploy.com/what-are-ground-control-points-gcps-and-how-do-i-use-them-4f4c3771fd0b>. Accessed on: August 30, 2018.
- DroneDeploy (2018). Ground Control Points for drone mapping. Retrieved from <https://www.groundcontrolpoints.com/>. Accessed on: August 30, 2018.
- Gleason, C. and Smith, L. (2014). Toward global mapping of river discharge using satellite images and at-many-stations hydraulic geometry. *Proceedings of the National Academy of Sciences of the United States of America*, 111(13):4788–91. DOI 10.1073/pnas.1317606111.
- Gordon, R. (1989). Acoustic measurement of river discharge. *Journal of Hydraulic Engineering*, 115(7):925–936. DOI 10.1061/(ASCE)0733-9429(1989)115:7(925).
- Government of Canada (2016). Concepts of Aerial Photography. Retrieved from <https://www.nrcan.gc.ca/earth-sciences/geomatics/satellite-imagery-air-photos/air-photos/about-aerial-photography/9687>. Accessed on: August 30, 2018.
- Henderson, F. (1966). *Open Channel Flow*. Prentice-Hall, Inc., Upper Saddle River. ISBN 0-02-353510-5.
- Herschy, R. (2009). *Streamflow measurement*. Taylor & Francis, New York, third edit edition. ISBN 978-0-415-41342-8.
- Hrachowitz, M., Savenije, H., Blöschl, G., McDonnell, J., Sivapalan, M., Pomeroy, J., Arheimer, B., Blume, T., Clark, M., Ehret, U., Fenicia, F., Freer, J., Gelfan, A., Gupta, H., Hughes, D., Hut, R. W., Montanari, A., Pande, S., Tetzlaff, D., Troch, P., Uhlenbrook, S., Wagener, T., Winsemius, H., Woods, R., Zehe, E., and Cudennec, C. (2013). A decade of Predictions in Ungauged Basins (PUB)-a review. *Hydrological Sciences Journal*, 58(6):1198–1255. DOI 10.1080/02626667.2013.803183.
- Jansen, P., Bendegom, v. L., Berg, v. d. J., Vries, d. M., and Zanen, A. (1979). *Principles of River Engineering The non-tidal alluvial river*. VSSD, Delft, first edit edition. ISBN 9065621466.
- Lamichhane, N. and Sharma, S. (2018). Effect of input data in hydraulic modeling for flood warning systems. *Hydrological Sciences Journal*, 63(6):938–956. DOI 10.1080/02626667.2018.1464166.
- Leon, J., Calmant, S., Seyler, F., Bonnet, M., Cauhopé, M., Frappart, E., Filizola, N., and Fraizy, P. (2006). Rating curves and estimation of average water depth at the upper Negro River based on satellite altimeter data and modeled discharges. *Journal of Hydrology*, 328(3-4):481–496. DOI 10.1016/j.jhydrol.2005.12.006.
- Luxemburg, W. and Coenders, A. (2015). *Hydrological Processes and Measurements*. Lecture notes, Delft University of Technology.
- Manning, R. (1891). On the flow of water in open channels and pipes. *Transactions of the Institution of Civil Engineers of Ireland*, (20):161–207.
- Mansurov, N. (2018a). Introduction to Aperture in Photography. Retrieved from <https://photographylife.com/what-is-aperture-in-photography>. Accessed on: August 30, 2018.
- Mansurov, N. (2018b). Introduction to ISO in Photography. Retrieved from <https://photographylife.com/what-is-iso-in-photography>. Accessed on: August 30, 2018.
- Moriasi, D., Arnold, J., Van Liew, M., Bingner, R., Harmel, R., and Veith, T. (2007). Model Evaluation Guidelines For Systematic Quantification Of Accuracy In Watershed Simulations. *American Society of Agricultural and Biological Engineers*, 50(3):885–900. DOI 10.13031/2013.23153.
- Mosley, M. and McKerchar, A. (1992). *Handbook of Hydrology*. McGraw-Hill, inc., New York.

- Mueller, D., Wagner, C., Rehm, M., Oberg, K., and Rainville, F. (2013). *Measuring Discharge with Acoustic Doppler Current Profilers from a Moving Boat*. DOI 10.3133/tm3A22.
- Pan, F. and Nichols, J. (2013). Remote sensing of river stage using the cross-sectional inundation area-river stage relationship (IARSR) constructed from digital elevation model data. *Hydrological Processes*, 27(25):3596–3606. DOI 10.1002/hyp.9469.
- Pan, F., Wang, C., and Xi, X. (2016). Constructing river stage-discharge rating curves using remotely sensed river cross-sectional inundation areas and river bathymetry. *Journal of Hydrology*, 540:670–687. DOI 10.1016/j.jhydrol.2016.06.024.
- Parodi, U. and Ferraris, L. (2004). Influence of stage discharge relationship on the annual maximum discharge statistics. *Natural Hazards*, 31(3):603–611. DOI 10.1023/B:NHAZ.0000024893.57284.0e.
- Petersen-Øverleir, A. (2005). A hydraulics perspective on the power-law stage-discharge rating curve. Technical Report 5-05, Norges vassdrags- og energidirektorat, Oslo. Technical report.
- Petersen-Øverleir, A. (2006). Modelling stage-discharge relationships affected by hysteresis using the Jones formula and nonlinear regression. *Hydrological Sciences Journal*, 51(3):365–388. DOI 10.1623/hysj.51.3.365.
- Petersen-Øverleir, A. (2014). Some challenges in hydrometry. *La Houille Blanche*, (4):53–56. DOI 10.1051/lhb/2014038.
- Pix4D (2018a). Ground sampling distance (GSD). Retrieved from <https://support.pix4d.com/hc/en-us/articles/202559809-Ground-sampling-distance-GSD->. Accessed on: August 30, 2018.
- Pix4D (2018b). How to select Camera Focal Length and Flight Altitude considering the desired Ground Sampling Distance and Terrain to map? Retrieved from <https://support.pix4d.com/hc/en-us/articles/202558849>.
- Pix4D (2018c). How to verify that there is Enough Overlap between the Images. Retrieved from <https://support.pix4d.com/hc/en-us/articles/203756125-How-to-verify-that-there-is-Enough-Overlap-between-the-Images>. Accessed on: August 30, 2018.
- Pix4D (2018d). TOOLS - GSD calculator. Retrieved from <https://support.pix4d.com/hc/en-us/articles/202560249>. Accessed on: August 30, 2018.
- Pix4D (2018e). Using GCPs. Retrieved from <https://support.pix4d.com/hc/en-us/articles/202558699-Using-GCPs>. Accessed on: August 30, 2018.
- Rantz, S. (1982). Measurement and Computation of Streamflow. *USGS Water Supply Paper*, Vol 1(2175):313. DOI 10.1029/WR017i001p00131.
- Sivapalan, M., Takeuchi, K., Franks, S., Gupta, V., Karambiri, H., Lakshmi, V., Liang, X., McDonnell, J., Mendiola, E., O'Connell, P., Oki, T., Pomeroy, J., Schertzer, D., Uhlenbrook, S., and Zehe, E. (2003). IAHS Decade on Predictions in Ungauged Basins (PUB), 2003-2012: Shaping an exciting future for the hydrological sciences. *Hydrological Sciences Journal*, 48(6):857–880. DOI 10.1623/hysj.48.6.857.51421.
- Strijker, B. (2017). *A Physics-Based approach for Rating Curves to Reduce Uncertainties A New Concept for Hydrological Model Calibration*. Additional thesis, Delft University of Technology.
- Teledyne Marine (2014). RiverRay ADCP datasheet. Technical report.
- The World Bank (2010). The Zambezi River Basin. Technical report, The World Bank, Washington DC. ISBN 9781315282053.
- Trimble Navigation Limited (2003). Real-Time Kinematic Surveying Training Guide. Technical report. ISBN 1408481774.
- Trimble Navigation Limited (2013). Trimble R4 User Guide. Technical Report April.

- Veldhuis, S. (2018). *Using River Geometry for Rating Curve Computation A step towards Remote River Rating*. Master thesis, Delft University of Technology.
- Vriend, H., Havinga, H., Prooijen, B., Visser, P., and Wang, Z. (2011). *River Engineering*. Lecture notes, Delft University of Technology.
- Walford, A. (2017). What is Photogrammetry? Retrieved from <http://www.photogrammetry.com/>. Accessed on: August 30, 2018.
- Wanninger, L. (2008). Introduction to Network RTK. Retrieved from <http://www.wasoft.de/e/iagwg451/intro/introduction.html>. Accessed on: August 30, 2018.
- WARMA (2016). Luangwa Catchment. Retrieved from <http://www.warma.org.zm/index.php/catchments/luangwa-catchment>. Accessed on: August 8, 2018.
- Wu, W. and Wang, S. (1999). Movable Bed Roughness in Alluvial Rivers. *Journal of Hydraulic Engineering*, 125(12):1309–1312.
- Yan, K., Di Baldassarre, G., Solomatine, D., and Schumann, G. (2015). A review of low-cost space-borne data for flood modelling: topography, flood extent and water level. *Hydrological Processes*, 29(15):3368–3387. DOI 10.1002/hyp.10449.



## Backwater derivation and calculation

The assumption that flow in the river is normal or uniform is not always valid. This can be caused by the following reasons:

- Natural variation in river flow rates e.g. flood events.
- Spatial variations in width.
- Spatial variations in friction.
- Change in sediment supply.

In such cases it can be necessary to compute the disequilibrium state e.g. the gradually varied flow. Gradually varied flow means that the flow is varying over large distances, which means that it gradually adapts to uniform flow after local disturbances. Therefore it is different from flow around structures where flow rapidly changes.

The backwater equation for steady gradually varying flow can be derived from the 1D shallow water equations (Jansen et al., 1979; Vriend et al., 2011).

$$\underbrace{\frac{\partial A}{\partial t}}_{\text{storage}} + \underbrace{\frac{\partial Q}{\partial x}}_{\text{net mass transport}} = 0 \quad \text{continuity equation} \quad (\text{A.1})$$

$$\underbrace{\frac{\partial Q}{\partial t}}_{\text{local inertia}} + \underbrace{\frac{\partial}{\partial x} \left( \frac{Q^2}{A} \right)}_{\text{advective inertia}} + \underbrace{gA \frac{\partial h}{\partial x}}_{\text{gravity forcing}} + \underbrace{c_f \frac{Q^2}{Ad}}_{\text{resistance}} = 0 \quad \text{momentum equation} \quad (\text{A.2})$$

After assuming a rectangular channel where  $A = Bd$  and a constant width  $B$  the equations reduce to:

$$\frac{\partial d}{\partial t} + \frac{\partial ud}{\partial x} = 0 \quad (\text{A.3})$$

$$\frac{\partial ud}{\partial t} + \frac{\partial u^2}{\partial x} + gd \frac{\partial (d + z_b)}{\partial x} + c_f u^2 = 0 \quad (\text{A.4})$$

In case of steady flow the  $\partial/\partial t$  terms drop. The equation of water mass conservation than reduces to:

$$\frac{\partial ud}{\partial x} = 0 \quad \rightarrow \quad ud = q_w = \text{constant} \quad \rightarrow \quad u = \frac{q_w}{d} \quad (\text{A.5})$$

Integration and applying the chain rule results in:

$$\frac{\partial ud}{\partial x} = u \frac{\partial d}{\partial x} + d \frac{\partial u}{\partial x} = 0 \quad \rightarrow \quad \frac{du}{dx} = -\frac{q_w}{d^2} \frac{dd}{dx} \quad (\text{A.6})$$

Under steady-state conditions the conservation equation of streamwise momentum reduces to:

$$\frac{\partial u^2 d}{\partial x} + gd \left( \frac{\partial d}{\partial x} + \frac{\partial z_b}{\partial x} \right) - c_f u^2 = 0 \quad (\text{A.7})$$

Applying the chain rule for the second term results in:

$$\frac{du^2 d}{dx} = u \frac{du d}{dx} + ud \frac{du}{dx} \quad (\text{A.8})$$

Integration and dividing by the water depth  $d$  leads to the following reduced expression for the momentum equation:

$$u \frac{du}{dx} + g \left( \frac{dd}{dx} + \frac{dz_b}{dx} \right) - c_f \frac{u^2}{d} = 0 \quad (\text{A.9})$$

Use the following expressions:

$$u = \frac{q_w}{d}, \quad \frac{du}{dx} = -\frac{q_w}{d^2} \frac{dd}{dx} \quad (\text{A.10})$$

To get the backwater equation:

$$\frac{dd}{dx} = \frac{i_b - i_w}{1 - \text{Fr}^2} \quad (\text{A.11})$$

where:

$$i_b = \frac{\partial z_b}{\partial x}, \quad \text{Fr}^2 = \frac{q_w^2}{gd^3} = \frac{u^2}{gd}, \quad i_w = c_f \text{Fr}^2 \quad (\text{A.12})$$

Instead of using the momentum equation, one could also derive the backwater equation from the energy equation (Vriend et al., 2011):

$$\frac{dH}{dx} \stackrel{\text{def}}{=} -i_w \quad (\text{A.13})$$

The gradient specific energy head than becomes:

$$\frac{dE}{dx} = \frac{d(H - z_b)}{dx} = -i_w + i_b \quad (\text{A.14})$$

When steady-state is considered,  $Q$  is constant over time which results in the following expression:

$$\frac{dE}{dx} = \frac{d}{dx} \left( d + \frac{Q^2}{2gA^2} \right) = \frac{dd}{dx} - \frac{2Q^2}{2gA^3} \frac{dA}{dx} \quad (\text{A.15})$$

If  $B$  is constant,  $dA/dx = Bdd/dx$  this reduces the gradient specific energy head to:

$$\frac{dE}{dx} = \frac{dd}{dx} - \frac{u^2}{gBd} B \frac{dd}{dx} \quad (\text{A.16})$$

Rewriting gives the backwater equation:

$$\frac{dd}{dx} = \frac{i_b - i_w}{1 - \text{Fr}^2} \quad (\text{A.17})$$

For the hydraulic model it is important to know how far local disturbances can travel upstream. The area of interest needs to be outside this influence area, otherwise your model results cannot be judged fairly. In other words some backwater calculations are needed.

The following solutions are used to estimate the characteristic backwater length scale:

- First order approximation
- Empirical fit to Bresse

The characteristic length scale of adaptation of the flow towards normal can in case of the first order approximation be estimated by the following formula:

$$L \cong \frac{d_e}{3i_b} \quad (\text{A.18})$$

where  $d_e$  is the equilibrium or normal flow depth, which is given by the following equation:

$$d_e = \left( \frac{c_f q^2}{i_b g} \right)^{1/3} \quad (\text{A.19})$$

The second method for estimating the backwater length scale is the empirical fit to Bresse. Here the half length can be calculated by the following expression:

$$L_{1/2} = 0.24 \frac{d_e}{i_b} \left( \frac{d_0}{d_e} \right)^{4/3} \quad (\text{A.20})$$

$$L \approx L_{1/2} \cdot 4 \quad (\text{A.21})$$

To be able to calculate the backwater length scales the following assumptions are made:

- The bed slope is equal  $i_b = 4e - 4$ .
- A low and high Manning's roughness is assumed, respectively  $n = 0.025$  and  $n = 0.060$ .
- This corresponds with the following values of the dimensionless friction coefficient,  $c_f = 0.004$  and  $c_f = 0.019$ .
- A rectangular channel is assumed, which means that  $q = Q/B$ .

Table A.1 Variables for both backwater estimations.

Variable	27/04/2018	12/05/2018
$Q$ [m <sup>3</sup> /s]	435	245
$B$ [m]	216	185
$i_b$ [m/m]	$4 \cdot 10^{-4}$	$4 \cdot 10^{-4}$

Table A.2 Variables for the first order approximation.

First order approximation	27/04/2018	12/05/2018
$d_e$ (low cf) [m]	7.4	5.6
$d_e$ (high cf) [m]	12.4	9.3
$L$ (low cf) [m]	6129	4635
$L$ (high cf) [m]	10303	7791

Table A.3 Variables for the empirical fit to Bresse.

Empirical fit to Bresse	27/04/2018	12/05/2018
$d_0$ [m]	4.1	3.4
$L_{1/2}$ (low cf) [m]	2051	1704
$L_{1/2}$ (high cf) [m]	1725	1433
$L$ (low cf) [m]	8204	6817
$L$ (high cf) [m]	6900	5733



# B

## Error estimation GCPs

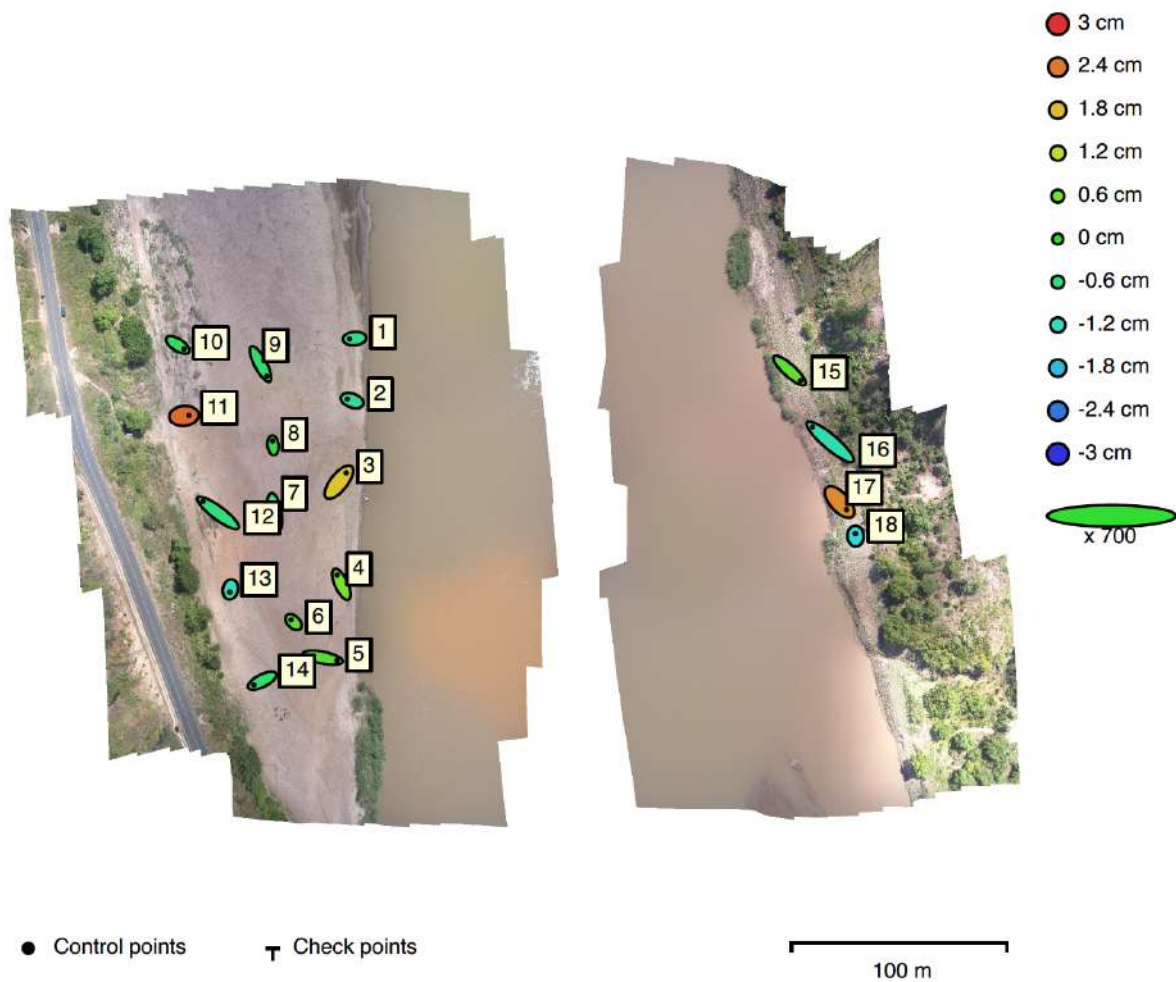


Figure B.1 GCP locations and error estimates. X (Easting) and Y (Northing) errors are represented by ellipse shape. Z (altitude) error is represented by ellipse color.

Table B.1 GCP errors for X, Y and Z.

<b>Label</b>	<b>X error [cm]</b>	<b>Y error [cm]</b>	<b>Z error [cm]</b>	<b>Total [cm]</b>
1	-0.66	-0.06	-0.77	1.02
2	-0.62	0.22	-0.86	1.08
3	0.96	1.22	1.72	2.32
4	-0.58	1.25	0.65	1.52
5	1.90	-0.37	0.32	1.96
6	-0.34	0.32	0.39	0.61
7	0.27	-1.72	-0.85	1.94
8	-0.06	0.58	-0.09	0.59
9	0.85	-1.62	-0.43	1.88
10	0.83	-0.52	-0.37	1.05
11	0.65	0.07	2.53	2.61
12	-2.02	1.51	-0.65	2.61
13	-0.07	-0.35	-1.21	1.26
14	-1.13	-0.56	-0.47	1.34
15	1.48	-1.33	0.40	2.03
16	-2.33	1.97	-1.09	3.24
17	0.90	-0.99	2.22	2.60
18	-0.02	0.32	-1.53	1.56
<b>Total</b>	<b>1.09</b>	<b>1.03</b>	<b>1.13</b>	<b>1.88</b>

# C

## Cross-sections analysis

This appendix provides the analysis of the ADCP measurements at the downstream measurement site of the Great East Road bridge. The first measurement day was on the 27th of April 2018 and the second one on the 12th of May 2018.

Figure C.1 shows an estimation of the location of the transects on the 12th of May 2018. It is assumed that the three transects on the 27th of April are more or less taken at the same position. On both days an upstream, middle and downstream transect is measured, preferably a transect is measured four times.

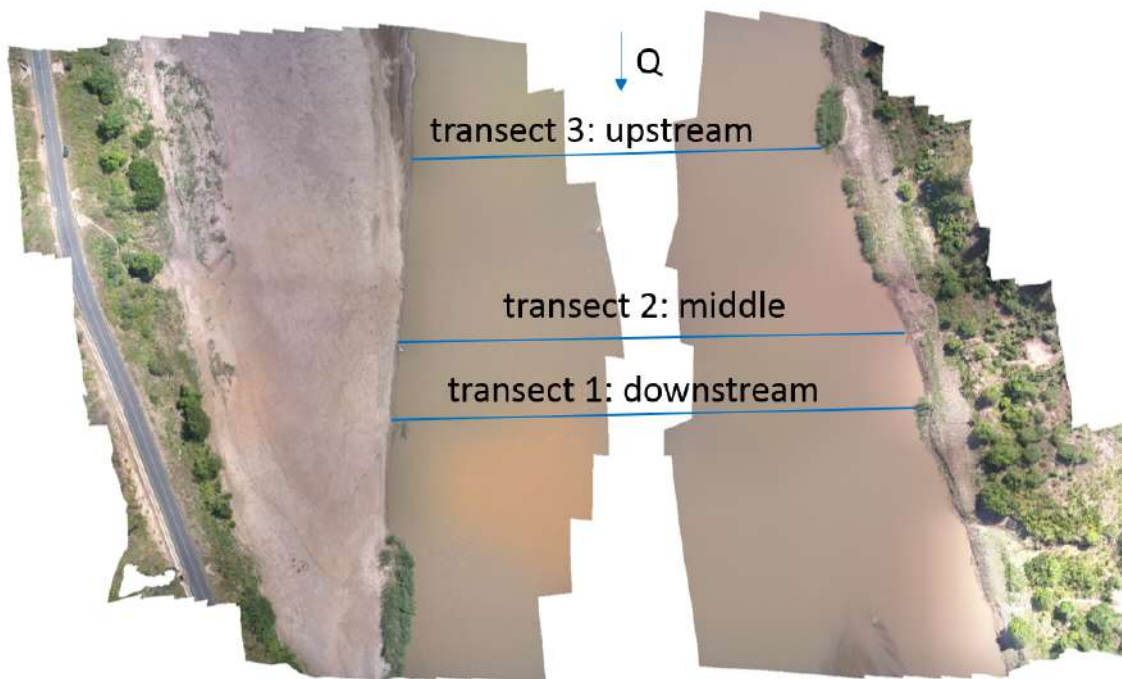


Figure C.1 Transects ADCP measurements for downstream location of the Great East Road bridge.

## C.1 Bathymetry measurements

### C.1.1 Depth profiles

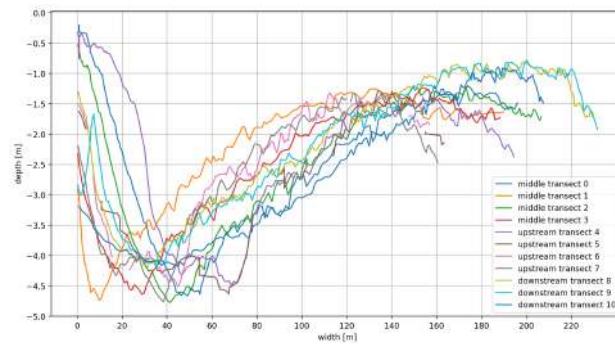


Figure C.2 Depth profiles for the downstream transect on the 27<sup>th</sup> of April 2018.

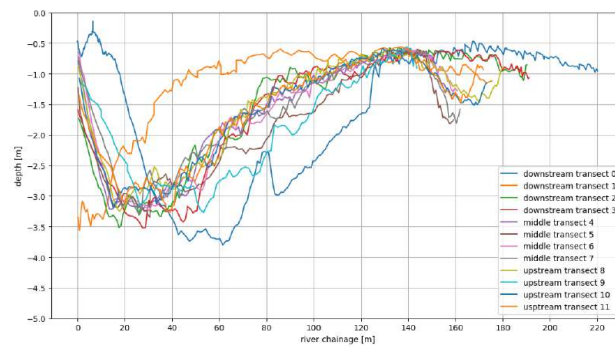


Figure C.3 Depth profiles for the downstream transect on the 12<sup>th</sup> of May 2018.

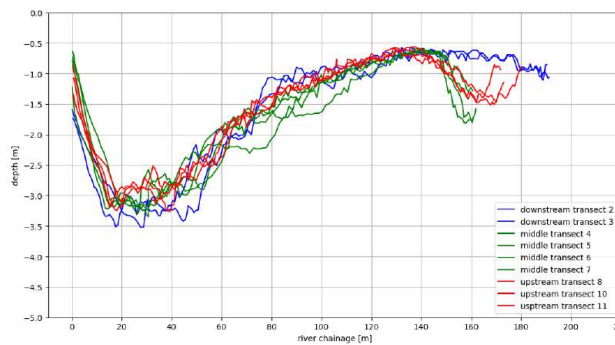


Figure C.4 Selection of depth profiles for the downstream transect on the 12<sup>th</sup> of May 2018.

## C.2 Velocity profiles

### C.2.1 Downstream transect

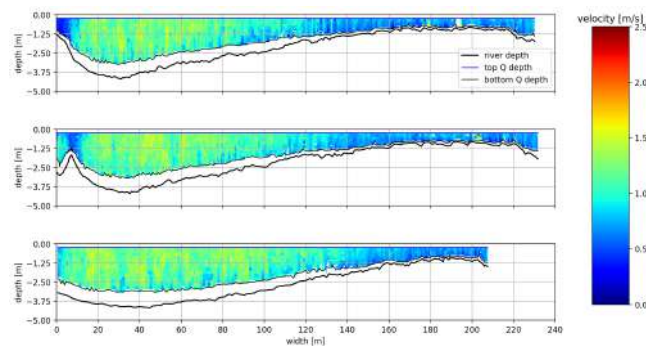


Figure C.5 Velocity profiles for the downstream transect on the 27<sup>th</sup> of April 2018.

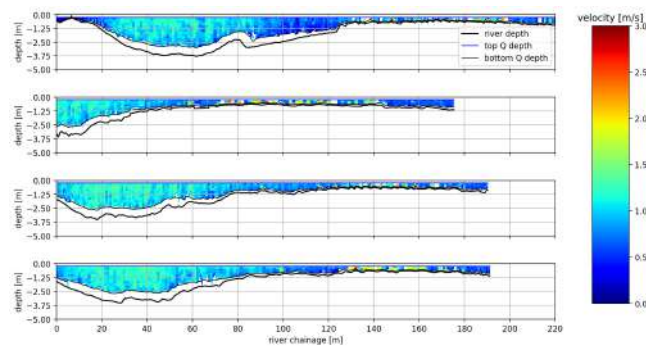


Figure C.6 Velocity profiles for the downstream transect on the 12<sup>th</sup> of May 2018.

### C.2.2 Middle transect

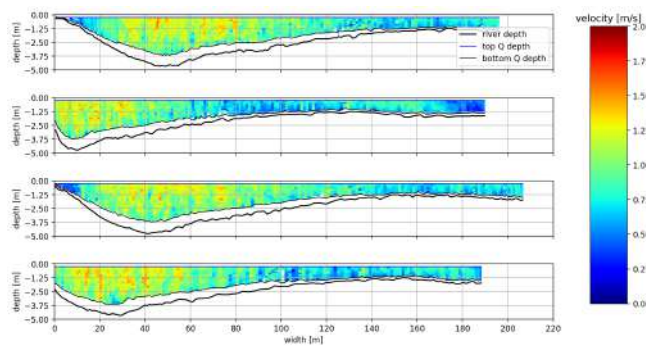


Figure C.7 Velocity profiles for the middle transect on the 27<sup>th</sup> of April 2018.

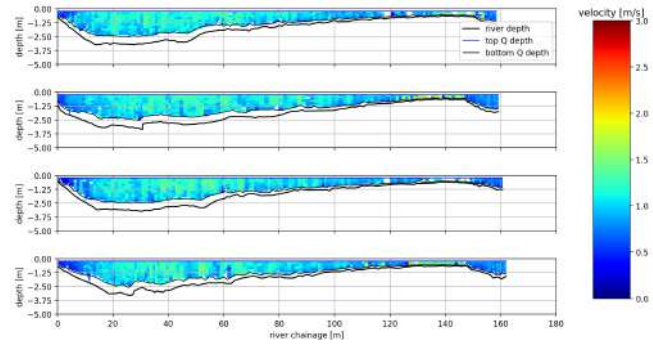


Figure C.8 Velocity profiles for the middle transect on the 12<sup>th</sup> of May 2018.

### C.2.3 Upstream transect

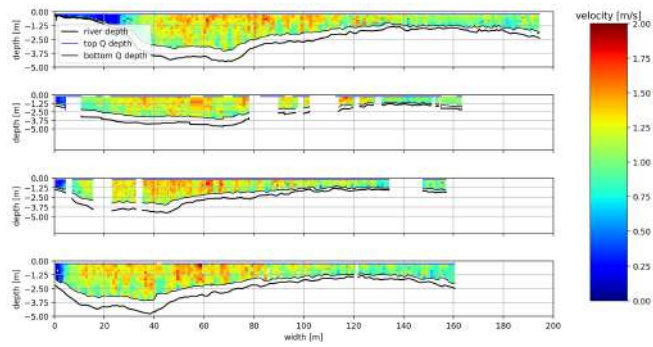


Figure C.9 Velocity profiles for the upstream transect on the 27<sup>th</sup> of April 2018.

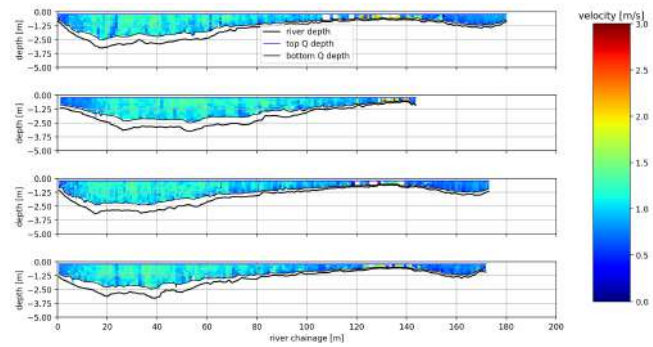


Figure C.10 Velocity profiles for the upstream transect on the 12<sup>th</sup> of May 2018.

### C.2.4 Discharge summary tables

Table C.1 Discharge summary table of the ADCP measurements on the 27<sup>th</sup> of April 2018.

transect	start bank	start time	total Q [m3/s]	delta Q [%]	top Q [m3/s]	meas. Q [m3/s]	bottom Q [m3/s]	left Q [m3/s]	right Q [m3/s]	left dist. [m]	right dist. [m]	width [m]	total area [m2]
down 0	left	18:04:53	-	-	-46.7	-	-89.3	-0.2	-1.3	1	3	221.9	461.2
			437.3	412.7		299.9							
down 1	right	18:12:12	434	210.3	46.5	300.8	84	0.8	1.9	2	2	214.5	443
down 2	left	18:16:13	422.9	202.3	43.5	291.5	82.2	1	4.6	3	4	212.6	458.3
middle 3	right	17:32:53	421.7	-3.3	39.3	295.1	86	0.8	0.6	2	5	208.8	475.4
middle 4	left	17:36:23	433.8	-0.6	38.6	303.2	85.1	0.5	6.4	2	5	192.8	493.9
middle 5	right	17:39:03	441.4	1.2	41.5	308.5	90	0.9	0.5	2	5	201.6	485.6
middle 6	left	17:41:38	448	2.7	39.8	314.3	88.4	0.8	4.7	2	5	193.9	499.5
up 7	left	17:48:46	-	0.4	-41.8	-	-93.2	0.3	-3.2	5	4	181.6	415.4
			440.8			302.8							
up 8	right	17:52:40	-	0.3	-41.5	-302	-90.9	-3.3	-2.9	7	4	169.7	418.5
			440.5										
up 9	left	17:55:03	-	-1.9	-40.5	-	-91.2	-1.9	-2.4	7	4	161.2	395.5
			430.7			294.8							
up 10	right	17:58:06	-	1.2	-41.6	-	-93.4	-3.3	-3	7	4	169.2	427.8
			444.5			303.3							
<b>average</b>			436	0	41.9	301.5	88.5	1.2	2.9	3.6	4.1	193.4	452.2
<b>std. dev.</b>			8.4	138.5	2.7	6.4	3.7	1.1	1.8	2.4	0.9	20.6	34.8

Table C.2 Discharge summary table of the ADCP measurements on the 12<sup>th</sup> of May 2018.

transect	start bank	start time	total Q [m3/s]	delta Q [%]	top Q [m3/s]	meas. Q [m3/s]	bottom Q [m3/s]	left Q [m3/s]	right Q [m3/s]	left dist. [m]	right dist. [m]	width [m]	total area [m2]
down 0	right	16:46:57	260.2	6.3	28.4	174.8	55.8	1.2	0.0	5.0	2.0	201.5	336.1
down 1	left	16:52:12	207.5	-15.2	27.0	132.6	42.9	1.1	3.9	5.0	3.0	181.5	259.6
down 2	right	16:54:34	250.2	2.2	29.6	165.9	52.2	0.6	1.9	3.0	3.0	191.1	291.3
down 3	left	16:57:42	249.8	2.0	31.4	163.8	52.3	0.7	1.6	3.0	3.0	195.5	298.1
middle 4	right	17:02:29	242.2	-1.1	29.3	162.1	49.2	1.4	0.2	5.0	2.0	157.8	262.1
middle 5	left	17:04:52	249.4	1.8	30.6	165.2	50.3	2.4	0.7	5.0	2.0	163.6	278.8
middle 6	right	17:07:11	241.8	-1.3	30.2	162.1	48.0	1.2	0.3	5.0	2.0	156.2	257.6
middle 7	left	17:09:46	253.0	3.3	31.6	166.7	51.8	2.3	0.4	5.0	2.0	168.3	283.4
up 8	right	17:12:56	245.8	0.4	30.6	162.1	51.1	1.0	0.9	3.0	3.0	176.3	274.2
up 9	left	17:15:57	227.4	-7.2	27.4	148.8	49.3	1.1	0.7	7.0	2.0	152.2	253.1
up 10	right	17:17:46	251.7	2.8	31.3	165.9	52.2	1.2	1.1	3.0	3.0	173.9	280.7
up 11	left	17:20:43	259.5	6.0	34.1	170.2	53.3	0.9	1.0	3.0	2.0	176.0	287.2
<b>average</b>			244.9	0.0	30.1	161.7	50.7	1.3	1.1	4.3	2.4	174.5	280.2
<b>std. dev.</b>			14.6	6.0	2.0	11.0	3.2	0.6	1.1	1.3	0.5	15.9	22.7

### C.3 Width versus depth

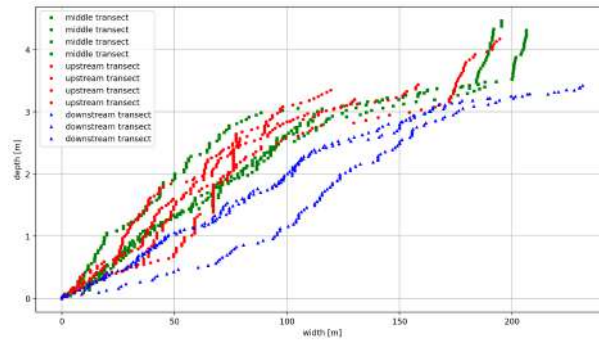


Figure C.11 Top width versus modelled depth on the 27<sup>th</sup> of April 2018.

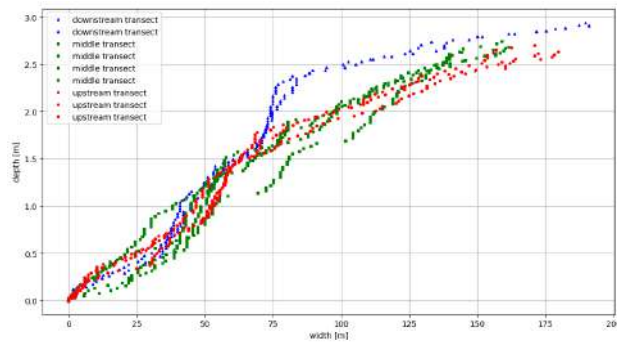


Figure C.12 Top width versus modelled depth on the 12<sup>th</sup> of May 2018.

### C.4 Cross-sectional area versus depth

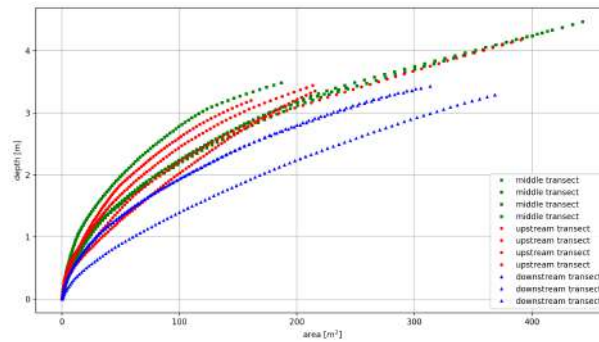


Figure C.13 Cross-sectional area versus modelled depth on the 27<sup>th</sup> of April 2018.

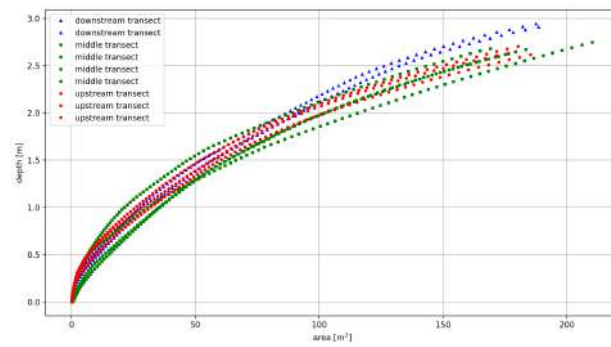


Figure C.14 Cross-sectional area versus modelled depth on the 12<sup>th</sup> of May 2018.

### C.5 Perimeter versus depth

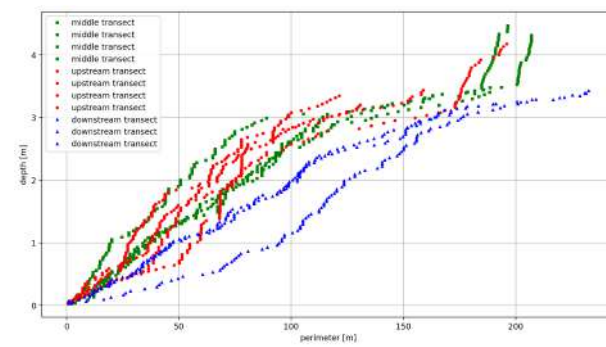


Figure C.15 Perimeter versus modelled depth on the 27<sup>th</sup> of April 2018.

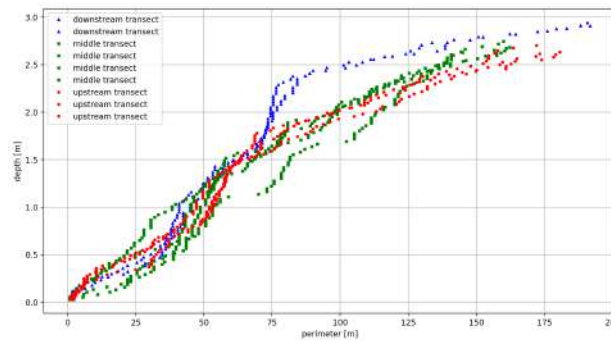


Figure C.16 Perimeter versus modelled depth on the 12<sup>th</sup> of May 2018.

## C.6 Hydraulic radius versus depth

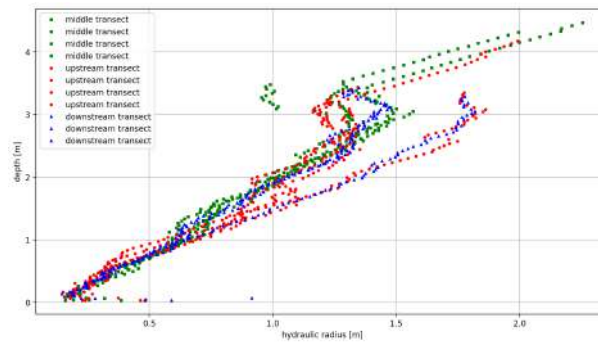


Figure C.17 Hydraulic radius versus modelled depth on the 27<sup>th</sup> of April 2018.

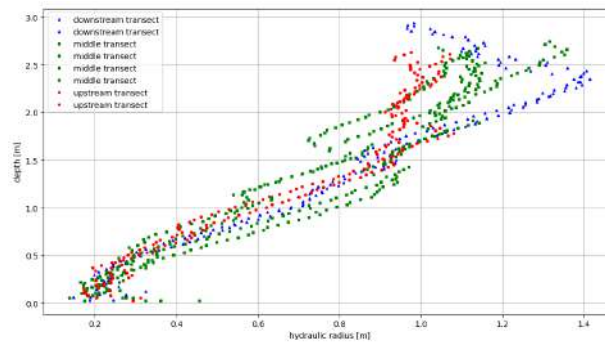


Figure C.18 Hydraulic radius versus modelled depth on the 12<sup>th</sup> of May 2018.

## C.7 Conveyance versus depth

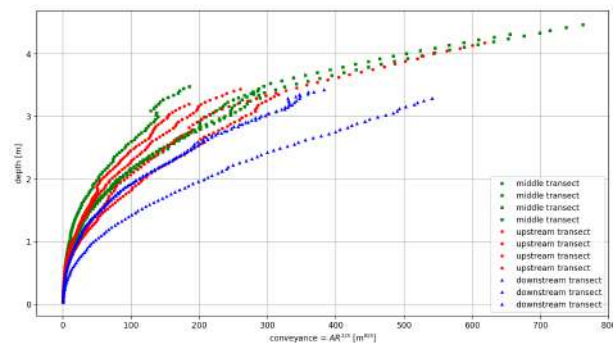


Figure C.19 Conveyance versus modelled depth on the 27<sup>th</sup> of April 2018.

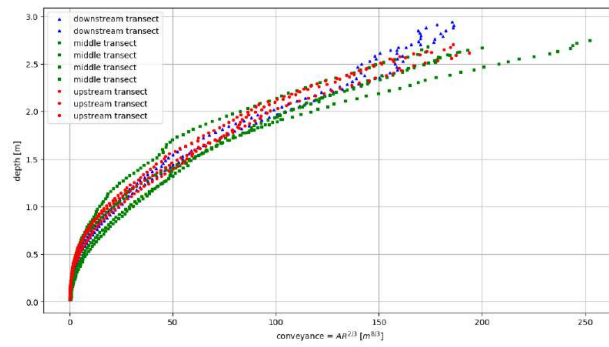


Figure C.20 Conveyance versus modelled depth on the 12<sup>th</sup> of May 2018.

## C.8 Averaging depth profiles

### C.8.1 Downstream transect

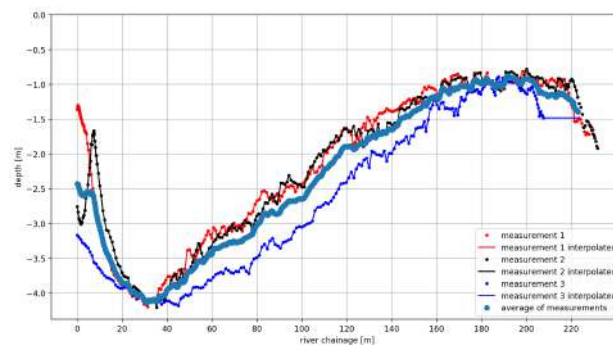


Figure C.21 Averaging the downstream transect on the 27<sup>th</sup> of April 2018.

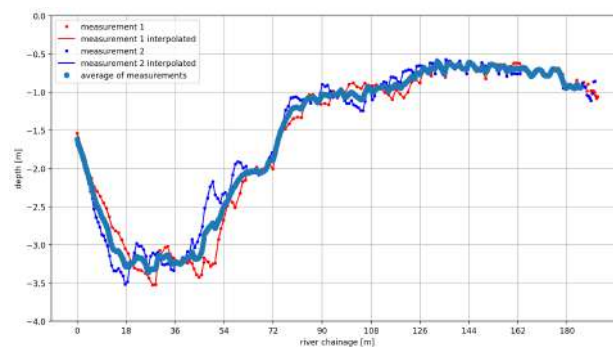


Figure C.22 Averaging the downstream transect on the 12<sup>th</sup> of May 2018.

### C.8.2 Middle transect

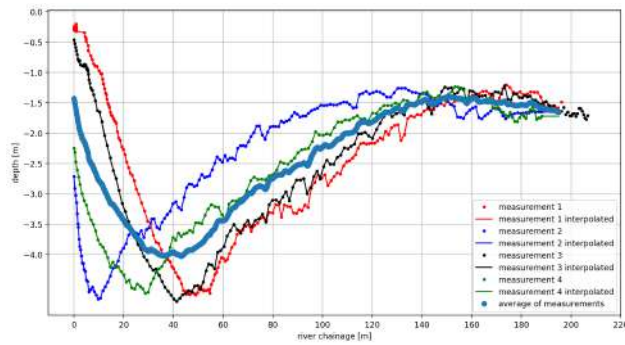


Figure C.23 Averaging the middle transect on the 27<sup>th</sup> of April 2018.

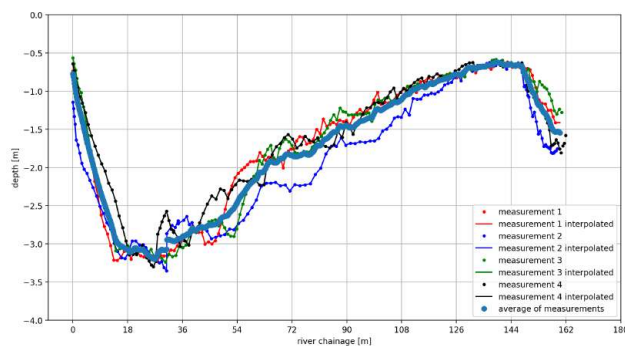


Figure C.24 Averaging the middle transect on the 12<sup>th</sup> of May 2018.

### C.8.3 Upstream transect

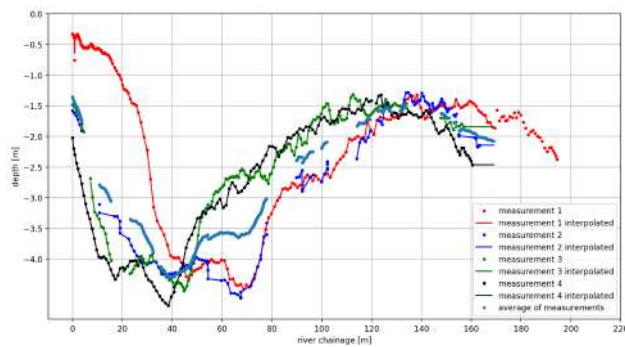


Figure C.25 Averaging the upstream transect on the 27<sup>th</sup> of April 2018.

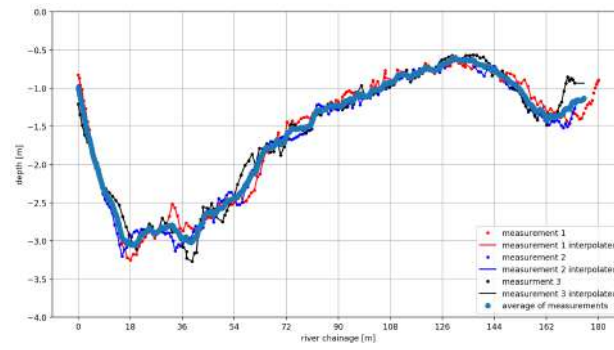


Figure C.26 Averaging the downstream transect on the 12<sup>th</sup> of May 2018.



# D

## Additional graphs results

### D.1 Hydraulic slope estimation

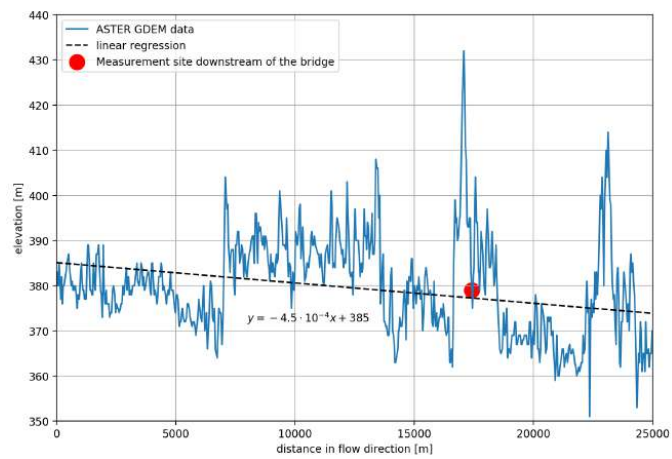


Figure D.1 Hydraulic slope estimation from the ASTER GDEM data (Broekema, 2018).

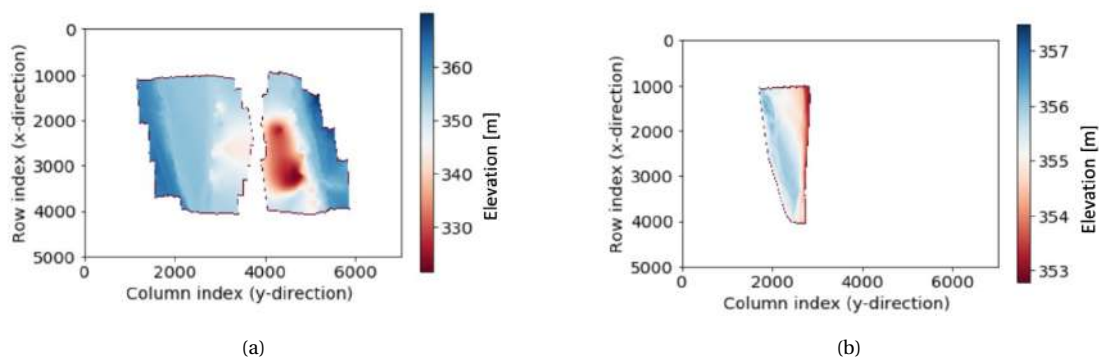


Figure D.2 (a) DEM in python with water surface and (b) DEM of only the floodplain, where the slope is estimated (Broekema, 2018).

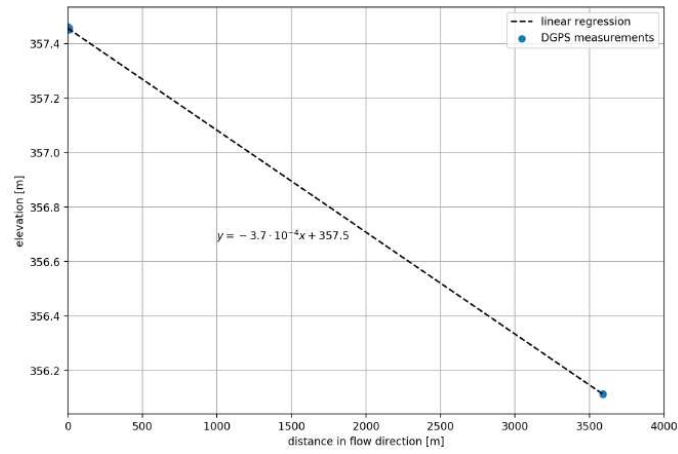


Figure D.3 DGPS measurements of the water surface elevation over a large distance.

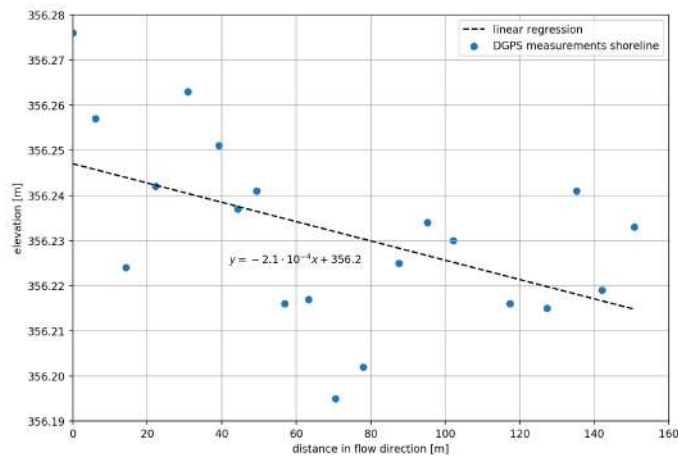


Figure D.4 DGPS measurements of the water surface over a short distance.

## D.2 Model evaluation

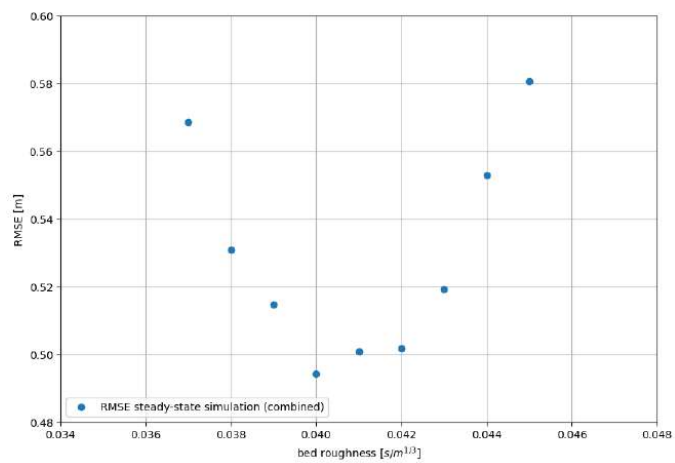


Figure D.5 The RMSE for varying Manning's coefficients for both measurement days.

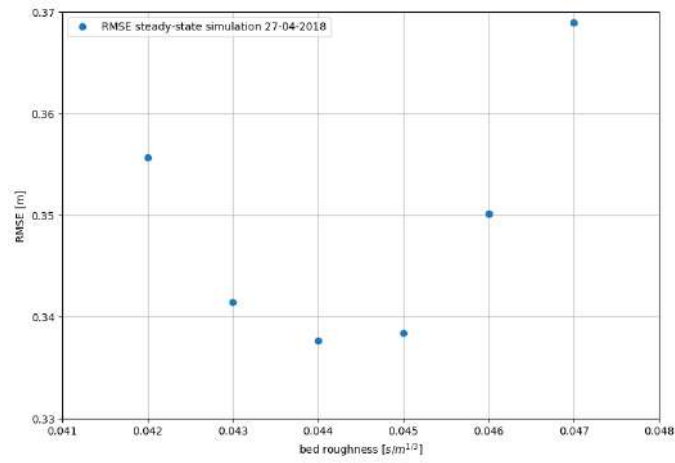


Figure D.6 The RMSE for varying Manning's coefficients on April 27, 2018.

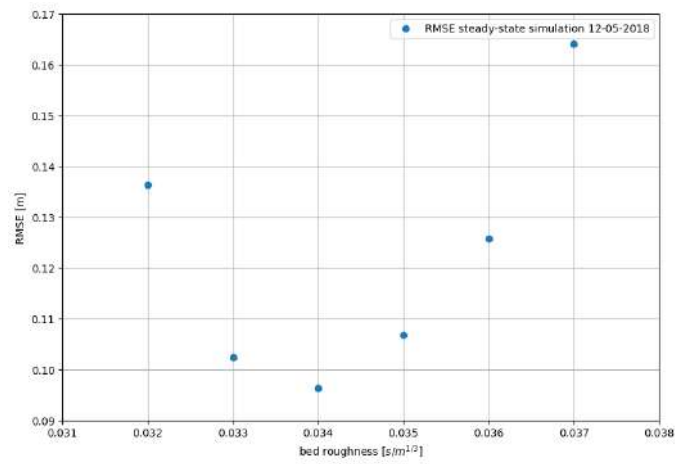


Figure D.7 The RMSE for varying Manning's coefficients on May 12, 2018.

## D.3 Rating curves

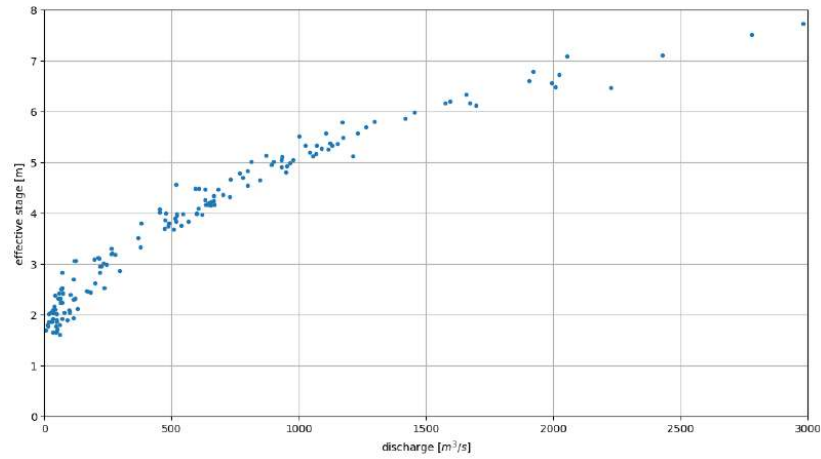


Figure D.8 The discharge stage measurements of WARMA.

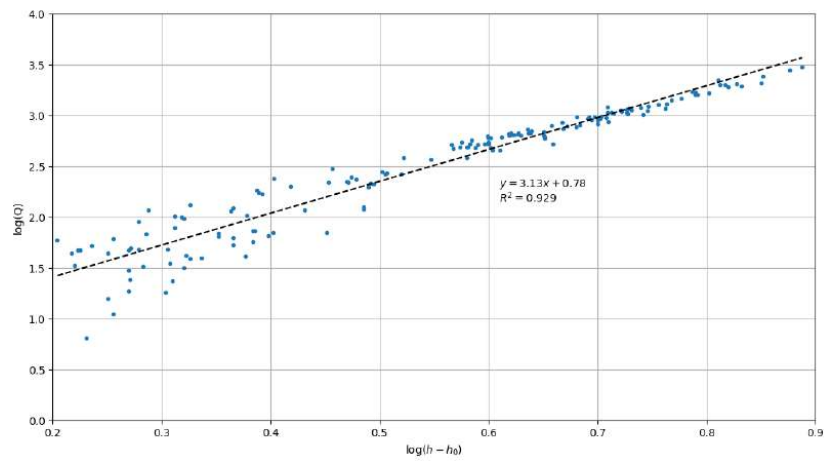


Figure D.9 Determination of stage-discharge relationship WARMA measurements.

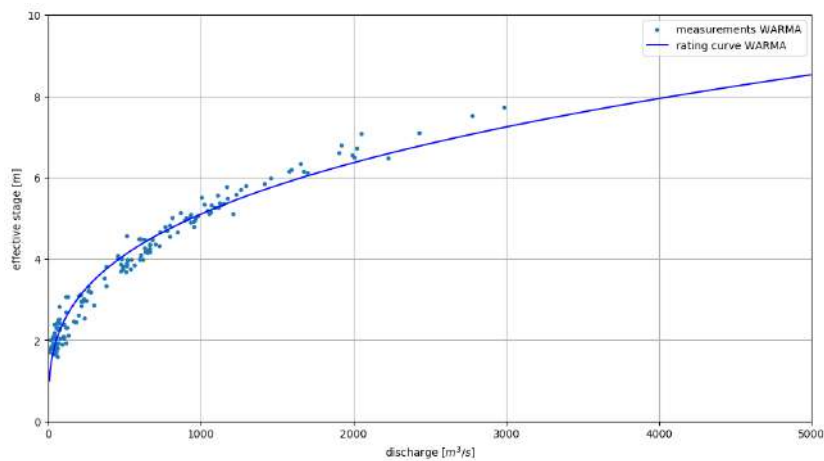


Figure D.10 The discharge stage measurements and corresponding rating curve of WARMA.

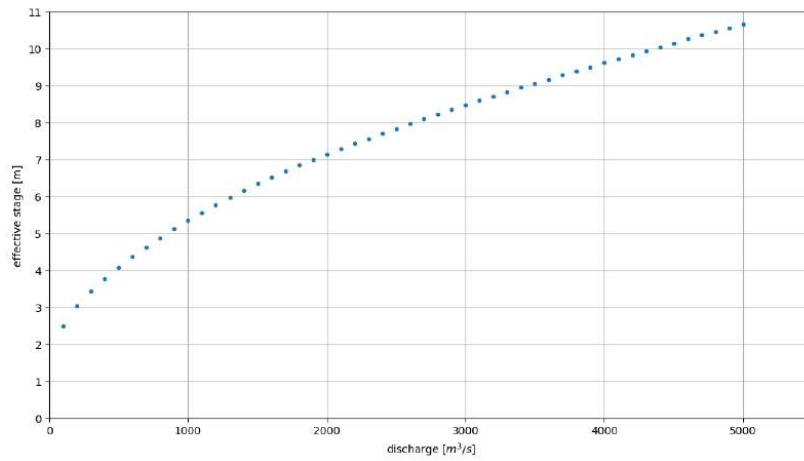


Figure D.11 The simulated stage discharge values for the HEC-RAS model, where  $iw=4e-4$  and  $n=0.040$ .

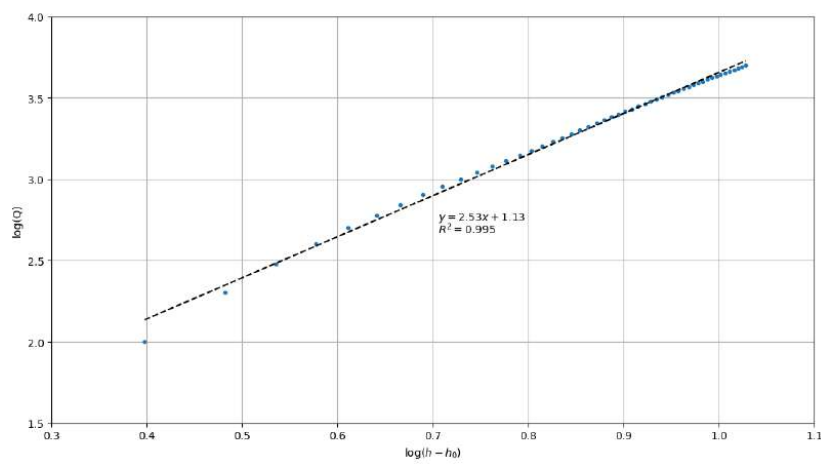


Figure D.12 Determination of stage-discharge relationship HEC-RAS model, where  $iw=4e-4$  and  $n=0.040$ .

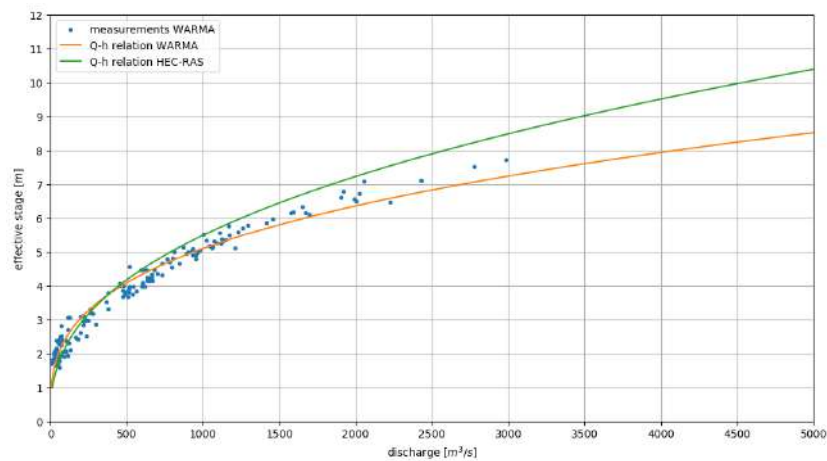


Figure D.13 Comparison of rating curve WARMA with the HEC-RAS rating curve.

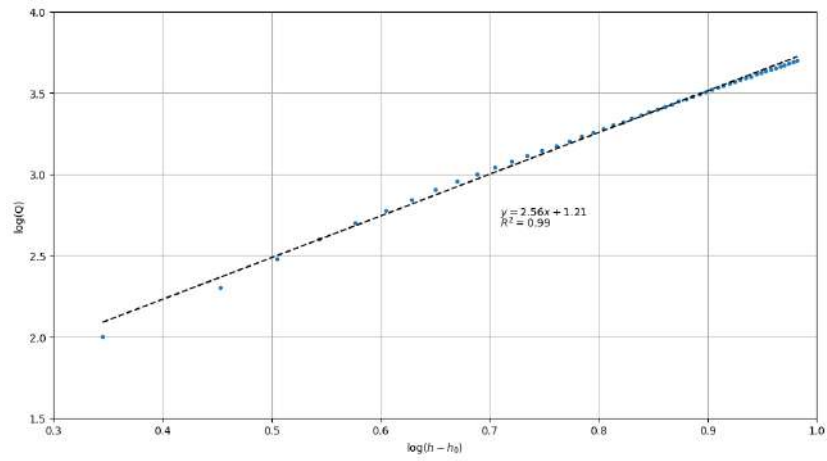


Figure D.14 Determination of stage-discharge relationship HEC-RAS model, where  $iw=4e-4$  and  $n=0.032$ .

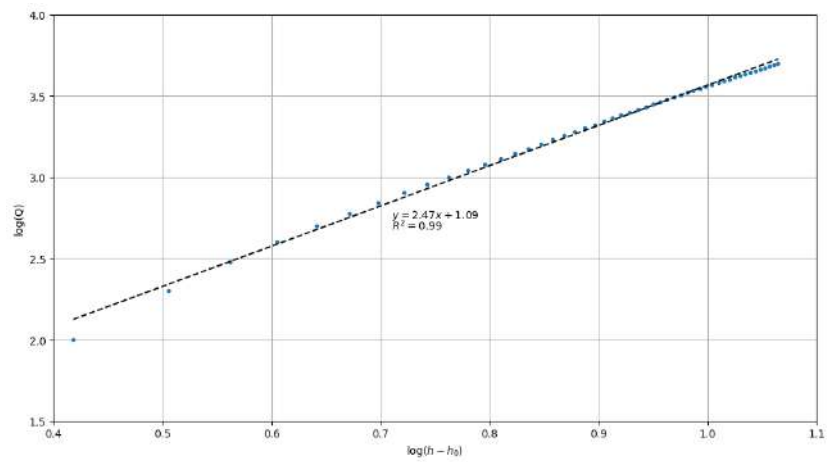


Figure D.15 Determination of stage-discharge relationship HEC-RAS model, where  $iw=4e-4$  and  $n=0.048$ .

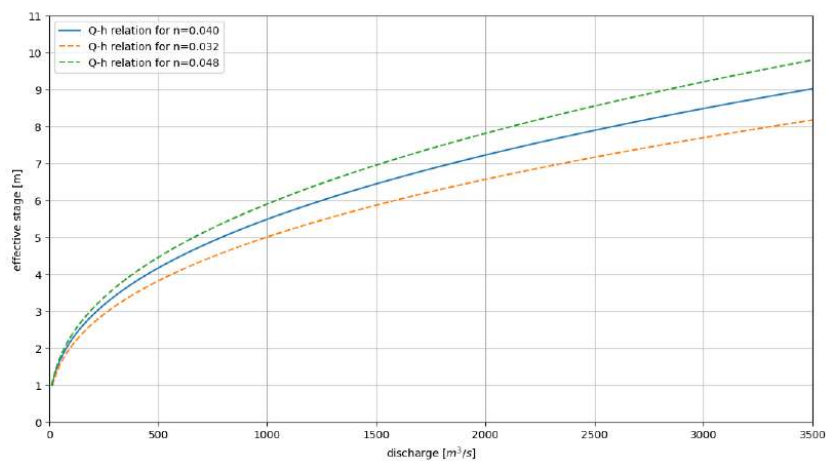


Figure D.16 Rating curve sensitivity for changes in Manning's coefficient and constant hydraulic slope.

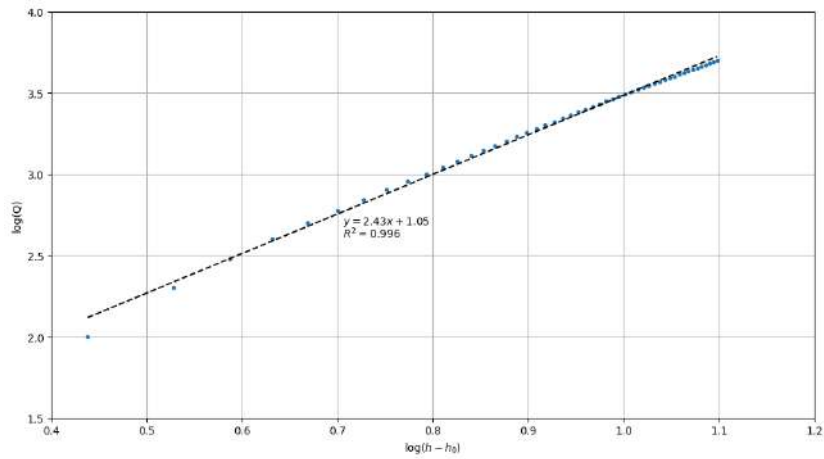


Figure D.17 Determination of stage-discharge relationship HEC-RAS model, where  $i_w=2e-4$  and  $n=0.040$ .

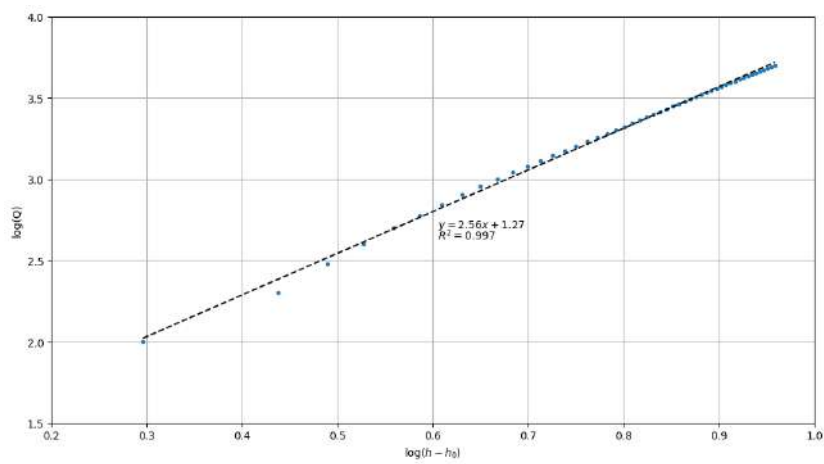


Figure D.18 Determination of stage-discharge relationship HEC-RAS model, where  $i_w=8e-4$  and  $n=0.040$ .

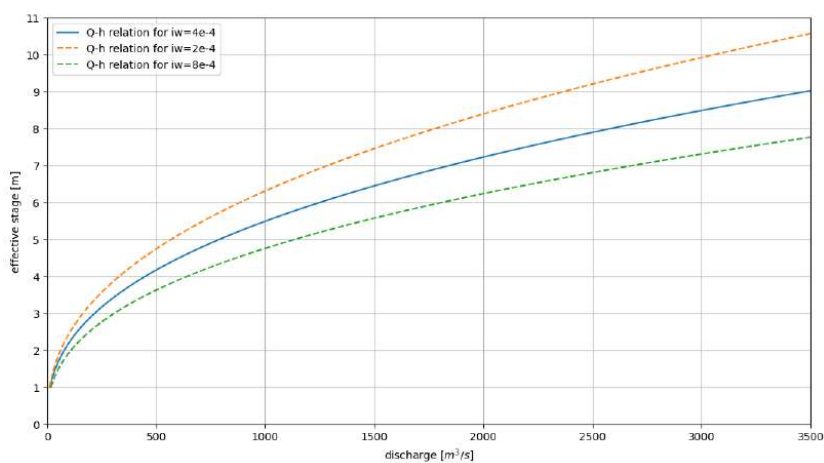


Figure D.19 Rating curve sensitivity for changes in hydraulic slope and constant bed roughness.

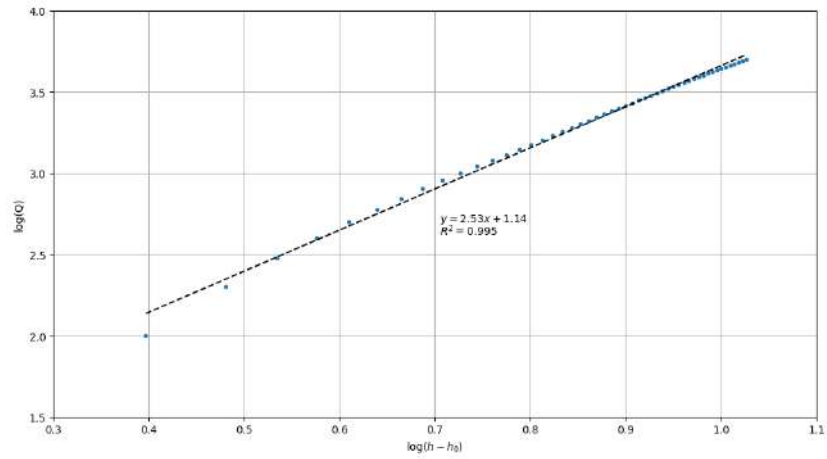


Figure D.20 Determination of stage-discharge relationship HEC-RAS model, where  $iw=2e-4$  for  $n=0.028$ .

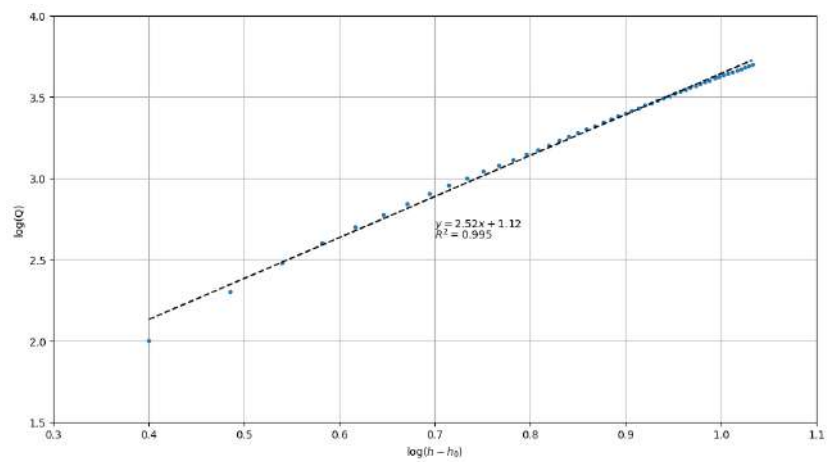


Figure D.21 Determination of stage-discharge relationship HEC-RAS model, where  $iw=8e-4$   $n=0.058$ .

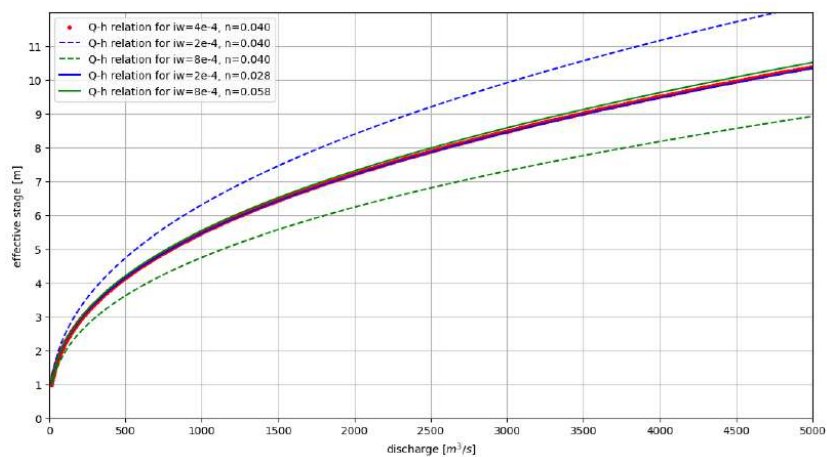


Figure D.22 Rating curve sensitivity for changes in hydraulic slope with new optimum bed roughness values.

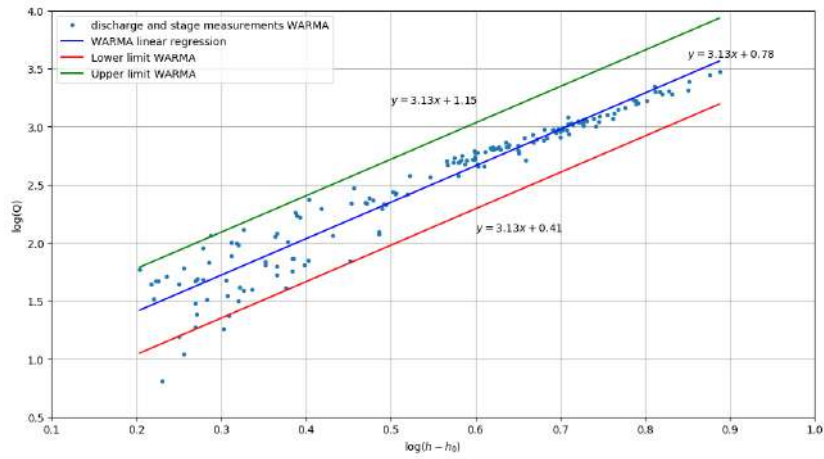


Figure D.23 Determination of the 95% confidence interval of the WARMA rating curve.

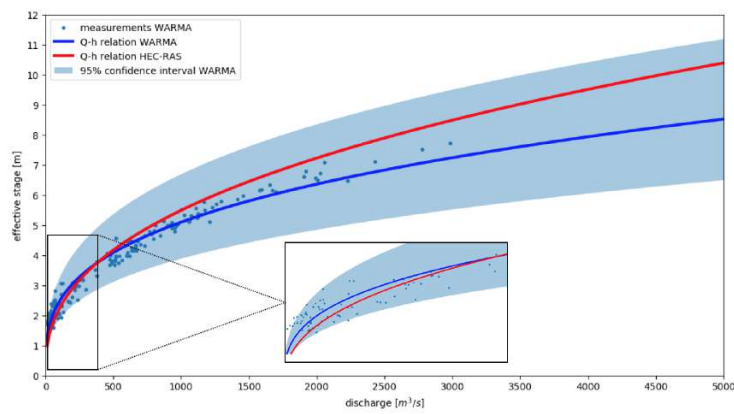


Figure D.24 Rating curve comparison with error bounds of the 95% confidence interval and WARMA measurements.

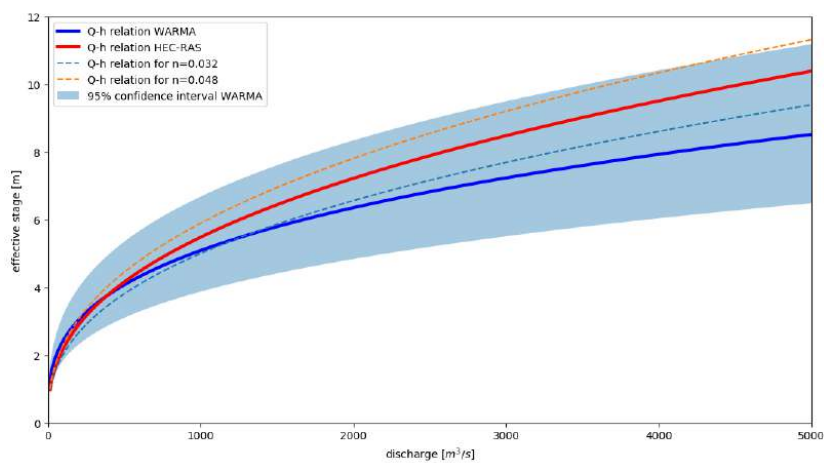


Figure D.25 Rating curve comparison with error bounds and the sensitivity of a change in bed roughness.





## Manning values and calculations

Type of Channel and Description	Minimum	Normal	Maximum
Natural streams - minor streams (top width at floodstage < 100 ft)			
<b>1. Main Channels</b>			
a. clean, straight, full stage, no rifts or deep pools	0.025	0.030	0.033
b. same as above, but more stones and weeds	0.030	0.035	0.040
c. clean, winding, some pools and shoals	0.033	0.040	0.045
d. same as above, but some weeds and stones	0.035	0.045	0.050
e. same as above, lower stages, more ineffective slopes and sections	0.040	0.048	0.055
f. same as "d" with more stones	0.045	0.050	0.060
g. sluggish reaches, weedy, deep pools	0.050	0.070	0.080
h. very weedy reaches, deep pools, or floodways with heavy stand of timber and underbrush	0.075	0.100	0.150
<b>2. Mountain streams, no vegetation in channel, banks usually steep, trees and brush along banks submerged at high stages</b>			
a. bottom: gravels, cobbles, and few boulders	0.030	0.040	0.050
b. bottom: cobbles with large boulders	0.040	0.050	0.070
<b>3. Floodplains</b>			
a. Pasture, no brush			
1. short grass	0.025	0.030	0.035
2. high grass	0.030	0.035	0.050
b. Cultivated areas			
1. no crop	0.020	0.030	0.040
2. mature row crops	0.025	0.035	0.045
3. mature field crops	0.030	0.040	0.050
c. Brush			
1. scattered brush, heavy weeds	0.035	0.050	0.070
2. light brush and trees, in winter	0.035	0.050	0.060
3. light brush and trees, in summer	0.040	0.060	0.080
4. medium to dense brush, in winter	0.045	0.070	0.110
5. medium to dense brush, in summer	0.070	0.100	0.160
d. Trees			
1. dense willows, summer, straight	0.110	0.150	0.200
2. cleared land with tree stumps, no sprouts	0.030	0.040	0.050
3. same as above, but with heavy growth of sprouts	0.050	0.060	0.080
4. heavy stand of timber, a few down trees, little undergrowth, flood stage below branches	0.080	0.100	0.120
5. same as 4. with flood stage reaching branches	0.100	0.120	0.160

Figure E.1 Manning's roughness values for main channel and flood plain (Chow, 1959).

$$Q = n^{-1} \sqrt{i_w} AR^{2/3} \quad (\text{E.1})$$

Table E.1 Parameter values for plain Manning calculation.

<b>Parameters</b>	<b>Values</b>
$i_w$ [m/m]	4
$Q_1$ [ $m^3/s$ ]	435
$Q_2$ [ $m^3/s$ ]	245
$A_1$ [ $m^2$ ]	414
$A_2$ [ $m^2$ ]	274
$d_1$ [m]	4.3
$d_2$ [m]	3.1



